

INFORMATION TO USERS

This manuscript has been reproduced from the microfilm master. UMI films the text directly from the original or copy submitted. Thus, some thesis and dissertation copies are in typewriter face, while others may be from any type of computer printer.

The quality of this reproduction is dependent upon the quality of the copy submitted. Broken or indistinct print, colored or poor quality illustrations and photographs, print bleedthrough, substandard margins, and improper alignment can adversely affect reproduction.

In the unlikely event that the author did not send UMI a complete manuscript and there are missing pages, these will be noted. Also, if unauthorized copyright material had to be removed, a note will indicate the deletion.

Oversize materials (e.g., maps, drawings, charts) are reproduced by sectioning the original, beginning at the upper left-hand corner and continuing from left to right in equal sections with small overlaps.

Photographs included in the original manuscript have been reproduced xerographically in this copy. Higher quality 6" x 9" black and white photographic prints are available for any photographs or illustrations appearing in this copy for an additional charge. Contact UMI directly to order.

ProQuest Information and Learning
300 North Zeeb Road, Ann Arbor, MI 48106-1346 USA
800-521-0600

UMI[®]

UNIVERSITY OF ALBERTA

**AN INVESTIGATION ON THE OPERATING CHARACTERISTICS
OF A NOVEL THYRISTOR LINKED REACTOR**

By

Xiqin Zhang



A thesis

submitted to the faculty of graduate studies and research
in partial fulfillment of the requirements for the degree of
Master of Science

Department of Electrical and Computer Engineering

Edmonton, Alberta

Spring 2001



National Library
of Canada

Acquisitions and
Bibliographic Services

395 Wellington Street
Ottawa ON K1A 0N4
Canada

Bibliothèque nationale
du Canada

Acquisitions et
services bibliographiques

395, rue Wellington
Ottawa ON K1A 0N4
Canada

Your file Votre référence

Our file Notre référence

The author has granted a non-exclusive licence allowing the National Library of Canada to reproduce, loan, distribute or sell copies of this thesis in microform, paper or electronic formats.

The author retains ownership of the copyright in this thesis. Neither the thesis nor substantial extracts from it may be printed or otherwise reproduced without the author's permission.

L'auteur a accordé une licence non exclusive permettant à la Bibliothèque nationale du Canada de reproduire, prêter, distribuer ou vendre des copies de cette thèse sous la forme de microfiche/film, de reproduction sur papier ou sur format électronique.

L'auteur conserve la propriété du droit d'auteur qui protège cette thèse. Ni la thèse ni des extraits substantiels de celle-ci ne doivent être imprimés ou autrement reproduits sans son autorisation.

0-612-60519-1

UNIVERSITY OF ALBERTA

LIBRARY RELEASE FORM

Name of Author: Xiqin Zhang

Title of Thesis: An Investigation on the Operating Characteristics of a
Novel Thyristor Linked Reactor

Degree: Master of Science

Year this Degree Granted: 2001

Permission is hereby granted to the University of Alberta Library to reproduce single copies of this thesis and to lend or sell such copies for private, scholarly or scientific research purposes only.

The author reserves all other publication and other rights in association with the copyright in the thesis, and except as herein before provided, neither the thesis nor any substantial portion thereof may be printed or otherwise reproduced in any material form whatever without the author's prior written permission.

Xiqin Zhang

Beitun, Luan Cheng, Hebei
051430 P. R. China

April 23. 2001

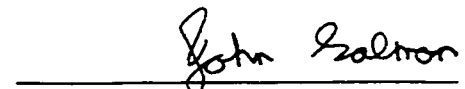
UNIVERSITY OF ALBERTA

FACULTY OF GRADUATE STUDIES AND RESEARCH

The undersigned certify that they have read, and recommend to the Faculty of Graduate Studies and Research for acceptance, a thesis An Investigation on the Operating Characteristics of a Novel Thyristor Linked Reactor submitted by Xiqin Zhang in partial fulfillment of the requirements for the degree of Master of Science.



Dr. Wilsun Xu



Dr. John Salmon



Dr. Edward S. Meadows

Abstract

This thesis investigates the operating characteristics of a novel variable reactor called Thyristor Linked Reactor (TLR). The objective is to determine the main factors that should be considered for designing such a device. Potential applications of the inductor include tunable harmonic filters and shunt reactive power compensators. In this project, a prototype device was constructed. Experimental and simulation studies were conducted to determine the voltage and current stress levels of the device.

The steady-state characteristics of the reactor are investigated first. Voltage stress on the main component of the reactor, thyristor switches, is assessed. The results are compared with those obtained from the tap-based variable inductors. Advantages of the new device are demonstrated. Transient characteristics of the device connected in RL and RLC circuits are then analyzed. Sensitivity studies are conducted to determine the impact of several factors, such as the instant of switching and the degree of inductor coupling, on the transient stress experienced by the thyristor components.

The results show that the thyristor linked reactor can be constructed economically. It has several advantages over existing devices. Key design issues have been identified.

Acknowledgement

I would like to express my sincere gratitude and appreciation to my research supervisor Dr. Wilsun Xu for his support and guidance. The prototype was constructed by Mr. Albert Huizinga, technician of power system lab. His contribution is acknowledged. In addition, I would like to thank all my colleagues and fellow students at the department for creating a productive environment.

At the end, I would like to mention my husband Daoping and my daughter Linan for their encouragement and love.

Xiqin Zhang

Table of Contents

	Page
Abstract	
List of Tables	
List of Figures	
List of Symbols	
Acknowledgement	
1. Introduction.....	1
1.0 Power Quality	1
1.1 Harmonic Distortion	4
1.2 Harmonic Mitigation.....	6
1.2.1 Harmonic Cancellation Schemes	6
1.2.2 Passive Filters	6
1.2.3 Active Filter	7
1.3 Objective and Scope	8
1.4 Outline of the Thesis	9
2. Thyristor Linked Reactor	11
2.0 Introduction.....	11
2.1 The Principle of Variable Reactor	12
2.2 Review of Existing Types of Variable Reactor	13
2.2.1 Saturable or Flux Controllable Reactor	14
2.2.2 Electronic Switch Controlled Reactor	16
2.2.3 Coil Turns Changeable Reactor	17
2.2.4 Tapped Reactor	18
2.3 Thyristor Linked Reactor.....	19
2.4 Potential Applications.....	21

2.4.1 Tunable Filter.....	21
2.4.2 Static VAR Compensation.....	25
3. Steady State Performance of the Thyristor Linked Reactor	28
3.0 Introduction.....	28
3.1 Experimental Setup and Results	29
3.2 Voltage Stress Analysis of Variable inductor.....	32
3.3 Case Studies of the Practical Applications	34
3.3.1 Pure Inductor Branch	34
3.3.2 TLR in a Filter	41
3.4 Impact of Harmonics on the Voltage Stress	47
3.4.1 Cases without Mutual Coupling.....	49
3.4.2 Cases with Mutual Coupling.....	50
3.5 Economical Feasibility.....	52
3.6 Conclusions.....	53
4. Transient Performance of the Thyristor Linked Reactor in RL Circuit.....	54
4.0 Introduction.....	54
4.1 Measurement Determination of Z Matrix of a Prototype	55
4.2 Transient Caused by Inductor Bypassing	58
4.2.1 Theoretical Analysis	58
4.2.2 Simulation and Experimental Study	65
4.2.3 Sensitivity Study on the Switch Timing	66
4.2.4 Effect of Some Factors on the Switching Transients.....	69
4.3 Transient Caused by Inductor Insertion.....	71
4.3.1 Theoretical Analysis	72
4.3.2 Simulation and Experimental Study	75
4.3.3 Sensitivity Study on the Switch Timing	76
4.3.4 Effect of Some Factors on the Switching Transients.....	78
4.4 Conclusions.....	81

5. Transient Performance of the Thyristor Linked Reactor in RLC Circuit.....	82
5.0 Introduction.....	82
5.1 Transient Caused by Inductor Bypassing	83
5.1.1 Theoretical Analysis	83
5.1.2 Simulation and Experimental Study	87
5.1.3 Sensitivity Study on Switch Timing	89
5.1.4 Effect of Some Factors on the Switching Transients.....	91
5.2 Transient Caused by Inductor Insertion.....	92
5.2.1 Theoretical Analysis	93
5.2.2 Simulation and Experimental Study	95
5.2.3 Sensitivity Study on the Switch Timing	96
5.2.4 Effect of Some Factors on the Switching Transients.....	98
5.3 Analysis of Voltage Stress on the Switches.....	99
5.3.1 Inductor Bypassing	100
5.3.2 Inductor Insertion.....	103
5.4 The Duration of Switching Transients of <i>RLC</i> Circuit.....	106
5.5 Conclusions.....	109
6. Design Issues of Thyristor Linked Reactor	111
6.0 Inductor Design Issues.....	111
6.1 Selection of Thyristors.....	115
6.1.1 Thyristor Current Rating.....	115
6.1.2 Voltage Rating	116
6.1.3 di/dt Rating.....	117
6.1.4 Forward dv/dt Rating	117
6.2 Conclusions.....	118
Conclusions and Recommendations.....	119

References	122
-------------------------	------------

Appendices	126
-------------------------	------------

Appendix A: EMTP Script	126
-------------------------------	-----

Appendix B: Matlab Scripts.....	127
---------------------------------	-----

List of Tables

3.1	Analytical results of TLR without mutual coupling	36
3.2	Analytical results of tap connection without mutual coupling	37
3.3	Analytical results of TLR with mutual coupling	39
3.4	Analytical results of tap connection with mutual coupling	39
3.5	Analytical results of TLR without mutual coupling (filter)	43
3.6	Analytical results of tap connection without mutual coupling (filter)	44
3.7	Analytical results of TLR with mutual coupling (filter)	45
3.8	Analytical results of tap connection with mutual coupling (filter)	46
3.9	Analytical results of TLR without mutual coupling (with harmonics)	49
3.10	Analytical results of tap connection without mutual coupling (with harmonics)	49
3.11	Analytical results of TLR connection with mutual coupling (with harmonics)	50
3.12	Analytical results of tap connection with mutual coupling (with harmonics)	50
3.13	Cost comparison	52
4.1	Measurement results	56
5.1	Calculation results of R and δ for different power loss	109
6.1	Parameter comparison	114

List of Figures

2.1	Principle of saturable reactor	14
2.2	Variable reactor under Patent 4347489	15
2.3	Variable reactor under Patent 4393157	15
2.4	Thyristor-controlled reactor	16
2.5	TCR inductor current	16
2.6	Switched reactor	17
2.7	Voltage and current waveforms	17
2.8	Coil turns changeable reactor	18
2.9	Tapped reactor	19
2.10	Inductor segment arrangement	20
2.11	Topology of the variable reactor	20
2.12	Operating state of inductor segment	21
2.13	Passive shunt filters	22
2.14	Notch filter frequency response	23
2.15	Concept of a tunable filter	24
2.16	TCR-based static compensators	26
2.17	LC static VAR compensator	26
3.1	Prototypr of thyristor linked reactor	29
3.2	Switch structure	30
3.3	Experimental circuit	30
3.4	Measured voltage and current at terminal	30
3.5	Measured switch current	31
3.6	Measured switch voltage	31
3.7	Tap connection	33
3.8	TLR connection	33
3.9	Curves of V_{\max} and Z vs. case number for TLR connection (RL circuit, without mutual coupling)	37
3.10	Curves of V_{\max} and Z vs. case number for tap connection (RL circuit,	

	without mutual coupling)	37
3.11	Curves of V_{\max} and Z vs. case number for tap connection (RL circuit, with mutual coupling)	40
3.12	Curves of V_{\max} and Z vs. case number for TLR connection (RL circuit, with mutual coupling)	40
3.13	Single tuned shunt filter	41
3.14	Curves of V_{\max} and Z vs. case number for tap connection (RLC circuit, without mutual coupling)	44
3.15	Curves of V_{\max} and Z vs. case number for TLR connection (RLC circuit, without mutual coupling)	44
3.16	Curves of V_{\max} and Z vs. case number for tap connection (RLC circuit, with mutual coupling)	47
3.17	Curves of V_{\max} and Z vs. case number for TLR connection (RLC circuit, with mutual coupling)	47
3.18	Curves of V_{\max} and Z vs. case number for tap connection (RLC circuit, with harmonics and without mutual coupling)	50
3.19	Curves of V_{\max} and Z vs. case number for TLR connection (RLC circuit, with harmonics and without mutual coupling)	50
3.20	Curves of V_{\max} and Z vs. case number for tap connection (RLC circuit, with harmonics and mutual coupling)	51
3.21	Curves of V_{\max} and Z vs. case number for TLR connection (RLC circuit, with harmonics and mutual coupling)	51
3.22	Cost comparison	53
4.1	Experimental circuit	55
4.2	Circuit used in the analysis	59
4.3	Frequency domain equivalent circuit	59
4.4	Flow chart of the Matlab program	63
4.5	Switch transient at Angle=210°	64
4.6	Comparison of simulation and theoretical results of inductor bypassing	65
4.7	Measurement and simulation current waveforms of inductor bypassing	66

4.8	Definition of transient duration	67
4.9	Sensitivity study on switch timing for inductor bypassing	67
4.10	Curves of peak transient current and duration vs. switch angle	68
4.11	Curves of transient current and duration vs. R for inductor bypassing	69
4.12	Simulation of inductor bypassing transient for $R=0$	70
4.13	Curves of I_2 peak and transient duration vs. M for different L	71
4.14	Frequency domain equivalent circuit of inductor insertion	72
4.15	Inductor insertion transient current waveforms	75
4.16	Comparasion between simulation and theoretical results	75
4.17	Measurement and simulation current waveforms of inductor insertion	76
4.18	Sensitivity study on switch timing (inductor insertion)	77
4.19	Curves of I_2 peak and duration vs. switch angle (inductor insertion)	77
4.20	Curves of transient current and duration vs. R (inductor insertion)	79
4.21	Simulation of inductor insertion transient for $R=0$	80
4.22	Curves of I_2 peak and duration vs. M at different L (inductor insertion)	80
5.1	Frequency domain equivalent RLC circuit	83
5.2	Switch transient current of RLC circuit	87
5.3	Comparasion between simulation and theoretical result (inductor bypassing)	88
5.4	Measuring current waveforms for RLC switch transient	88
5.5	I_2 peak in p. u. vs. switch angle	89
5.6	Current waveforms when switch angle is 14°	90
5.7	Curve of I_2 peak in p. u. vs. R/X	91
5.8	The effect of L and M on transient peak current in RLC circuit	92
5.9	Transient current for inductor insertion	95
5.10	Comparison between analysis and simulation result of inductor insertion	95
5.11	Measurement and simulation current waveforms of inductor insertion	96
5.12	I_1 peak current in p. u. vs. switch angle	97
5.13	Curve of I_1 peak vs. R/X ratio	98
5.14	Peak current I_1 in per unit vs. M	99

5.15	Switch voltage waveforms for inductor bypassing	101
5.16	Curve of peak transient voltage v. s. switch angle (bypassing and $M/L=0.5$)	102
5.17	Curve of peak transient voltage v. s. switch angle (bypassing and $M/L=0.95$)	102
5.18	Switch voltage waveforms for inductor insertion	104
5.19	Curve of peak transient voltage v. s. switch angle (insertion)	105
5.20	Switch voltage waveforms for inductor insertion ($M/L=0.95$)	105
5.21	Duration cycles vs. percent of loss for a filter	108
6.1	Parameter comparison	114

List of Symbols

<i>TLR</i>	Abbreviation for thyristor linked reactor
<i>EMTP</i>	Electromagnetic Transient Program
<i>RMS</i>	Root mean square or effective value of voltage or current
<i>L</i>	Inductance
μ	Permeability of magnetic material
<i>N</i>	Number of turns of an inductor
<i>A</i>	Cross section area
ℓ	Length of inductor
λ	Flux linkage
<i>I</i>	Current
<i>B</i>	Flux density
<i>H</i>	Field intensity
<i>Z</i>	Complex impedance
<i>R</i>	Resistance
<i>C</i>	Capacitance
ω	Fundamental frequency in rad/sec
<i>THD</i>	Total harmonic distortion
X_C	Capacitive reactive reactance at the fundamental frequency
X_L	Inductive reactance at the fundamental frequency
X_{TC}	Total reactance
<i>Q</i>	Reactive power
<i>M</i>	Mutual coupling inductance
<i>h</i>	Harmonic order
V_P	Phase voltage
V_{LL}	Line to line voltage
K_h	Per unit harmonic current based on load current
ϕ	Phase angle
θ	Switch angle

t	Time
V_m	Peak magnitude of voltage
$I_L(0)$	Initial inductor current
$V_C(0)$	Initial capacitor voltage
$u(t)$	Voltage as a function of time
$V(s)$	Voltage as a function of complex frequency
p	Pole of a polynomial
V_C	Capacitor voltage as a function of complex frequency
f_N	Natural frequency
$p. u.$	Per unit

Chapter 1

Introduction

The quality of electric power has become an increasing concern for both utilities and end users in recent years due to the widespread proliferation of power electronic loads. This concern results in an area of study including methods and devices designed to maintain high quality power, as defined by achieving a near sinusoidal voltage waveform, at rated voltage magnitude and frequency for power systems. In this chapter, the concept of power quality is presented. The chapter ends with a statement of thesis objective and the outline of how the objective will be achieved.

1.0 Power Quality

Alternating current power systems are designed to operate at a sinusoidal voltage of a given frequency (typically 50 or 60Hz) and magnitude. However, due to the complex network between utilities and the end user, with the presence of a multitude of non-linear elements, the ideal case cannot be realized. Any significant deviation in the magnitude, frequency, or purity of waveform is a potential power quality problem. The ultimate measure of power quality is determined by the performance and productivity of end user equipment. Therefore, from the prospective of the customer, power quality (PQ) refers to the characteristics of the power supply required for the electrical equipment to operate correctly, and a power quality problem is defined as [1],

Any power problem manifested in voltage, current, or frequency deviations that result in failure or mis-operation of customer equipment.

Power quality problems can result from system transient or the presence of non-linear load components. Many different types and sources of power quality disturbances exist in power systems. They are usually classified according to the electrical characteristics of the voltage experienced by customers' equipment. The characteristics include waveforms, RMS¹ values and phase voltage balances. According to recent international efforts to standardize the definitions of power quality terms, the common power quality disturbances are classified as [1]:

- Transients: Transients are disturbances that last less than three cycles, and they have many possible origins, for example, capacitor switching, lightning strikes, etc. Transients can be further classified into two categories: impulsive and oscillatory. Impulsive transients are unidirectional in polarity and have sharp rise and fall edges. Oscillatory transients consist of a voltage or current whose instantaneous value changes polarity rapidly.
- Short duration voltage variations: Short duration voltage variations refer to voltage abnormality from 0.5 cycles to one minute, including sags, swells and interruptions. The causes of this kind of disturbances could be faults in the system, connection or disconnection of large loads.
- Long duration voltage variations: These are steady-state voltage abnormalities with duration of longer than one minute, including over-voltages, under voltages and sustained interruptions. In these types of voltage variations, the RMS voltage goes outside of the contract service voltage band. The causes could be poor system design and/or operation or excessive loads.
- Waveform distortions: This type of disturbance is characterized by steady state

¹ RMS stands for root-mean-square, which is effective value of voltage or current. The effective value of a

function i is defined as
$$I_{eff} = \sqrt{\frac{1}{T} \int_0^T i^2 dt} .$$

distortions of the 60Hz sinusoidal waveform. Examples of distortions are harmonics, voltage notching, DC offset and broadband noise. The causes could be non-linear loads such as power-electronic loads.

- **Voltage unbalance:** These are steady state disturbances with unbalance of the voltages among the three-phase power supplies. The causes could be unbalanced load or unbalanced system.
- **Voltage fluctuations:** Repetitive voltage sags and swells appear as voltage fluctuations. A typical spectral content of voltage fluctuation is less than 25Hz. Causes could be repeated motor starting, industry processes such as arc furnace, etc.
- **Power frequency variations:** This type of disturbance is defined as the deviation of the power system fundamental frequency from its specified nominal value. The typical duration of the frequency variation of interest is less than 10 seconds.

All these types of power quality disturbances are not necessarily new. They are drawing more and more attention in recent years due to many factors. First, end use equipment, such as microprocessor-based and power electronic devices, is more sensitive to power quality problems. Secondly, the growth of application of high-efficiency devices, such as adjustable-speed motor drives and shunt capacitors, increase the severity of waveform distortion. These devices inject significant amounts of distorted currents into power system, which not only disturb loads that are sensitive to waveform distortion, but also cause many undesirable effects on power system elements. Finally, more things are now interconnected in a network. Integrated processes mean that the failure of any component has many more important consequences.

Over the years, the increase in the general awareness on the subject, along with the increasing concerns over productivity and efficiency, have made the development and application of technologies for the analysis and mitigation of power quality disturbance a new area of power quality research [3]. Many techniques and applications such as

transient simulation programs and suppression methods have been developed and tested for power system networks. However, there is still a need for improvement to meet the industry.

1.1 Harmonic Distortion

Harmonics started to become a significant factor in the design of power systems with the invention of silicon controlled rectifier (SCR) in 1957; then, there was a gradual move towards the application of solid state devices. This has continued to increase to the present day and is expected to continue to increase in future decades. It is worth noting that industry standards did not start to reflect the consideration of harmonics until the last 10 to 20 years [3].

Harmonics are a mathematical model used to analyze distorted current or voltage waveforms appearing on an electrical system [4]. Technically, harmonics are sinusoidal voltages or currents having frequencies that are integer multiples of the frequency at which the supply system is designed to operate (which is termed the fundamental frequency, usually 50 or 60Hz.). Typical harmonics for a 60Hz system are the 3rd (180Hz), the 5th (300Hz), the 7th (420Hz) and the 11th (660Hz). Since harmonic distortion is in steady state, the distorted waveforms can be expressed in the form of a Fourier series. Each Fourier component is called a harmonic.

Harmonic distortion is caused by nonlinear devices in the power system. A nonlinear device is one in which the current is not proportional to the applied voltage [1]. The main harmonic source is electronic power converter, including ac/dc motor drives, electronic power supplies, battery chargers, electronic ballasts and many other rectifier/inverter applications. Another major harmonic source is arcing devices, including arc furnaces, arc welders, and discharge-type lighting. Saturable devices, such as transformers and other electromagnetic devices with steel cores, are also big harmonic contributors.

Many power system problems arise due to harmonic distortion. The problems can be categorized as follows [1]:

- **Over-heating of transformer.** Transformers are designed to deliver the required power to the connected loads with minimum losses at fundamental frequency. The additional harmonic losses require the equipment to be de-rated, so that the total losses are within the specified equipment ratings.
- **Malfunction of power electronic based devices.** These devices usually rely on various characteristics of the ac supply voltage to determine proper firing angles. Therefore, any distortion may cause a functional failure.
- **Capacitor bank failure.** A major concern arising from the use of capacitors in a power system is the possibility of system resonance. This effect imposes voltages and currents that are considerably higher than what would be the case without resonance. These high currents and voltages shorten the life of or even destroy the capacitor bank.
- **Communication interference.** Noise originating from the harmonic currents and voltages in power systems can be coupled into wire communication circuits through magnetic and electrostatic fields.
- **Errors on metering.** Metering and instrumentation are affected by harmonic currents, particularly if resonant conditions occur, which cause high harmonic voltage on the circuits. Induction disk devices, such as watt-hour, normally see only fundamental current, but phase unbalance, caused by harmonic distortion, can cause error in the operation of these devices.

1.2 Harmonic Mitigation

Much effort has been made to study the origins, propagation and mitigation of harmonics within power systems, which leads to the methods that eliminate or reduce the harmonics to an acceptable level. At present there are two general methods for reducing and eliminating harmonics in power systems. One is to reduce the harmonic currents produced by the load. The other is to install harmonic filters near the current injection source. A review of present day literature and industrial practice highlights several methods.

1.2.1 Harmonic Cancellation Schemes

Utilities have little control over the type of loads connected to their systems. It is possible, however, for a utility to arrange connection schemes that can reduce the net harmonic current injection from the load into the system. An effective method is the transformer-based harmonic cancellation scheme. In this method, the transformer Y and Δ connections are employed to reduce harmonics in three-phase systems [5]. The effectiveness of the transformer cancellation schemes is dependent on the operating characteristics of the loads. If the harmonic currents produced by the loads are relatively constant and consistent over time, the scheme can be quite effective.

1.2.2 Passive Filters

There are two types of passive harmonic filters: shunt and series filters [1]. A shunt filter is employed to shunt the harmonic off the line. It is the most commonly used filter in the industry because of its economical structure and benefits, such as power factor correction [12]. Depending on the frequency response characteristics, there are different types of shunt filters. Some examples are the single-tuned filter, the 2nd order filter and the high pass filter.

The series filter has the capability of blocking harmonic currents. It is a parallel-tuned circuit that offers high impedance to the harmonic current. It is not widely used because it is difficult to insulate, and load voltage is very often distorted. One common application is in the neutral of a grounded capacitor where it blocks the flow of zero sequence harmonics while retaining a good ground at the fundamental frequency.

The passive filter has the disadvantage of potential adverse interactions with the power system [1]. It creates a sharp parallel resonance point at a frequency below the filter-tuned frequency. This could result in a worse situation than without a filter if the changes of filter parameters shift the parallel resonance into a harmonic frequency.

1.2.3 Active Filter

Active filters are relatively new types of devices for eliminating harmonics. The basic idea is to replace the portion of the sine wave that is missing in the current in a nonlinear load. It is implemented by monitoring the line voltage and/or current and injecting harmonic current into the system at an appropriate instant to restore the voltage and/or current, so that the current, seen by the system, is much more sinusoidal [11].

Active filters have distinct advantages over passive filters. They do not resonate with the system; they can provide elimination to more than one harmonics at a time and suppress other power quality problems such as voltage flicker. However, they are much more expensive than passive filter due to their complexity, which greatly limits its application in industry.

1.3 Objective and Scope

Harmonic filtering is most commonly conducted by a passive filter. In spite of its advantages, the active filter is not very attractive to the industry because of its high cost

and complexity of design. In view of the increasing of harmonic injection, a more flexible filter is in high demand. In response to this demand, a novel tunable filter is proposed at University of Alberta [2].

A tunable filter is a filter that can be tuned automatically to different harmonics in response to different system conditions. The core component of this filter is a variable reactor. The proposed filter employs a new variable reactor named thyristor linked reactor, which uses thyristors to bypass or insert inductor coils, thereby achieving variable inductance. The objective of this research is to investigate the performance characteristics of the variable inductor. The work will be focused on the analysis of the steady state and transient performance of the variable reactor in different applications. The scope of this thesis is summarized as follows:

- Introduce the schematic of the thyristor linked reactor. Compared with existing types of variable reactors, the advantages of the proposed device are addressed. Also, the potential areas of application are investigated.
- Investigate the steady-state performance of the device. The voltage stress on the device and its components are examined in both first order and second order circuits. Voltage stress is actually a cost related-issue. Based on stress study, economical feasibility are conducted.
- Investigate the electromagnetic transients associated with the device. Since the variable reactor has switching elements, the switch transient is of great concern. Therefore, the transient response of the device in RL and RLC circuits is analyzed theoretically and experimentally.
- A set of criteria is developed to select components of the variable inductor. The switches should have a certain level of voltage and current tolerance, and the inductor segments should meet the parameter requirement for the designed application.

1.4 Outline of the Thesis

This thesis investigates the steady state and transient characteristics of a novel variable reactor. To implement this work the following methodologies are adopted: (1) Experiments--A prototype variable reactor is constructed and tested. A data acquisition system Nicolet is used to attain experimental voltage and current waveforms. The measurement results are used to verify the feasibility of the new inductor and also facilitate theoretical analysis. (2) Simulation-- The EMTP² program is used to conduct transient analysis in time domain. The results of the simulation are taken as a reference. (3) Analytical study--Laplace transform is employed to perform theoretical analysis in frequency domain, and the time domain response is obtained by partial fraction expansions. The chapters of the thesis are organized as follows:

Chapter 2 gives the general principle of the variable inductor. The existing types of variable inductors are reviewed and classified, showing their advantages and disadvantages. The topology and structure of the thyristor linked reactor are given and its potential applications are also explored.

Chapter 3 deals with the steady-state performance of the thyristor linked reactor. The experimental setup is introduced and the experimental results are demonstrated graphically. As a cost associated issue, voltage stress is a major concern to industry applications and it is studied in first order and second order circuit. Comparison is made with a tapped inductor. Economical feasibility study is also presented.

Chapter 4 presents the transient performance of the proposed inductor in RL circuit. Theoretical analysis is conducted on inductor bypassing and insertion transient,

² EMTP - Electromagnetic Transient Program. First developed by H. W. Dommel at the Bonneville Power Administration, Portland, U.S. A.

Chapter 1: Introduction

using Laplace transform. The prototype parameters are used in the analysis so that comparison with test results is made possible. Aided by a Matlab program, the analytical results are demonstrated in waveforms. The switch point with minimum transient is found by switch sensitivity study. The duration and the severity of the transient are discussed. The EMTP simulation is also conducted to confirm the analytical results and further illustrate the performance of the inductor.

Chapter 5 performs transient study of the thyristor linked reactor in the RLC circuit. Following the same procedures as chapter 4, but at a more complicated level, the theoretical analysis is conducted. Simulation and tests are also performed. Different from chapter 4 due to the nature of the circuit, the duration of the transient is discussed separately.

Chapter 6 develops a set of criteria for the selection of components and their evaluation. The necessary voltage and current tolerance of the components is discussed. The selection of inductor segment parameters is also dealt with in this section.

Chapter 7 shows the conclusions derived from this thesis, and suggestions for future research are given.

Chapter 2

Thyristor Linked Reactor

In this chapter, the basic principles of variable reactors are presented. The existing types of variable reactors are reviewed and the performance of them is analyzed. It is concluded that each of them suffers from certain drawbacks and that their applications are limited. The thyristor linked reactor is introduced. It is simple in structure and easy to implement. Its topology is given, and its potential applications are discussed.

2.0 Introduction

Variable reactors can be found in many industrial applications. The main applications are power quality and efficiency improvement, for instance, voltage regulation, power factor correction in long transmission lines and shunt reactor control of reactive KVA of a static capacitor bank. Another potential application of a variable reactor is a tunable harmonic filter. With more harmonic current injected into the power system, an effective and economical measure of mitigating harmonics is in high demand.

Great efforts have been made in constructing a variable reactor branch, which lead to several types of devices. These devices are playing important roles in many industrial applications. Some variable reactors, such as the variable air-gap type inductor, tap-changing inductor and dc premagnetized type inductor, can be smoothly varied. However, these devices suffer from certain drawbacks such as the necessity of mechanical operation and slow time response. This has led to the development of static arrangements using thyristor switches. Thyristor-controlled variable reactors which are free from the drawbacks mentioned above have been developed; however, their main

disadvantage is the harmonic distortion of the input current, particularly at delayed firing angles.

In this chapter, the existing types of variable reactors are reviewed, and their performance briefly analyzed. It will be seen that the drawbacks or disadvantages of the existing variable reactors either limit the application of the device or cause power quality problems. A new device proposed at the University of Alberta is then discussed along with its potential applications.

2.1 The Principle of Variable Reactors

A reactor is usually composed of a coil and a core. Considering a solenoid core, the inductance can be represented as:

$$L = \frac{\mu N^2 A}{\ell} \quad (2.1)$$

where μ is the permeability of the material of the core.

N is the number of turns carrying current around the coil.

A is the cross sectional area of the coil.

ℓ is the length of the coil.

Two methods can be derived from Equation 2.1 to realize a variable reactor. One is through the change of μ , which results in a flux controllable inductor; the other is varying the number of turns.

The inductance can also be expressed by flux as the following equation:

$$\lambda = LI \quad (2.2)$$

where λ is the flux linkage of the coil, and I is the current flowing through the coil. From this equation another method of varying L is introduced, which is changing the flux linkage of the coil externally. In this way, I stays the same but λ is changed. Therefore, the inductance is changed equivalently.

The material of the core also plays an important role in inductance. The core is usually made of ferromagnetic material, such as iron, which shows the effect of saturation. Therefore, when the inductor is working in the saturated region, the relationship between the flux density B and field intensity H is non-linear, referred to in equations as:

$$H = KI \quad (2.3)$$

$$\lambda = NBA \quad (2.4)$$

where K is a constant related to the structure of the coil and the material of the core, N is the number of turns of the coil.

Then, to this end, the relationship between λ and I is non-linear. Consequently, the inductance is inherently changeable. This kind of variable inductor is known as a saturable inductor. Another way to achieve a variable reactor is to use an electronic component to control the current applied to the inductor; the most widely used one is the thyristor-controlled reactor (TCR).

2.2 Review of Existing Types of Variable Reactors

An extensive survey on variable inductors shows that the existing devices fall into four basic categories: saturable or flux controllable reactor, electronic switch controlled reactor, winding turns changeable reactor and tapped reactor.

2.2.1 Saturable or Flux Controllable Reactor

A saturable reactor exploits the effect of saturation of ferromagnetic material. Fig. 2.1 depicts the simplest way to implement a saturable reactor. There are basically two coils mounted on the same core; one is the main coil and the other is a control coil. An additional variable DC source is necessary to supply the control coil. With the change of the DC current, the flux in the core is also changed, so the saturation degree of the core can be controlled by the control coil. The inductance of the main coil will change accordingly [6, 7] .

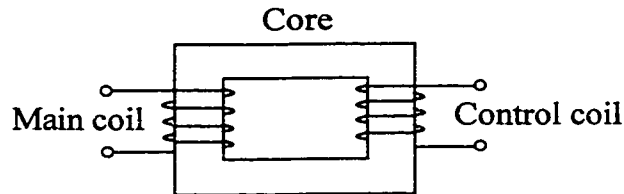


Fig. 2.1: Principle of saturable reactor.

It is obvious that this inductor has a non-linear response since it works in the saturated region. In turn, it will generate harmonics that is not favorable to the system. The core losses are high due to the amount of stored energy, and the variation range is low because of its working region.

A flux changeable inductor uses mechanical devices to control either the number of flux linkages of the inductor or the reluctance of the magnetic circuit passing through the coils. The number of flux linkages is altered mechanically by using a tapped inductor coil and a tap-changing mechanism, which is a relay-controlled motor. Altering, again mechanically, the reluctance of the coil is achieved by controlling the movement of a low reluctance material within the inductor. A typical example is shown in Fig. 2.2. It is the

device under Patent 4347489 [8], which uses a hand crank to move an iron core into a current carrying coil.

An electrical way to change the permeability of the core and, hence, to change flux linkage is realized by two orthogonally placed cores. Fig. 2.3 shows the device under Patent 4393157 [6]. The two cores intersect in two areas. One core carries an alternative magnetic field, and the other circulates an adjustable direct current magnetic field. The change of direct current alters the permeability of the intersecting regions, and in this way the overall permeability of the core and therefore the inductance of the alternating current coil. This type of device has the following disadvantages:

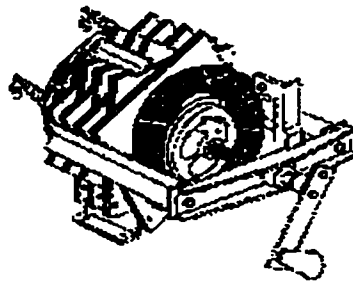


Fig. 2.2: Variable Reactor under Patent 4347489.

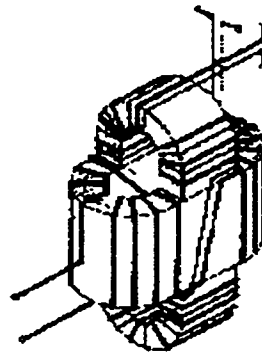


Fig. 2.3: Variable inductor under Patent 4393157.

- Requirement for extra equipment in the form of motors or relays or additional DC source.
- Slow response time.

2.2.4 Electronic Switch Controlled Reactor

The most widespread electronic switch controlled reactor is the thyristor-controlled reactor (TCR). It is mainly employed in shunt static VAR compensators [13~18]. Fig. 2.4 shows a typical single-phase schematic diagram for a thyristor-controlled reactor.

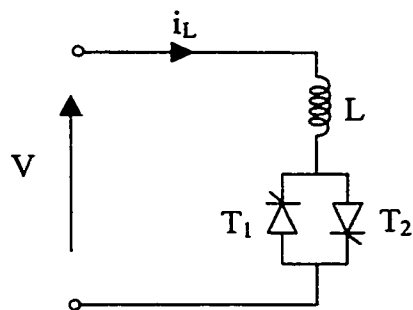


Fig. 2.4: Thyristor-controlled reactor.

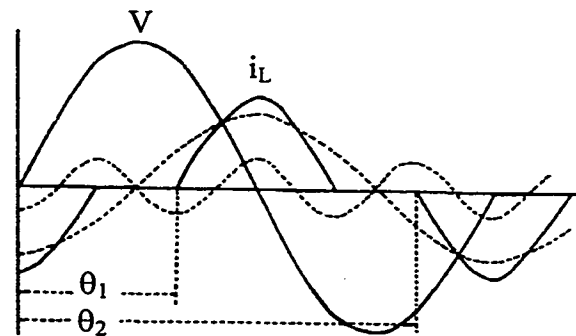


Fig. 2.5: TCR inductor current.

When thyristor T_1 is fired at θ_1 and thyristor T_2 is fired at $\theta_2 (=180+\theta_1)$, the resulting input current i_L is shown in Fig. 2.5. The current contains all odd harmonics among which the third harmonic is predominant. As θ_1 is varied, the fundamental component of input current varies in magnitude, so the impedance of the inductor at fundamental frequency is equivalently changed.

The main disadvantage of TCR is harmonic generation. It is designed only for fundamental frequency applications, i.e., it is a variable reactor only at fundamental frequency. At harmonic frequencies, it behaves as harmonic sources do.

Another device worth mentioning is a switched-reactor [9], which tries to solve the harmonic problem of TCR. Its operating principle is illustrated in Fig. 2.6. In Fig. 2.6, S_1 and S_2 represent two self-commutated bi-directional switches with complementary gatings. Through high-frequency switching, the fundamental component of the inductor current i_L can be controlled by changing the duty cycle of the switch. Fig. 2.7 shows the voltage and input current waveforms of this circuit.

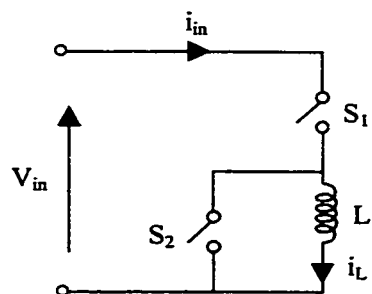


Fig. 2.6: Switched reactor.

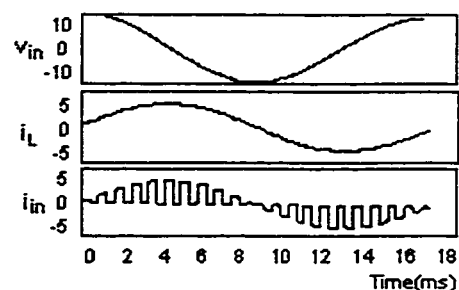


Fig. 2.7: Voltage and current waveforms.

From Fig. 2.7, it can be seen that the currents are fairly smooth, which means the low order harmonics are effectively eliminated. The drawbacks of this structure are

- Requirement for high frequency switches, which results in high switch losses.
- Complex control strategy.
- Use limited to being a variable reactor at fundamental frequency.

2.2.3 Coil Turns Changeable Reactor

The idea of this reactor is very simple: change the inductance by changing the number of turns of the coil. An example of this type of inductor is shown in Fig. 2.8 [10].

$S_1 \sim S_5$ are triac switches. Triac is a bidirectional triode thyristor, which can conduct both directions of current flow in response to a positive or negative gate signal

[21]. By operation of the switches, the effective number of turns of secondary winding is changed. Therefore the inductance seen from V_s is changed accordingly. In this case, the inductance is linearly varied causing no distortion to the supply current. This makes it superior to other existing devices.

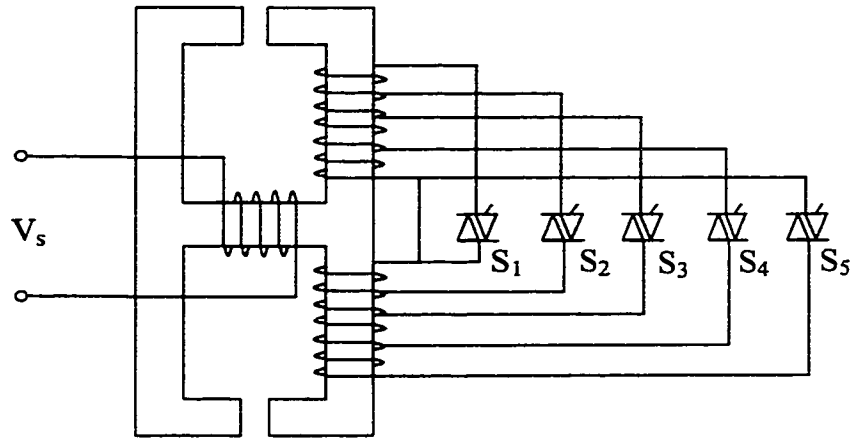


Fig. 2.8: Coil turns changeable.

Its disadvantage lies in the operation of its secondary winding. When one of the switches is forward biased, part of the coil is short-circuited. The switch conducts the short circuit current. When the switch is reverse-biased, it has to block the induced voltage across the winding. The drawbacks of this device are

- High switch current stress.
- Switch voltage stress.

2.2.4 Tapped Reactor

This kind of variable reactor is sometimes termed as a tap-changing reactor. As the name indicated, the inductance is varied by the changing of the tap connection. It is seen in the application of the furnace power supply [19] and it is also used as a voltage regulator [1]. Fig. 2.9 shows the principle of the tapped inductor.

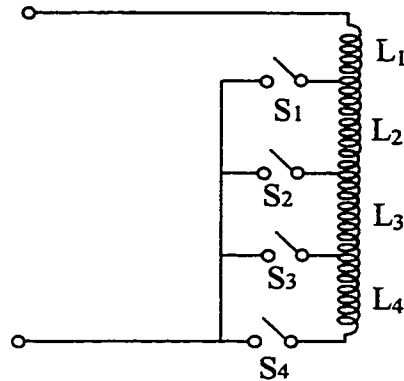


Fig. 2.9: Tapped reactor.

$S_1 \sim S_4$ are switches, which are triacs or back to back thyristors. When different switch is closed, the total inductance seen from the terminal is different. In this case, only one switch can be closed at one time. The inductance of this kind of variable inductor can be changed linearly. The disadvantages of this device are high voltage stress on switches and larger step of variation, which are further demonstrated in chapter 3.

With more and more load equipment sensitive to power quality variation installed in the power system, the drawbacks of the existing variable inductors are more manifested and their further application is limited. Hence, a better performing variable inductor is in high demand.

2.3 Variable Reactor to Be Investigated

The variable reactor to be investigated is called thyristor linked reactor. It is implemented by changing the number of the connected inductor segments. The inductor segments are mounted on the same core; the arrangement is shown in Fig. 2.10 (with 4 segments). The topology of the device is given in Fig. 2.11. Each inductor segment is connected with two pairs of thyristors, one is in parallel, and the other is in series with the

segment, i.e. the segments are linked by thyristors; that is where the name thyristor linked reactor (TLR) comes from.

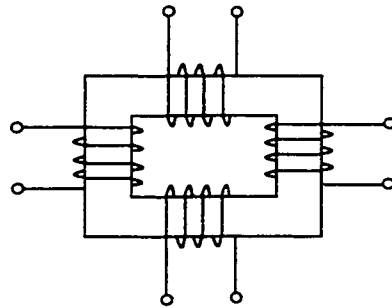


Fig. 2.10: Inductor segment arrangement.

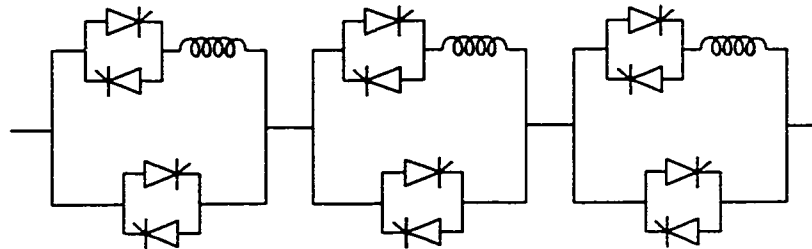


Fig. 2.11: Topology of variable reactor.

The thyristor pair is connected in anti-parallel. Therefore, triggering the thyristor gates simultaneously will allow current to flow in either direction. After the triggering signal is removed, the thyristor keeps conducting until the current becomes zero. The thyristors act as switches. By controlling the operation of the thyristors, the individual inductor segment can be either included or bypassed. Fig. 2.12 shows the operating state of the inductor segment. Several segments connected in series form a discretely variable reactor.

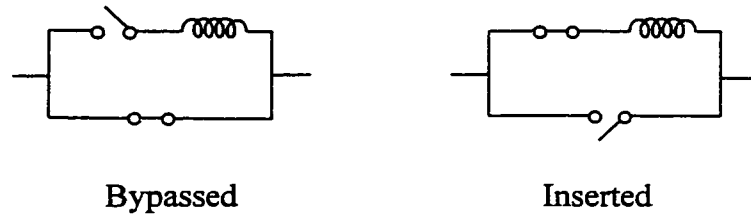


Fig. 2.12: Operating state of inductor segment.

This arrangement will result in a linearly variable reactor at all frequency ranges. It has the following advantages over other types:

- The structure is simple, no auxiliary dc source is needed.
- The inductor does not generate harmonics, so no additional filters are needed.
- It has smooth transient performance; detailed analysis will be presented in chapters 4 and 5.

2.4 Potential Applications

The advantages of the proposed device make it very promising in industry applications. As mentioned before, the ultimate motivation of developing this variable reactor is to implement a tunable filter. Some other applications are static VAR compensation and preinsertion reactor.

2.4.1 Tunable Filter

Passive filter has remained the most favored method for harmonic current confinement. A passive filter is composed of capacitor, reactor and resistor. The parameters of these components are chosen and connected so that the filter branch presents either a high impedance to the concerned frequencies (passive series filter) or a

low shunt impedance to the concerned frequencies (passive shunt filter). Shunt filter is the most utilized method of harmonic mitigation [1].

Three common types of shunt filters are depicted in Fig. 2.13. The first order and second order filters are high pass filters, which are used to significantly attenuate all non-fundamental frequency currents. The single-tuned filter provides a low impedance path to the current of a concerned harmonic frequency. The single-tuned filter is taken as an example to demonstrate the principle of shunt filters.

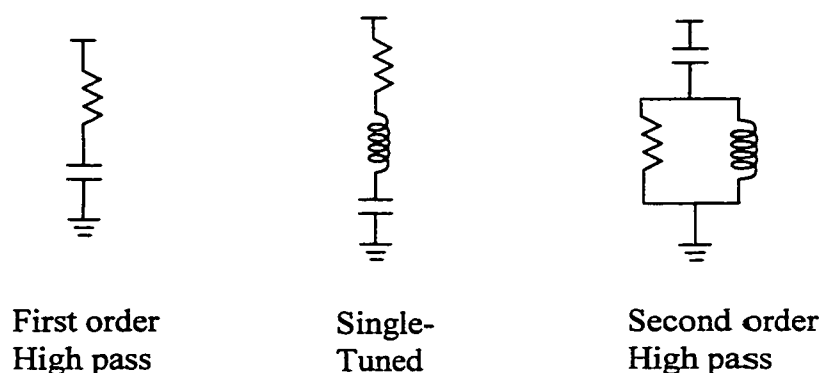


Fig. 2.13: Passive shunt filters.

A single-tuned filter is also termed as a *notch filter* because of its frequency response curve. The frequency response is expressed as

$$|Z| = \left| R + j(2\pi fL - \frac{1}{2\pi fC}) \right| \quad (2.5)$$

Fig. 2.14 shows the frequency response of a notch filter tuned to the 5th harmonic (300Hz). From the frequency response, it can be seen that the impedance of the filter is minimum at $f=300\text{Hz}$, ωL and $1/\omega C$ cancel out at this point. In practice, filters are commonly tuned slightly lower than the harmonic to be filtered in order to provide a margin of safety.

The prime disadvantage of passive filters stems from their static frequency response. If the source system impedance changes, harmonic content will vary, possibly rendering the filter ineffective. Furthermore, the installation of a passive filter has an adverse side effect in that it creates a sharp parallel resonance point at a frequency below the tuned frequency. The drift of filter element parameters due to temperature or damage may create a situation worse than without a filter. Detailed case studies can be found in [2], which demonstrates that the fluctuation of the filter capacitor causes high total harmonic distortion (THD) level.

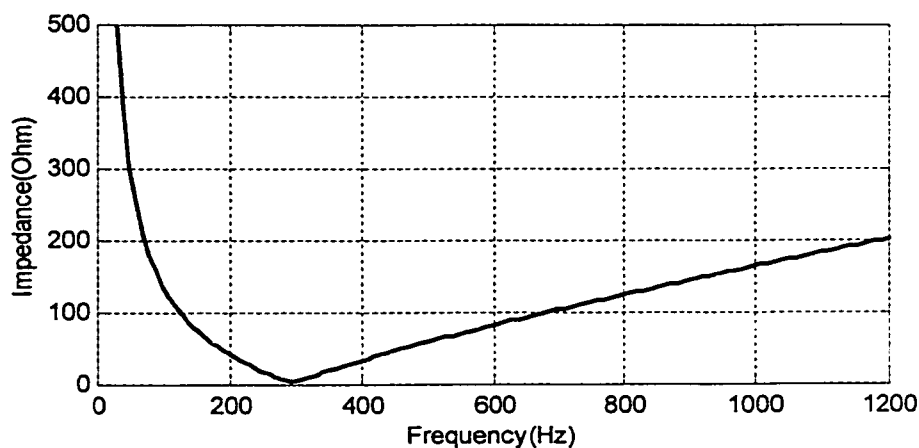


Fig. 2.14: Notch filter frequency response.

To solve this problem, an active filter is the most suitable alternative, but the high cost and complexity of design keep it far from being an industrial application. A flexible solution to the problem is a tunable filter, which is based on a passive filter. A variable capacitor or inductor is introduced into the filter to compensate for any fluctuations that occur in the filter. In this way, if the filter becomes de-tuned, the reactive impedance of the variable device can be changed to re-tune the filter. A conceptual tunable filter is shown in Fig. 2.15.



Fig. 2.15: Concept of tunable filter.

The variable component could be a capacitor or an inductor. Presently the most commonly used variable capacitor in power system is a set of parallel switch-able capacitors. The capacitance value of the variable device is equal to the sum of each capacitor with a closed switch. It is applied mainly for power factor correction and voltage support [24, 25]. The primary drawback of using a variable capacitor for a tunable filter is the financial cost due to the fact that multiple capacitors each with full voltage rating are required. A variable reactor is more suitable in this situation.

For tunable filter application, a variable reactor should meet the following requirements:

- Easy and economical in implementation.
- Non-harmonic generating.
- Self-reliant, which means that no continual maintenance is required.

There are tunable harmonic filters designed and implemented using variable reactors [26, 27]. In [26] the variable reactor is a tapped inductor controlled by a tap changing mechanism. The system is designed to compensate for capacitance changes due to ambient temperature variation and temperature variation due to self-heating. It is slow in response due to its changing mechanism. In [27], ABB implements a variable inductor using a DC current to alter the permeability of the inductor core. The system is designed

to optimize filter performance by maintaining specified filter tuning. The drawback of it is the requirement for additional DC source.

The proposed variable reactor will meet the three requirements mentioned above. Its performance will be discussed in length in chapters 3, 4 and 5.

2.4.2 Static VAR Compensation

Static VAR compensators (SVC) have been used in electric power systems for a number of application purposes [16]. The main purpose is to support the voltage of transmission lines during disturbances of both loads and generation. This voltage support is achieved by the rapid control of the SVC reactance and, thus, its reactive power (VAR) output. Thereby, the reactive current flow is controlled in the transmission lines. The primary objectives of dynamic VAR compensation are to increase the transient stability limit of the ac power system, to decrease terminal voltage fluctuation during load variations and, at times, to limit overvoltages following large disturbances.

The static VAR compensators currently used in utilities are mainly thyristor-controlled reactor (TCR) based. To achieve both leading and lagging reactive power regulation, fixed capacitors (FC) or thyristor-switched capacitors (TSC) are used together with the reactors [16, 17]. TCR-based compensators have simple power structures and control schemes. The circuit of a typical TCR-based compensator and a compensator of TCR-TSC structure are depicted in Fig. 2.16.

TCR-based static compensators achieve reactive power variation by controlling the firing angle of the thyristors, which results in non-sinusoidal current. Referring to Fig. 2.5, the inductor current is discontinuous and, hence, harmonics are generated. The harmonics are mainly in low-order, so harmonic filters are needed to keep the system in a low harmonic level.

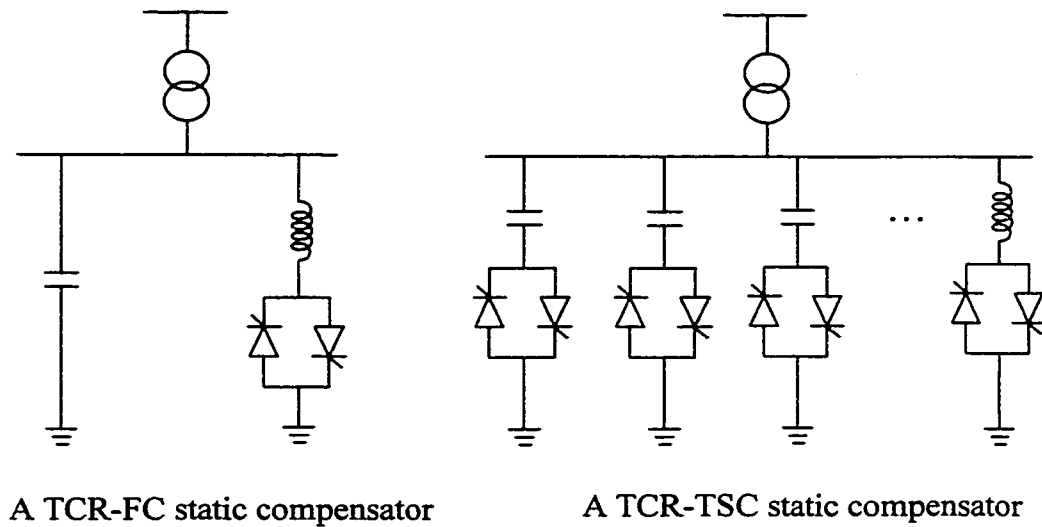


Fig. 2.16 TCR-based static compensators.

The proposed variable reactor can be used to make a new type of static VAR compensation called a LC static VAR compensator. Different from conventional static compensator, the variable reactor is in series with the capacitor. This idea is illustrated in Fig. 2.17.

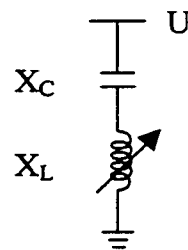


Fig. 2.17: LC static VAR compensator.

Here X_C , and X_L are impedances of the capacitor and variable reactor, respectively. X_L is a certain percentage of X_C , for example 20%. The total impedance of the compensator and the reactive power provided by the compensator are

$$X_{TC} = |X_C - X_L| \quad (2.6)$$

$$Q = \frac{U^2}{X_{TC}} \quad (2.7)$$

By varying the value of X_L , a variable VAR output can be achieved. The device does not generate harmonics. This arrangement can be utilized in power distribution system for reactive power compensation.

Chapter 3

Steady-State Performance of the Thyristor Linked Reactor

In this chapter, the behavior of the thyristor linked reactor at steady state is investigated. Its performance is observed experimentally, and the voltage stresses on TLR switches at different conditions are analyzed in detail. A brief economical feasibility study is performed. The results are compared with a tapped variable inductor.

3.0 Introduction

Variable reactors are used in many industrial applications. They are mainly used for power quality and efficiency improvement. Besides performing their intended functions, some reactors have some undesirable impacts on the systems. For example, the saturable reactor and thyristor-controlled reactor inject harmonic current to the system. It is important to investigate the performance of a newly designed device prior to its application. There are basically two areas to be studied: (1) steady-state performance. (2) transient performance. The transient performance of the TLR is presented in chapters 4 and 5.

The steady-state performance of the device is assessed in this chapter, which includes the characteristics of inductor variation, voltage stress on the thyristors, and impact of harmonics on voltage stress. The following works are conducted in this chapter:

- Experimental assessment of the device characteristics.

- Voltage stress analysis of the device, which is conducted by case studies of practical applications.
- The assessment of the impact of harmonics on the voltage stress.
- Brief study of economical feasibility based on the analyzed voltage stress.

3.1 Experimental Setup and Results

To conduct steady state performance study experimentally, a prototype has been designed and constructed. It is composed of a control box and several inductor segments. The control box consists of six pairs of thyristors connected in anti-parallel with triggering circuit, functioning as switches. The box provides internal and external triggering signal, which makes the switch timing possible. Several air core inductors are chosen as the inductor segments. The inductance of each of them is around $45mH$. They are piled together to get mutual coupling inductance. The prototype is shown in Fig. 3.1.

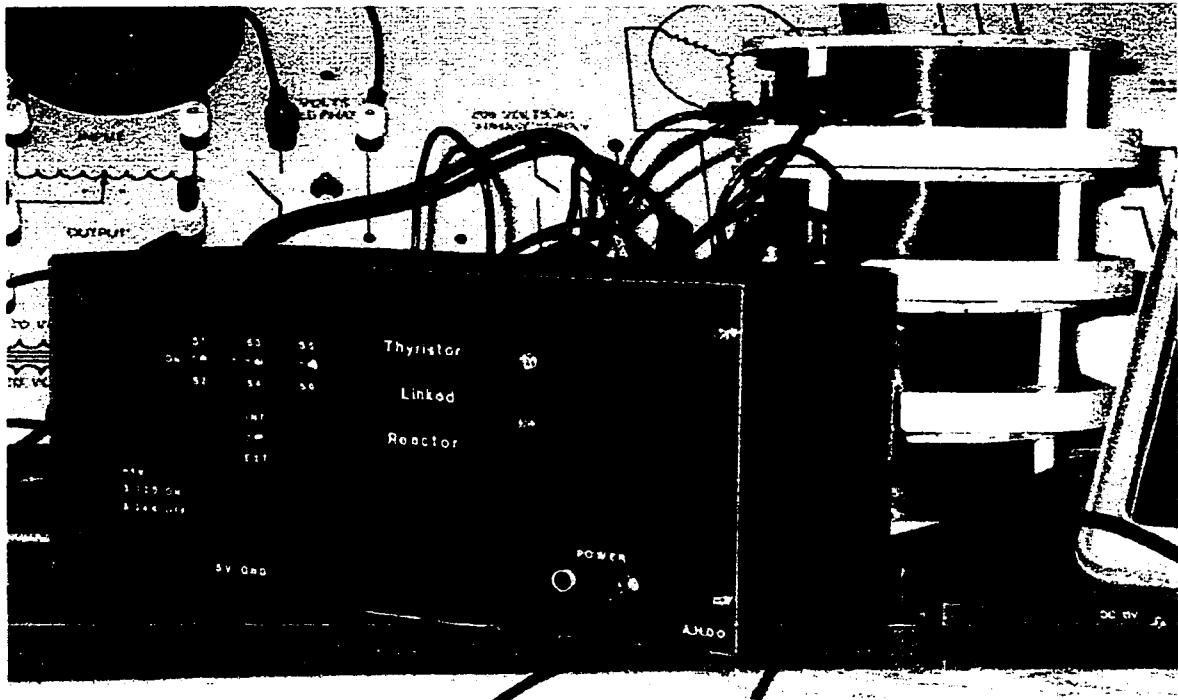


Fig. 3.1: Prototype of the thyristor linked reactor.

Fig. 3.2 shows the anti-parallel connected thyristors. An experimental circuit as in Fig. 3.3 is set up and a data acquisition system, Nicolet system, is employed to record voltage and current waveforms. The operation of switches has complementary logic, i.e., when S_1 is on, S_2 is off, and vice versa.

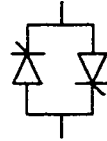


Fig. 3.2: Switch structure.

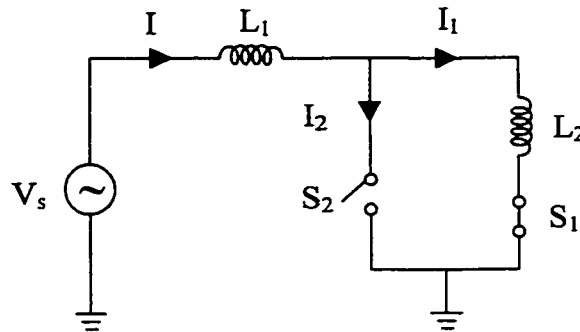


Fig. 3.3: Experimental circuit.

Fig. 3.4 shows the measured terminal voltage and current during switch operation. In this case, initially S_1 is closed and S_2 is open. At $t = 30ms$, L_2 is bypassed by opening S_1 and closing S_2 . The results show that the total current is increased after the switching; therefore, the total inductance is reduced accordingly.

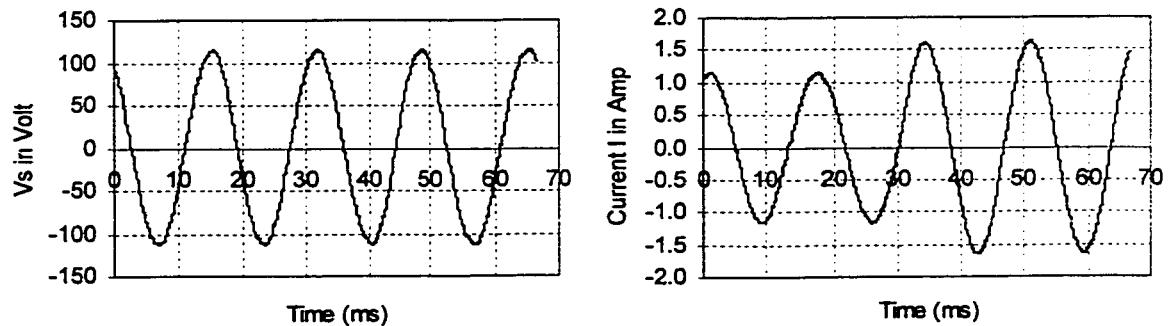


Fig. 3.4: Measured voltage and current at terminal.

It is observed that the currents before and after switching are almost pure sinusoidal. The currents transfer from one state to another smoothly. The measured currents for both switches are shown in Fig. 3.5. It can be seen that the current commutates from S_1 to S_2 instantly, almost without transient. Although this is not always the case, it indicates that non-transient switching is possible. Switch sensitivity studies are presented in chapters 4 and 5.

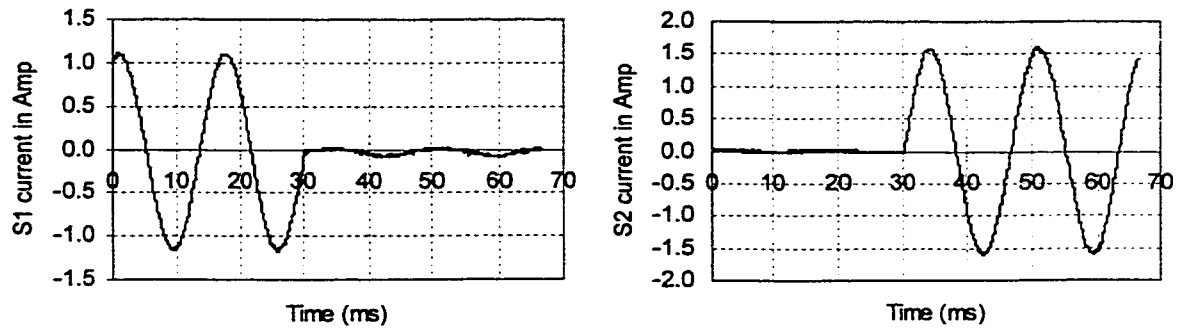


Fig. 3.5: Measured switch current.

The measured voltages for both switches are shown in Fig. 3.6. It can be seen that there is no noticeable voltage stresses. The voltage sparks are due to the thyristor commutation.

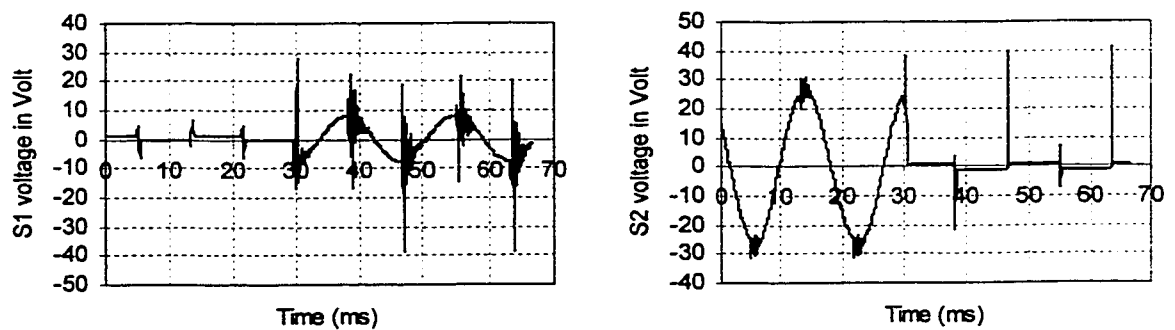


Fig. 3.6: Measured switch voltage.

Similarly, for inductor insertion, the current decreases after switch operation due to the increase of impedance. It is observed that there is no harmonic distortion in total current before and after switch operation and that the current increases or decreases with the bypassing or insertion of inductor segment. It can be concluded that the novel device is a linearly variable reactor. Therefore, the variable inductor is a linear inductor seen from the system, and the impact of it on the system is the same as that of a common inductor.

3.2 Voltage Stress Analysis of Variable inductor

Voltage stress on inductor and switches is an important factor to consider when applying the device. Since excessive high voltage may destroy the insulation between the reactor winding turns, and thyristors have a breakdown voltage at which the elements will begin to conduct even if there is no gate signal present, to maintain normal operation, the voltage across the thyristors must not exceed the breakdown voltage. The voltage stress analysis is conducted in comparison with a tapped inductor.

As introduced in chapter 2, the tapped inductor is a well-recognized device. Now, the topology of the inductor is redrawn in Fig. 3.7. When a different tap is connected, the inductance included in the circuit is different. The steady-state performance of the tapped inductor is analyzed only for the purpose of comparison with the proposed inductor.

The topology of the thyristor linked reactor is shown in Fig. 3.8. In both tapped inductor and thyristor linked reactor (TLR), the switches consist of two thyristors connected in anti-parallel, which are treated as ideal switches in this chapter. The variable reactor consists of four inductor segments. One fixed segment is always connected in the circuit. The other segments can be switched in or out of the circuit.

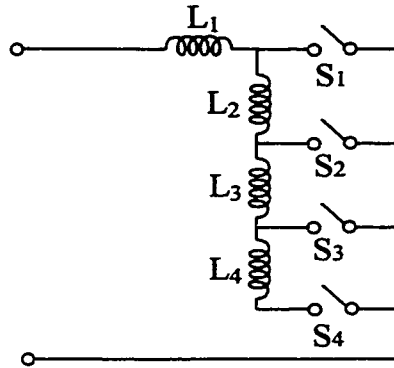


Fig. 3.7: Tap connection.

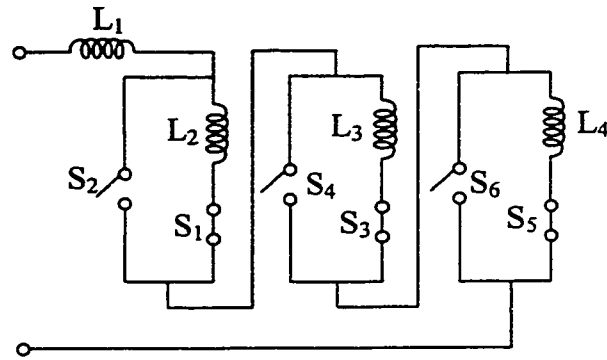


Fig. 3.8: TLR connection.

At steady-state, the sinusoidal current and voltage can be represented by phasors and the impedance can be expressed by complex. By solving simple phasor equations, the desired current and voltage can be obtained. Suppose the inductor is in a branch, given the voltage level of the branch to be connected and the branch component parameters, the following procedures should be taken to perform voltage stress analysis:

- According to the switch states, calculate the total branch impedances and then the branch currents.
- Calculate the voltage drop on each branch component by multiplying the current with the impedance of the component.
- Compute the voltage stress on switches based on the component voltage drop, according to the connection.

Besides the voltage stress, some other aspects will also be compared between the tapped inductor and the thyristor linked reactor. The aspects to be compared are

- Number of segment combinations (i.e., the number of possible inductance variations)
- Number of switches needed for each variation step.
- Maximum current and voltage stress on switches.

3.3 Case Studies of the Practical Applications

We will analyze the voltage stress through case studies of several practical applications. One is the application of the TLR in a pure inductor branch. Although this is not the intended application of the TLR, it is used to highlight the nature of switch voltage stresses. The other is the application in a tunable filter.

3.3.1 Pure Inductor Branch

For TLR connection, two switches are connected with each switch-able segment; one is in series with the segment and the other is in parallel. These two switches are operated in complementary logic; i. e., when one switch is on, the other one is off. Therefore, when the series switch is on, the segment is switched in; otherwise it is off. For tap connection, there is one switch for each switch-able segment.

Assume that the fixed inductor is 800KVA with 480V voltage rating, the parameters are

$$X_{L1} = \frac{480^2}{800 \times 1000} = 0.288\Omega \quad (3.1)$$

$$L_1 = \frac{X_{L1}}{\omega} = \frac{0.288}{2 \times 60\pi} = 0.764mH \quad (3.2)$$

Take this parameter as the fixed segment of the inductor. The other three segments are obtained by dividing the fixed part in binary order, so other parameters are

$$L_2 = \frac{0.764}{2} = 0.382mH, \quad L_3 = \frac{0.764}{2^2} = 0.191mH$$

Similarly, we have $L_4=0.0095mH$.

3.3.1.1 Cases without Mutual Coupling

A pair of inductor segments without mutual coupling means that there is no presence of a common magnetic flux, which links these two segments. In other words, they are not magnetically coupled such as being mounted on the same core. For the four-segment-inductor, the inductance matrix is

$$X = \begin{bmatrix} 0.288 & 0 & 0 & 0 \\ 0 & 0.144 & 0 & 0 \\ 0 & 0 & 0.072 & 0 \\ 0 & 0 & 0 & 0.036 \end{bmatrix} \Omega \quad (3.3)$$

Except for the fixed part, the TLR structure enables each inductor segment to be switched in or out separately. Therefore, there are 2^3 combinations. Suppose that the switch state is denoted as 1 and 0; 1 stands for the segment being switched in and 0 for out; the switch state matrix is shown as below:

$$S = \begin{bmatrix} 1 & 1 & 1 & 1 & 1 & 1 & 1 & 1 \\ 0 & 0 & 0 & 0 & 1 & 1 & 1 & 1 \\ 0 & 0 & 1 & 1 & 0 & 0 & 1 & 1 \\ 0 & 1 & 0 & 1 & 0 & 1 & 0 & 1 \end{bmatrix} \quad (3.4)$$

When one segment is switched in, the series thyristor pair (switch) conducts current and, ideally, there is no voltage drop on it. The parallel switch has to block the voltage drop on the inductor segment, i.e., the reverse voltage of the parallel switch equals to the inductor segment voltage. Likewise, while the segment is switched off, the parallel switch conducts current, and the series switch has to block the induced voltage on the segment. In this case, there is no mutual coupling between inductor segments, so there is no voltage on the series switch when the segment is off.

A Matlab program is developed to calculate the branch current and voltage drop on inductor segments and the total impedance. The complete program is attached in Appendix B. The results are shown in Table 3.1. Here Z is the total impedance for each switch state. L_x series refers to the switch in series with segment L_x . Likewise, L_x parallel is the switch in parallel with L_x . V_{max} is the maximum voltage stress of each case, based on a rating voltage of 480V.

Table 3.1: Analytical results for TLR without mutual coupling.

Switch	Case#	I(A)	Z(Ohm)	Voltage stress experienced by switches (V)						
				L2 series	L2 parallel	L3 series	L3 parallel	L4 series	L4 parallel	Vmax(%)
1000	Case1	1667	0.288	0	0	0	0	0	0	0
1001	Case2	1481	0.324	0	0	0	0	0	53	11
1010	Case3	1333	0.360	0	0	0	96	0	0	20
1011	Case4	1212	0.396	0	0	0	87	0	44	18
1100	Case5	1111	0.432	0	160	0	0	0	0	33
1101	Case6	1026	0.468	0	148	0	0	0	37	31
1110	Case7	952	0.504	0	137	0	69	0	0	29
1111	Case8	889	0.540	0	128	0	64	0	32	27

It can be seen that the largest current the thyristor has to conduct is 1666.7A in case 1, and the largest voltage the thyristor has to block is 160V, which weighs 33% of the rating voltage.

For tap connection, one side of all the switches is connected to the system common (refer to Fig. 3.7), so there is only one switch that can be connected for each operation. For example, if S_1 is on, segments L_2 , L_3 and L_4 are all shorted and the other switches whether on or off have no effect on total inductance. Therefore, there are only 4 segment combinations and the switch state matrix is

$$S = \begin{bmatrix} 1 & 1 & 1 & 1 \\ 0 & 1 & 1 & 1 \\ 0 & 0 & 1 & 1 \\ 0 & 0 & 0 & 1 \end{bmatrix} \quad (3.5)$$

When one switch is on, this switch conducts the branch current and there are no voltage drops on the switches that are shorted, since there are no induced voltages on the shorted inductors. The voltage on the switches that are not shorted could be accumulating. For example, when S_4 is on, all four segments are included. The reverse voltage for S_1 is the summation of the voltage on L_2 , L_3 and L_4 . The current and segment voltages are calculated and, hence, the voltages on switches are also obtained, which are shown in Table 3.2.

From Table 3.2, we observe that the maximum current flowing through the switch is $1666.67A$, and the maximum voltage on the switch is $224V$, 46.67% of the rating voltage. Compared with the TLR connection, the maximum current is the same, while the maximum voltage is much higher due to the voltage summation.

Table 3.2: Analytical results for tap connection without mutual coupling

Switch	Case#	I(A)	Z(Ohm)	S1(V)	S2(V)	S3(V)	S4(V)	Vmax(%)
1000	S1 on	1667	0.288	0	0	0	0	0
1100	S2 on	1111	0.432	160	0	0	0	33
1110	S3 on	952	0.504	206	69	0	0	43
1111	S4 on	889	0.540	224	96	32	0	47

Curves of impedance and V_{max} versus case number are plotted and shown in Fig. 3.9 and Fig. 3.10. Comparing the results in the tables and the curves, we can draw the following conclusions:

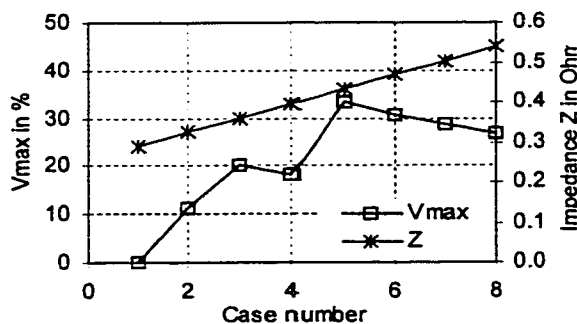


Fig. 3.9: Curves of V_{max} & Z vs. case number for TLR connection.

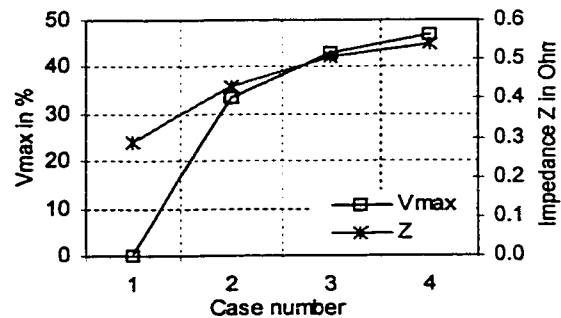


Fig. 3.10: Curves of V_{max} & Z vs. case number for tap connection.

- The TLR connection has more combinations for the same number of inductor segments, which means a smaller variation step of inductance. In the case studied, the TLR connection has $2^3 = 8$ combinations or steps, while the tap connection has only 4 combinations.
- The TLR needs fewer switches for the same variation step than the tap connection does. The switches per step for TLR are $6/8 = 0.75$, while the tap connection is 1 switch per step.
- The voltage stress on switches of TLR connection is lower than that of the tap connection. For example, the maximum voltage stress for TLR cases is 33.33%, while for the tap connection, it is 46.67%.

3.3.1.2 Cases with Mutual Coupling

In this case, the inductor segments are magnetically coupled. Suppose the coupling coefficient $K=0.9$ and the mutual inductance can be obtained as

$$M_{12} = M_{21} = K\sqrt{L_1 L_2} \quad (3.6)$$

The impedance matrix of variable reactor with mutual coupling is

$$X = \begin{bmatrix} 0.288 & 0.1833 & 0.1296 & 0.0916 \\ 0.1833 & 0.144 & 0.0916 & 0.0648 \\ 0.1296 & 0.0916 & 0.072 & 0.0458 \\ 0.0916 & 0.0648 & 0.0458 & 0.036 \end{bmatrix} \Omega \quad (3.7)$$

For the TLR connection, the switch state matrix is the same as Equation 3.4. Following the same procedure as the analysis of the TLR connection without coupling, the current and voltage across each inductor segment are obtained. Here the voltage on each inductor segment is the summation of the voltage drop on self-inductance and

mutual inductance. When the corresponding segment is shorted, the voltage on the series switch is the induced voltage of the segment. The voltages on series and parallel switches are also calculated. The results are shown in Table 3.3.

Examining Table 3.3, it is noted that the maximum voltage the switch has to block is 306V, 63.65% of rating voltage and the maximum current is 1666.7A at case 1. This maximum voltage is much higher than that of the no coupling case due to the mutual coupling.

Table 3.3: Analytical results for TLR with mutual coupling

Switch	Case#	I(A)	Z(Ohm)	Switch Voltage(V)						
				L2 series	L2 parallel	L3 series	L3 parallel	L4 series	L4 parallel	Vmax(%)
1000	Case1	1667	0.288	306	0	216	0	153	0	64
1001	Case2	946	0.507	235	0	166	0	0	121	49
1010	Case3	775	0.619	213	0	156	0	107	0	44
1100	Case4	601	0.799	0	197	133	0	94	0	41
1011	Case5	516	0.930	175	0	0	128	0	89	37
1101	Case6	418	1.147	0	164	112	0	0	80	34
1110	Case7	366	1.313	0	153	0	107	74	0	32
1111	Case8	274	1.753	0	132	0	93	0	65	28

For the tap connection, the same impedance matrix as Equation 3.7 is used in this case and the switch states are the same as Equation 3.5. The current and voltage are calculated. Taking mutual coupling into consideration, the switch voltages are obtained and shown in Table 3.4.

Table 3.4: Analytical results for tap connection with mutual coupling

Switch	Case#	I(A)	Z(Ohm)	S1(V)	S2(V)	S3(V)	S4(V)	Vmax(%)
1000	S1 on	1667	0.288	0	306	522	674	140
1100	S2 on	601	0.799	197	0	133	227	47
1110	S3 on	366	1.313	260	107	0	74	54
1111	S4 on	274	1.753	290	158	65	0	61

The maximum current the switch has to conduct is $1666.67A$, and the maximum voltage on the switch is $674V$, 140% of the rating voltage. Comparing the TLR inductor with the coupling case, this current is the same but the voltage is much higher.

Curves of impedance and V_{max} versus case number are plotted and shown in Figures 3.11 and 3.12. Comparing the results and the curves between TLR and the tap connection and, also, with the cases without coupling, we have the following conclusions:

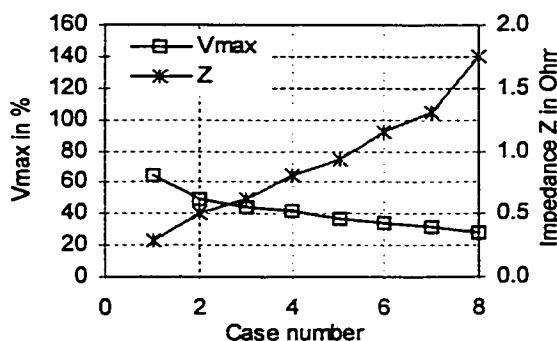


Fig. 3.11: Curves of V_{max} & Z vs. case number for TLR connection.

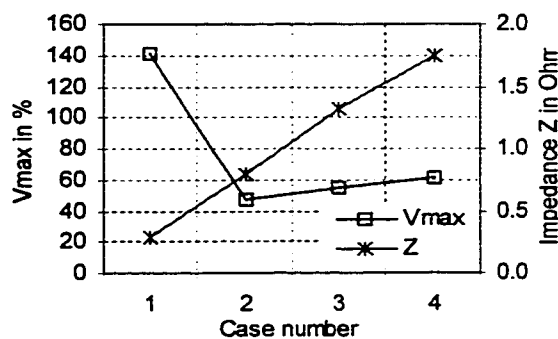


Fig. 3.12: Curves of V_{max} & Z vs. case number for tap connection.

- Compared with the cases without mutual coupling, the coupling cases have much wider impedance variation range. For non-coupling cases, the range is $0.288 \sim 0.54\Omega$, while the coupling cases have a range of $0.288 \sim 1.753\Omega$.
- The voltage stress for coupling cases is higher than non-coupling cases.
- The voltage stress of tap connection is much higher than the TLR connection for coupling cases.
- The maximum current stress is the same for all four cases.

3.3.2 TLR in a Filter

The intended application of the thyristor linked reactor is a tunable filter, in this part, the study of voltage stress on the variable reactor within a filter is conducted. A single tuned shunt filter is considered, which is tuned to the 7th harmonic. The filter simply consists of a variable reactor and a capacitor. The variable reactor has the same configuration as Fig. 3.7 (tap connection) or Fig. 3.8 (TLR). The circuit diagram of a single tuned shunt filter is shown in Fig. 3.13.

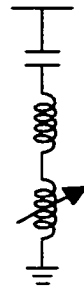


Fig. 3.13: Single tuned shunt filter.

The parameters are calculated from the capacitor size and the voltage level. Given the three-phase capacitor size $2400KVar$ and the voltage rating $V_{LL} = 44KV$, the single-phase capacitor size is $800Kvar$ and the impedance is calculated as follows:

$$X_C = \frac{(44 \times 1000 / \sqrt{3})^2}{800 \times 1000} = 781.25\Omega \quad (3.8)$$

The filter is designed for the 7th harmonic and tuned slightly below the harmonic frequency of concern. Here we tune it to $h = 6.9$, and the impedance is

$$X_{L1} = \frac{X_C}{h^2} = \frac{781.25}{6.9^2} = 16.41\Omega \quad (3.9)$$

Taking this parameter as the impedance of the fixed segment, the other segment parameters are

$$X_{L2} = \frac{X_{L1}}{2} = \frac{16.41}{2} = 8.205\Omega \quad (3.10)$$

$$X_{L3} = \frac{X_{L2}}{2} = \frac{8.205}{2} = 4.102\Omega \quad (3.11)$$

Similarly, $X_{L4} = 2.051\Omega$. When the inductance changes, the tuned frequency of the filter is shifted. The shifted frequency can be calculated as

$$h = \sqrt{\frac{X_C}{X_L}} \quad (3.12)$$

3.3.2.1 Cases without Mutual Coupling

The impedance of the filter consists of two parts, one is the reactance of the capacitor X_C , and the other is the reactance of the variable inductor X_L . X_L is the impedance matrix of the inductor, shown as below:

$$X_L = \begin{bmatrix} 16.41 & 0 & 0 & 0 \\ 0 & 8.205 & 0 & 0 \\ 0 & 0 & 4.102 & 0 \\ 0 & 0 & 0 & 2.05 \end{bmatrix} \Omega \quad (3.13)$$

The total impedance of the filter is the summation of X_C and the reactance of the inductor segments in effect, X_{Ltotal} , i. e.,

$$X_{total} = |X_{Ltotal} - X_C| \quad (3.14)$$

The fundamental current flowing through the filter is

$$I = \frac{V_P}{X_{total}} \quad (3.15)$$

Here V_P is phase voltage. The voltage across each inductor segment can be obtained simply by multiplying segment impedance with the filter current.

For the TLR connection, the switch state matrix is the same as Equation 3.4. A Matlab script is written to calculate the filter current and the voltage drop on all the components. The tuned frequency is also obtained using the formula given in Equation 3.12 and the switch voltage stress is derived from the component voltages. The results are tabulated in Table 3.5. Here Z is the total impedance of the filter for each switch state. h is the tuned frequency. L_x series refers to the switch in series with segment L_x . Likewise, L_x parallel is the switch in parallel with L_x . V_{max} is the maximum voltage stress of each case, based on a rated phase voltage of $44/\sqrt{3} KV=25KV$.

The results in Table 3.5 indicate that the filter current is relatively small due to the large capacitor reactance. The largest current is $33.33A$ and occurs in case 8. The maximum voltage the switch has to block is $273V$ and weighs on by 1.09% of the rating voltage. The tuned harmonic order is from 5.04 to 6.9 , so the filter can be tuned to the 5th and the 7th harmonics.

Table 3.5: Analytical results for TLR without mutual coupling

Switch	Case#	I(A)	Z(Ohm)	h(order)	Voltage stress experienced by switches (V)						
					L2 series	L2 parallel	L3 series	L3 parallel	L4 series	L4 parallel	Vmax(%)
1000	Case1	32.7	765	6.90	0	0	0	0	0	0	0.00
1001	Case2	32.8	763	6.51	0	0	0	0	0	67	0.27
1010	Case3	32.9	761	6.17	0	0	0	135	0	0	0.54
1011	Case4	33.0	759	5.88	0	0	0	135	0	68	0.54
1100	Case5	33.0	757	5.63	0	271	0	0	0	0	1.08
1101	Case6	33.1	755	5.41	0	272	0	0	0	68	1.09
1110	Case7	33.2	753	5.22	0	273	0	136	0	0	1.09
1111	Case8	33.3	750	5.04	0	273	0	137	0	68	1.09

For tap connection, the switch state matrix is the same as Equation 3.5. The segment parameters are the same as Equation 3.13. Following the same procedure, the results for tap connection without mutual coupling are obtained and shown in Table 3.6.

From Table 3.6, we observe that the maximum current flowing through the switch is 33.3A, which is the same as that of TLR connection, and the maximum voltage on the switch is 478V, 1.9% of the rating voltage. The tuned harmonic order is from 5.04 to 6.9, so the filter can be tuned to the 5th and 7th harmonic. Compared with the TLR connection, the maximum current is the same, while the maximum voltage is higher due to the voltage summation.

Table 3.6: Analytical results for tap connection without mutual coupling

Switch	Case#	I(A)	Z(Ohm)	h(order)	S1(V)	S2(V)	S3(V)	S4(V)	Vmax(%)
1000	S1 on	32.7	765	6.90	0	0	0	0	0.0
1100	S2 on	33.0	757	5.63	271	0	0	0	1.1
1110	S3 on	33.2	753	5.22	409	136	0	0	1.6
1111	S4 on	33.3	750	5.04	478	205	68	0	1.9

Curves of harmonic order and V_{max} versus case number are plotted and shown in Fig. 3.14 and Fig. 3.15. Comparing the results in the tables and the curves, we can draw the following conclusions

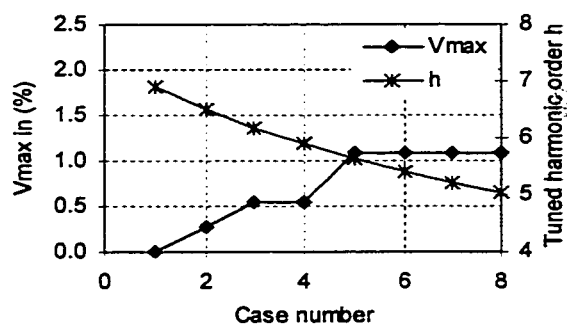


Fig. 3.14: Curves of V_{max} & h vs. case number for TLR connection.

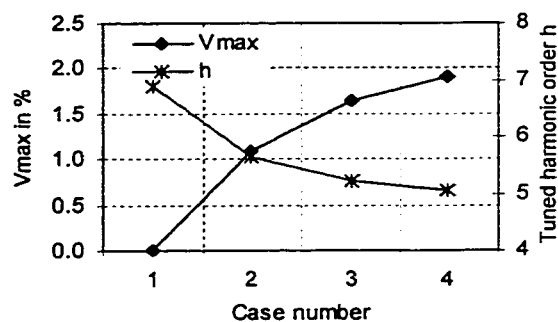


Fig. 3.15: Curves of V_{max} & h vs. case number for tap connection.

- The TLR connection has more combinations for the same number of inductor segments, which means a smaller variation step of inductance. Therefore when the component parameter has a small shift, TLR will provide more accurate adjustment.
- The tuned range of harmonic order is the same for both the tap and TLR connection.
- The voltage stress on switches of TLR connection is lower than on that of tap connection. For example, the maximum voltage stress for TLR cases is 1.09%, while for the tap connection, it is 1.9%.

3.3.2.2 Cases with Mutual Coupling

In this case, the inductor segments are coupled together. Suppose the coupling coefficient $K=0.9$ and the mutual inductance can be obtained as in Equation 3.6. The impedance matrix of a variable reactor with coupling is

$$X = \begin{bmatrix} 16.41 & 10.44 & 7.384 & 5.221 \\ 10.44 & 8.205 & 5.221 & 3.692 \\ 7.384 & 5.221 & 4.102 & 2.611 \\ 5.221 & 3.692 & 2.611 & 2.051 \end{bmatrix} \Omega \quad (3.16)$$

For the TLR connection, using Equation 3.16 as the impedance matrix of the variable reactor and Equation 3.4 as the switch state matrix, the current and voltage of inductor and capacitor are calculated and the results are shown in Table 3.7.

Table 3.7: Analytical results for TLR with mutual coupling

Switch	Case#	I(A)	Z(Ohm)	h(order)	Voltage stress experienced by switches (V)						
					L2 series	L2 parallel	L3 series	L3 parallel	L4 series	L4 parallel	Vmax(%)
1000	Case1	32.7	765	6.90	341	0	241	0	171	0	1.4
1001	Case2	33.2	752	5.20	470	0	332	0	0	242	1.9
1010	Case3	33.5	746	4.71	525	0	0	385	262	0	2.1
1011	Case4	34.3	728	3.84	664	0	0	484	0	339	2.7
1100	Case5	34.0	736	4.14	0	634	428	0	303	0	2.5
1101	Case6	34.9	716	3.46	0	780	531	0	0	383	3.1
1110	Case7	35.4	706	3.23	0	845	0	591	408	0	3.4
1111	Case8	36.7	681	2.80	0	1011	0	709	0	498	4.0

From Table 3.7, it is concluded that the maximum current is 36.7A, and the maximum switch voltage is 1101V, 4% of the rating voltage. The tuned harmonic order is from 2.8 to 6.9. Compared with Part 3.2.1 without coupling, the maximum current and voltage are higher but the tuned harmonic range is wider. It can be tuned to the 3rd, 5th and 7th harmonics.

For tap connection, the impedance matrix is as in Equation 3.16, and the switch state matrix is the same as in Equation 3.5. Calculating the current and voltage of inductor segments and capacitor, the results are tabulated in Table 3.8. The maximum current is 36.7A, the same as that of the TLR connection, while the maximum voltage is 2218V, 8.87% of the rating voltage, which is more than twice of that of the TLR connection (4%). The tuning range is the same as the TLR connection, but it cannot be tuned to the 5th harmonic.

Table 3.8: Analytical results for tap connection with mutual coupling

Switch	Case#	I(A)	Z(Ohm)	h(order)	S1(V)	S2(V)	S3(V)	S4(V)	Vmax(%)
1000	S1 on	32.7	765	6.90	0	341	583	753	3.01
1100	S2 on	34.0	736	4.14	634	0	428	731	2.92
1110	S3 on	35.4	706	3.23	1436	591	0	408	5.74
1111	S4 on	36.7	681	2.80	2218	1207	498	0	8.87

Curves of harmonic order h and maximum voltage V_{max} versus case number are plotted and shown in Fig. 3.16 and Fig. 3.17. Comparing the results and the curves between the TLR and the tap connection and also with the cases without coupling, we draw the following conclusions:

- Compared with the cases without mutual coupling, the coupling cases have wider tuning range. For no coupling cases, the range is 5.04 ~ 6.9, while with coupling cases the range is 2.8 ~ 6.9.
- The voltage stress for coupling cases is higher than that of non-coupling cases.

- The voltage stress of the tap connection is higher than TLR connection for coupling cases.
- TLR connection is more flexible than the tap connection due to more variation in steps. For example, TLR connection with mutual coupling filter can be tuned to the 3rd, 5th and 7th harmonics, while the tap connection can only be tuned to the 3rd and 5th harmonics.

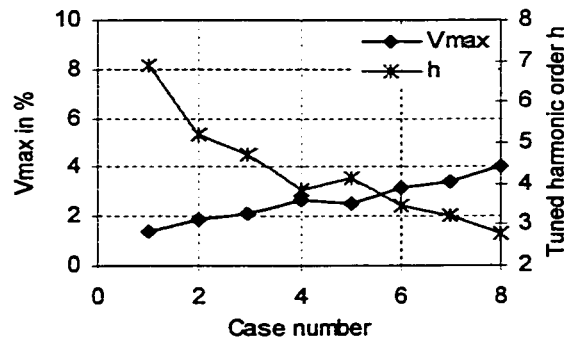


Fig. 3.16: Curves of V_{max} & h vs. case number for TLR connection.

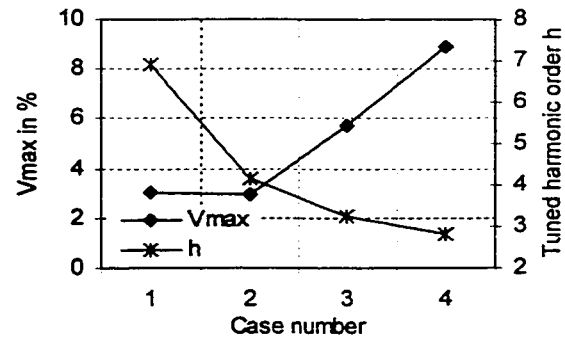


Fig. 3.17: Curves of V_{max} & h vs. case number for tap connection.

3.4 Impact of Harmonics on the Voltage Stress

The presence of one or more significant harmonics would surely increase the voltage stress on filter components. The effect of harmonics is investigated through a practical case study.

Assume a filter is designed for a nonlinear load with size S . The harmonic spectrum of the load is usually given; i. e., the per unit harmonic current based on full load current is known. Considering the worst case that all harmonic currents flow through the filter, the current and voltage on filter components can be obtained as follows:

$$I_{rms} = \sqrt{I_1^2 + \sum_{h=1} I_h^2} \quad (3.17)$$

$$V_{rms} = \sqrt{V_1^2 + \sum_{h=1} V_h^2} \quad (3.18)$$

where: I_{rms} and V_{rms} are root mean square current and voltage,

I_1 and V_1 are current and voltage rms value of the fundamental component, and h is the order of harmonic.

I_1 and V_1 can be obtained as analyzed earlier in 3.2.2, and harmonic currents are calculated from the load size and the harmonic spectrum,

$$I_h = \frac{K_h S}{\sqrt{3} V_{LL}} \quad (3.19)$$

where: S is the load size,

V_{LL} is system line to line voltage, and

K_h is per unit harmonic current based on load current.

Harmonic voltages across capacitor and a certain inductor segment are derived as follows:

$$V_{Ch} = \frac{I_h X_C}{h} \quad (3.20)$$

$$V_{Lh} = I_h X_L h \quad (3.21)$$

Consider a practical case. Suppose the filter in 3.2.2 is designed for a nonlinear load with load size of 1186Kvar. The two dominant harmonics it generates are known as 5th, 18.24% of full load current, and 7th, 11.9% of full load current. The current and voltage stress for cases of TLR inductor with and without mutual coupling are calculated,

conducted by a Matlab program. The voltage stress on a tapped reactor is also investigated as comparison.

3.4.1 Cases without Mutual Coupling

The analytical results are shown in Table 3.9 and Table 3.10, and the curves of V_{max} versus case number with and without the presence of harmonics are given in Fig. 18 and Fig. 19.

Table 3.9: Analytical results for TLR connection

Switch	Case#	I(A)	h(order)	Voltage stress experienced by switches (V)						
				L2 series	L2 parallel	L3 series	L3 parallel	L4 series	L4 parallel	Vmax(%)
1000	Case1	32.9	6.9	0	0	0	0	0	0	0.00
1001	Case2	33.0	6.5	0	0	0	0	0	78	0.31
1010	Case3	33.0	6.2	0	0	0	157	0	0	0.63
1011	Case4	33.1	5.9	0	0	0	157	0	79	0.63
1100	Case5	33.2	5.6	0	315	0	0	0	0	1.26
1101	Case6	33.3	5.4	0	316	0	0	0	79	1.26
1110	Case7	33.4	5.2	0	316	0	158	0	0	1.26
1111	Case8	33.5	5.0	0	317	0	158	0	79	1.27

Table 3.10: Analytical results for tap connection

Switch	Case#	I(A)	h(order)	S1(V)	S2(V)	S3(V)	S4(V)	Vmax(%)
1000	S1 on	32.9	6.9	0	0	0	0	0.00
1100	S2 on	33.2	5.6	315	0	0	0	1.26
1110	S3 on	33.4	5.2	474	158	0	0	1.90
1111	S4 on	33.5	5.0	554	238	79	0	2.22

The maximum voltage stress on switch increases with the presence of harmonics for both TLR and the tap connection. The largest increment for TLR and the tap connection are 0.175% and 0.3%, respectively. Therefore, tap connection has a higher voltage stress increment than TLR connection.

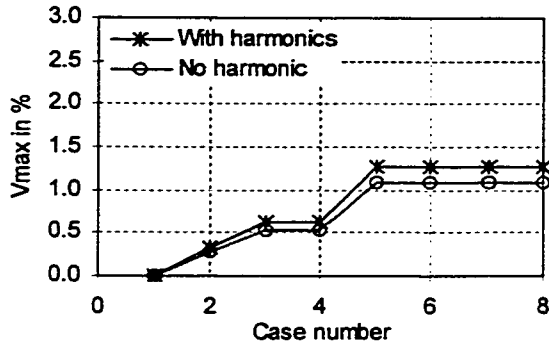


Fig. 3.18: Curves of V_{max} vs. case number for TLR connection.

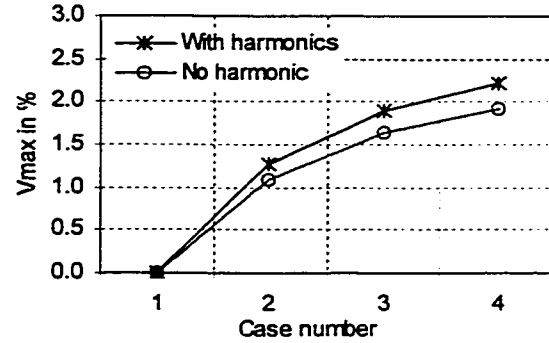


Fig. 3.19: Curves of V_{max} vs. case number for tap connection.

3.4.2 Cases with Mutual Coupling

With mutual coupling, the total inductance for each case is larger than that of the corresponding case without mutual coupling, and the voltage increase due to the presence of harmonics in this case is, therefore, larger than without mutual coupling. The analytical results and comparison curves are shown below:

Table 3.11: Analytical results for tap connection

Switch	Case#	I(A)	h(order)	S1(V)	S2(V)	S3(V)	S4(V)	Vmax(%)
1000	S1 on	32.9	6.9	0	398	679	878	3.51
1100	S2 on	34.2	4.1	731	0	494	843	3.37
1110	S3 on	35.6	3.2	1640	675	0	466	6.56
1111	S4 on	36.9	2.8	2513	1367	564	0	10.05

Table 3.12: Analytical results for TLR connection

Switch	Case#	I(A)	h(order)	Voltage stress experienced by switches (V)						Vmax(%)
				L2 series	L2 parallel	L3 series	L3 parallel	L4 series	L4 parallel	
1000	Case1	32.9	6.9	398	0	281	0	132	0	1.59
1001	Case2	33.4	5.2	545	0	385	0	0	280	2.18
1010	Case3	33.7	4.7	608	0	0	446	304	0	2.43
1011	Case4	34.5	3.8	765	0	0	557	0	390	3.06
1100	Case5	34.2	4.1	0	731	494	0	349	0	2.92
1101	Case6	35.1	3.5	0	894	609	0	0	439	3.58
1110	Case7	35.6	3.2	0	965	0	675	466	0	3.86
1111	Case8	36.9	2.8	0	1146	0	803	0	564	4.58

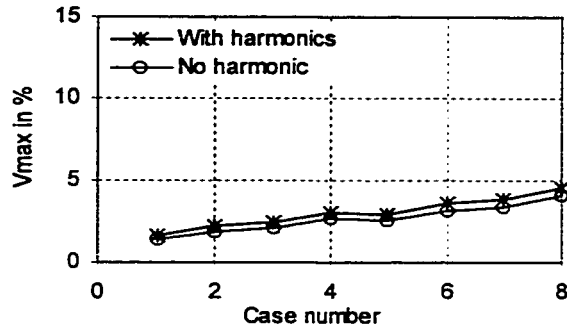


Fig. 3.20: Curves of V_{\max} vs. case number for TLR connection.

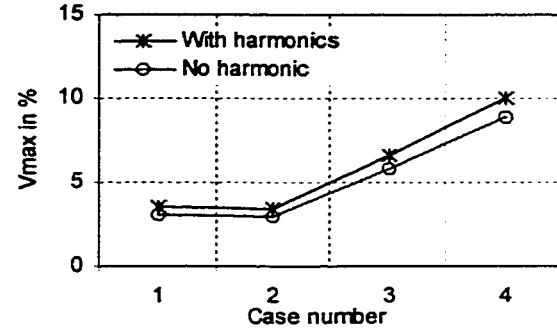


Fig. 3.21: Curves of V_{\max} vs. case number for tap connection.

It is obvious that the maximum stress increases for both TLR and the tap connection due to the presence of harmonics. The largest increments for both connections are 0.54% and 1.18% , respectively. As the case without mutual coupling, the situation is worse for the tap connection.

The analysis above illustrates that the presence of harmonics in the load current imposes more voltage stress on filter switches, and the increase of voltage stress of the tap connection is higher than that of TLR connection. However, the voltage increment is insignificant in this practical case. When the load size or the harmonic component is larger, the increase of voltage stress could be higher. However, noting that the analysis is based on the assumption that all harmonic currents, generated by the load, flow through the filter, the analytical results are for the worst case and, therefore, pessimistic. In a practical system, there are always other paths for the harmonic currents, so the voltage stress would not be as severe, and the voltage stress due to harmonics is not as big a concern. Therefore, the effect of harmonics on voltage stress can be taken into account by simply multiplying the fundamental voltage stress by a factor, for example 1.05 .

3.5 Economical Feasibility

In industrial applications, cost is an important factor to consider. To determine the economical feasibility of the proposed variable reactor, the cost of TLR is compared with that of a tap connection.

Consider a four-segment-inductor. For a tap connection and TLR, the cost on inductor segments is assumed to be the same, so only the cost on thyristors is considered. For thyristor (SCR) selection, there are usually several important parameters given: peak repetitive reverse or forward voltage V_{DRM} or V_{RRM} , on-state current and dV/dt & di/dt rate. These parameters cannot be exceeded in practical applications. At steady state, we only consider the basic requirement for voltage and current.

To select thyristor, the maximum on-state current and reverse voltage should be estimated. A thyristor must be rated to carry this on-state current and block this reverse voltage. If a suitable device is not available, several thyristors whose sum of rated currents exceed the estimated current may be used in parallel as well as several thyristors whose reverse breakdown voltage rating total to the required value may be used in series.

Taking the case in 3.2.2.3 as an example, the maximum current is only $36.7A$, so thyristors are chosen according to maximum reverse voltage V_{max} on the switch. The voltage V_{RRM} should be higher than V_{max} . All thyristors are chosen according to the worst cases, which will yield a pessimistic cost estimation. Table 3.13 is a comparison of costs between the tap connection and TLR.

Table 3.13 Cost comparison

	$V_{max}(V)$	$V_{RRM}(V)$	SCR Unit Price	Step #	SCR #	Cost/Step	Total Cost
Tap	2218	2400*	\$47.16	4	8	\$94.32	\$377.28
TLR	1011	1200	\$23.58	8	12	\$35.37	\$282.96

* Two $V_{RRM}=1200V$ thyristor in series.

The price for the SCR with $V_{RRM} = 1200V$ is from International Rectifier product catalog on web site www.nawark.com. The comparison bar graph is shown in Fig. 3.22. It

is obvious that the total cost as well as the cost per step for the tap connection is higher than that of TLR.

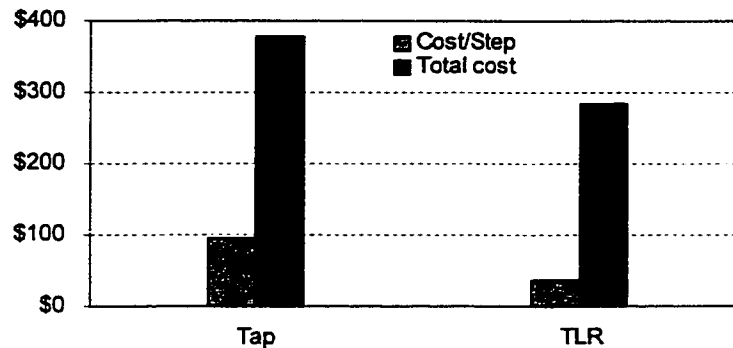


Fig. 3.22: Cost comparison.

3.6 Conclusions

The thyristor linked reactor is mainly designed for harmonic mitigation. The characteristic of it shown in the experimental waveforms demonstrates that it is a linearly variable reactor. This makes it superior to most of variable reactors mentioned in chapter 2 as well as suitable to serve the purpose of harmonic mitigation.

The steady state voltage stress on TLR switches are analyzed in different cases: when TLR is in a pure inductor branch, TLR in a filter and with the presence of harmonics. A tapped variable reactor is taken as comparison. The results show that the maximum voltage stress on a switch of TLR is lower than that of on a tapped reactor in all cases. Moreover, for the same number of inductor segment, TLR has more combinations and needs fewer switches per inductance variation step, which makes it a more flexible and accurately variable reactor. With the presence of harmonics, the voltage stress increases slightly, which can be taken into account by multiplying the fundamental voltage stress by a factor. A brief economical feasibility study is conducted, which shows that the TLR costs less than a same-sized tapped variable reactor.

Chapter 4

Transient Performance of the Thyristor Linked Reactor in RL Circuit

This chapter presents the analysis of the transient characteristics of the thyristor linked reactor in a RL circuit. Laplace transform is applied to conduct the theoretical analysis. A sensitivity study of switch timing is performed and the effects of resistance, self-inductance and mutual inductance on the switch transient are also investigated. EMTP simulation and experimental tests are taken to confirm the analytical results.

4.0 Introduction

With the presence of energy storing elements, capacitor and inductor, the operation of switches in a circuit usually results in transients of the form of over-current and over-voltage. It is well known that the voltage across the capacitor and the current through the inductor cannot change instantaneously. When the currents/voltages of the inductor/capacitor before and after switching are not equal, transient occurs with the switch operation. The thyristor linked reactor, as a switch controlled device, will also experience switching transients when the switches are operated randomly, which could impose extra current or voltage stress on the components of the device. The analysis of the transient characteristics of the device is therefore of great importance.

The objectives of this chapter are (1) to explore the transient stress that could be experienced by the TLR components in a RL circuit and the possible way to minimize it; (2) to investigate the impact of various factors on transient response to facilitate TLR design. In this chapter, the transient characteristic of the thyristor linked reactor in a pure

inductor branch is investigated in detail. Laplace transform is adopted to conduct the theoretical analysis due to its ability to avoid tedious calculation as required by classical procedure. Software tools such as Matlab and EMTP are used throughout the thesis for computation. The following aspects are investigated:

- Theoretical analysis of switching transients.
- Confirmation of the analytical results by EMTP simulation and experiments.
- Sensitivity study of the switch timing. The peak transient current and transient duration are taken as the indices for evaluation.
- Investigation of the effect of the resistance, the self-inductance and the mutual inductance on the switching transients.

4.1 Measurement Determination of Z Matrix of a Prototype

To demonstrate the transient characteristics of the TLR and facilitate the theoretical analysis and simulation study, an experimental prototype is set up as in Fig. 4.1. Four inductors are selected and connected with the thyristor switch box mentioned in chapter 3. The four inductor segments are coupled together and can be represented by an impedance matrix Z as follows:

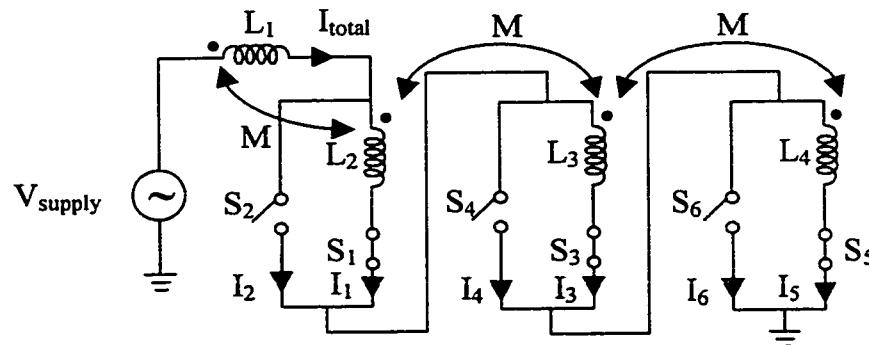


Fig. 4.1: Experimental circuit.

$$V = Z \times I \quad (4.1)$$

where V is the voltage across each inductor segment, a four-element vector,
 I is the current flowing through each inductor segment, a four-element vector,
 Z is the impedance matrix, which is a four by four square matrix.

The Z matrix is determined experimentally as follows. First, apply a sinusoidal voltage to one of the four inductor segments. Read the voltages across the inductor segments; one is the applied voltage and others are induced voltages, and the current through inductor segments; one is the current through the segment that applied voltage; others are zero. Second, form the voltage and the current vectors from the readings and substitute these vectors into Equation 4.1; then solve for the impedance. One column of the impedance matrix will be obtained. Third, apply the voltage to another inductor segment. Repeating steps 1 and 2, another column of the impedance matrix can be obtained. In this way, all the elements of the impedance matrix can be determined.

The value of the Z matrix of this prototype is determined experimentally. A 60Hz sinusoidal voltage of 80V is applied to one of the inductor segments each time. The measured results are presented in Table 4.1. The results can be represented as voltage and current matrices.

Table 4.1: Measured results

No.#	I(A)	ϕ (Degree)	V_{L1} (V)	V_{L2} (V)	V_{L3} (V)	V_{L4} (V)
1	4.56	-78	80.0	19.4	5.00	2.00
2	4.50	-79	19.4	80.0	18.8	4.90
3	4.54	-80	4.90	18.8	80.0	19.2
4	4.51	-80	2.00	4.90	19.2	80.0

$$V = \begin{bmatrix} 80.0 & 19.4 & 4.9 & 2.0 \\ 19.4 & 80.0 & 18.8 & 4.9 \\ 5.0 & 18.8 & 80.0 & 19.2 \\ 2.0 & 4.9 & 19.2 & 80.0 \end{bmatrix},$$

$$I = \begin{bmatrix} 4.56\angle -78^\circ & 0 & 0 & 0 \\ 0 & 4.5\angle -79^\circ & 0 & 0 \\ 0 & 0 & 4.54\angle -80^\circ & 0 \\ 0 & 0 & 0 & 4.51\angle -80^\circ \end{bmatrix}$$

The voltage and the current can still be related by Equation 4.1. Solving for Z , we have $Z = VI^{-1}$. The impedance matrix is obtained as

$$Z = \begin{bmatrix} 3.6476+17.1605i & 4.3111i & 1.1013i & 0.4435i \\ 4.2544i & 3.3922+17.4511i & 4.1410i & 1.0865i \\ 1.0746i & 4.1778i & 3.0599+17.3534i & 4.2572i \\ 0.4386i & 1.0889i & 4.2291i & 3.0802+17.4689i \end{bmatrix} \quad (4.2)$$

The self-inductance and the mutual inductance of the inductor segments can be computed from the inductive impedance, i.e. the imaginary part of the impedance Z , by simply dividing the inductive impedance by the radian frequency ω of the voltage source, i.e., $\omega = 2\pi f$, here frequency $f=60\text{Hz}$. Expressed in matrix, the self-inductance and mutual inductance are obtained as

$$L = \begin{bmatrix} 0.0455 & 0.0114 & 0.0029 & 0.0012 \\ 0.0113 & 0.0463 & 0.0110 & 0.0029 \\ 0.0029 & 0.0111 & 0.0460 & 0.0113 \\ 0.0012 & 0.0029 & 0.0112 & 0.0463 \end{bmatrix} \quad (4.3)$$

4.2 Transient Caused by Inductor Bypassing

There are basically two kinds of TLR operation involved in the transient analysis. One is the transient caused by bypassing an inductor segment coupled with the working inductor, while the other is caused by inserting an inductor segment into the working circuit. These are two inverse operations, which result in a different transient process. The transient caused by inductor bypassing is investigated in this section.

4.2.1 Theoretical Analysis

To simplify the circuit, only two inductors are considered. Fig. 4.2 is the circuit used in theoretical analysis. Some assumptions are adopted:

- The equivalent resistance R of the two inductors is the same.
- S_2 closes at the instant of switch operation; S_1 opens when the current flowing through it crosses zero (according to the characteristic of thyristor).
- The mutual inductance between the two inductors is the same, i.e., $M_{12}=M_{21}$.

Suppose a switch is operated at the time t with an initial current of $I_1(0)$. The frequency domain equivalent circuit is shown in Fig. 4.3. The equivalent resistance of the two inductors is R . The source voltage is sinusoidal with the form of $V_m \cos \omega t$, where V_m is peak magnitude of the source voltage, ω is frequency in radian per second.

The steady-state current i_t can be obtained as below:

$$Z = 2R + j\omega(L_1 + L_2 + 2M) = z \angle \varphi \quad \Omega \quad (4.4)$$

$$i_t(t) = \frac{V_m}{z} \cos(\omega t - \varphi) \text{ A} \quad (4.5)$$

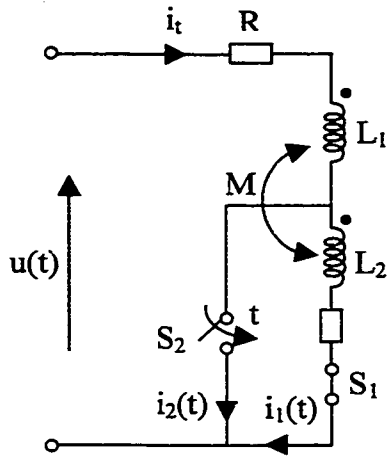


Fig. 4.2: Circuit used in the analysis.

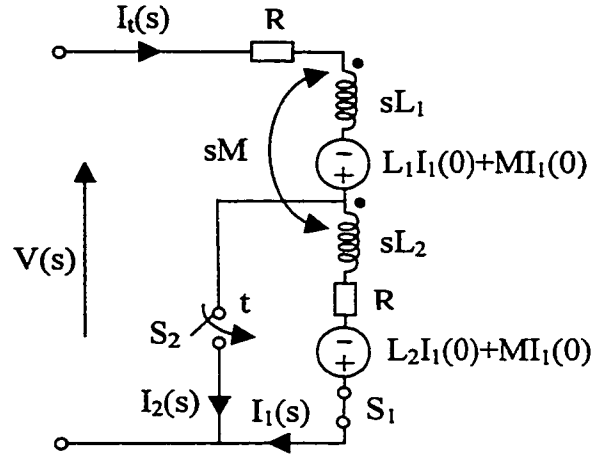


Fig. 4.3: Frequency domain equivalent circuit.

The switch is operated at time t when $\omega t = \theta$, and the initial currents for L_1 and L_2 are the same $I_l(0)$,

$$I_1(0) = \frac{V_m}{z} \cos(\theta - \varphi) \text{ A} \quad (4.6)$$

Referring to Fig 4.3, the switch S_2 closes at time t , and S_1 will open at the instant i_l crosses zero. Therefore, if the initial current $I_l(0)$ is zero, the switch S_1 would open at the same time as S_2 closes. Otherwise, it conducts till the instantaneous current of i_l equals zero. Taking the instant of switching as the beginning of transient, i.e. the switch operates at $t = 0$ based on the initial condition of Equation 4.6, the voltage source is represented as

$$u(t) = V_m \cos(\omega t + \theta) \text{ V} \quad (4.7)$$

The Laplace transform of it is

$$V(s) = \frac{V_m (s \cos \theta - \omega \sin \theta)}{s^2 + \omega^2} \quad (4.8)$$

The voltage equations are

$$\begin{cases} I_t (R + sL_1) + sMI_1 = (L_1 + M)I_1(0) + V(s) \\ I_t sM + I_1 (R + sL_2) = (L_2 + M)I_1(0) \end{cases} \quad (4.9)$$

Solve the equations to obtain I_t and I_1 ,

$$I_t = \frac{RI_1(0)(L_1 + M) + sI_1(0)(L_1L_2 - M^2) + (R + sL_2)V(s)}{s^2(L_1L_2 - M^2) + sR(L_1 + L_2) + R^2} \quad (4.10)$$

$$= \frac{[RI_1(0)(L_1 + M) + sI_1(0)(L_1L_2 - M^2)](s^2 + \omega^2) + V_m(R + sL_2)(s \cos \theta - \omega \sin \theta)}{[s^2(L_1L_2 - M^2) + sR(L_1 + L_2) + R^2](s^2 + \omega^2)}$$

$$I_1 = \frac{RI_1(0)(L_2 + M) + sI_1(0)(L_1L_2 - M^2) - sMV(s)}{s^2(L_1L_2 - M^2) + sR(L_1 + L_2) + R^2} \quad (4.11)$$

$$= \frac{[RI_1(0)(L_2 + M) + sI_1(0)(L_1L_2 - M^2)](s^2 + \omega^2) - V_m sM(s \cos \theta - \omega \sin \theta)}{[s^2(L_1L_2 - M^2) + sR(L_1 + L_2) + R^2](s^2 + \omega^2)}$$

Using the measured parameters to compute transient currents, $R=3.3922\Omega$, $L_1=0.0455H$, $L_2=0.0463H$, $M=0.0114H$, $V_m=80\sqrt{2} V$, $\omega=2\pi f=377 \text{ rad/s}$, determine the inverse Laplace transform by partial fraction expansions. The poles of the current functions are

$$p_1 = j\omega = j377 \quad p_1^* = -j\omega = -j377 \quad p_2 = -59.19 \quad p_3 = -98.34$$

Here p_1^* is the conjugate of p_1 . When θ is different, the residues of the poles are different. Taking $\theta = 210^\circ$ as an example, the residues for I_t are

$$R_1 = -2.31 - j2.52, R_1^* = -2.31 + j2.52, R_2 = -0.2363, R_3 = 3.0276$$

Residues for I_l are

$$R_4 = 0.6654 + j0.4915, R_4^* = 0.6654 - j0.4915, R_5 = -0.2448, R_6 = -2.9232$$

Therefore, the time-domain currents are obtained as

$$i_t = R_1 e^{p_1 t} + R_1^* e^{p_1^* t} + R_2 e^{p_2 t} + R_3 e^{p_3 t} \quad (4.12)$$

$$= 6.837 \cos(\omega t + 132.5^\circ) - 0.2363 e^{-59.19t} + 3.0276 e^{-98.34t}$$

$$i_l = R_4 e^{p_1 t} + R_4^* e^{p_1^* t} + R_5 e^{p_2 t} + R_6 e^{p_3 t} \quad (4.13)$$

$$= 0.8272 \cos(\omega t + 143.6^\circ) - 0.2448 e^{-59.19t} - 2.9232 e^{-98.34t}$$

$$i_2 = i_t - i_l \quad (4.14)$$

This is the first phase of the transient. The second phase of the transient begins when the current i_l crosses zero at time t_l and switch S_1 opens. The initial current of L_1 , $I_l(0)$, is the instantaneous value of i_l at the instant t_l . Suppose the voltage source has the form $V_m \cos(\omega t + \theta_l)$, the Laplace transform of the voltage source is of the same pattern as Equation 4.8. The voltage equation for the second phase is

$$(R + sL_1)I_t = V(s) + L_1 I_t(0) \quad (4.15)$$

Solve the equation for I_t , we have,

$$I_t = \frac{s^2 L_1 I_t(0) + s V_m \cos \theta_1 - V_m \omega \sin \theta_1 + \omega^2 L_1 I_t(0)}{S^3 L_1 + S^2 R + s L_1 \omega^2 + R \omega^2} \quad (4.16)$$

Following the first phase, the initial condition $I_t(0)$ and phase angle θ_1 can be obtained. Determining the inverse Laplace transform of the current by partial fraction expansions, the poles and residues are

$$p_1 = j377, \quad p_1^* = -j377, \quad p_2 = -74.52$$

$$R_1 = -0.6932 + j3.1576, \quad R_1^* = -0.6932 - j3.1576, \quad R_2 = 0.5019$$

Therefore, the time domain current is expressed as

$$\begin{aligned} i_t &= R_1 e^{p_1 t} + R_1^* e^{p_1^* t} + R_2 e^{p_2 t} \\ &= 6.4656 \cos(\omega t - 102.38^\circ) + 0.5019 e^{-74.52t} \end{aligned} \quad (4.17)$$

The above derivation is programmed in Matlab. The complete program is attached in Appendix B. Fig. 4.4 shows the flow chart of the program. This program basically consists of four parts. The first part completes the initiation of the program and the calculation of steady-state current before switch operation. The second part is devoted to Laplace transform, calculating poles and residues and obtaining time domain currents after switch S_2 closes. According to our assumption, S_1 opens after switching time t only when i_l crosses zero. Therefore, the third part of the program finds out the zero-cross point of i_l and sets i_l to zero after this point, computing the current of L_1 after S_1 opens. The fourth part gives out the plot of current waveforms. The current waveforms before

and after switch operation at $Angle = 210^\circ$ are shown below in Fig. 4.5. Here $Angle$ is the phase angle of source voltage at time t when $\omega t = Angle = 210^\circ$.

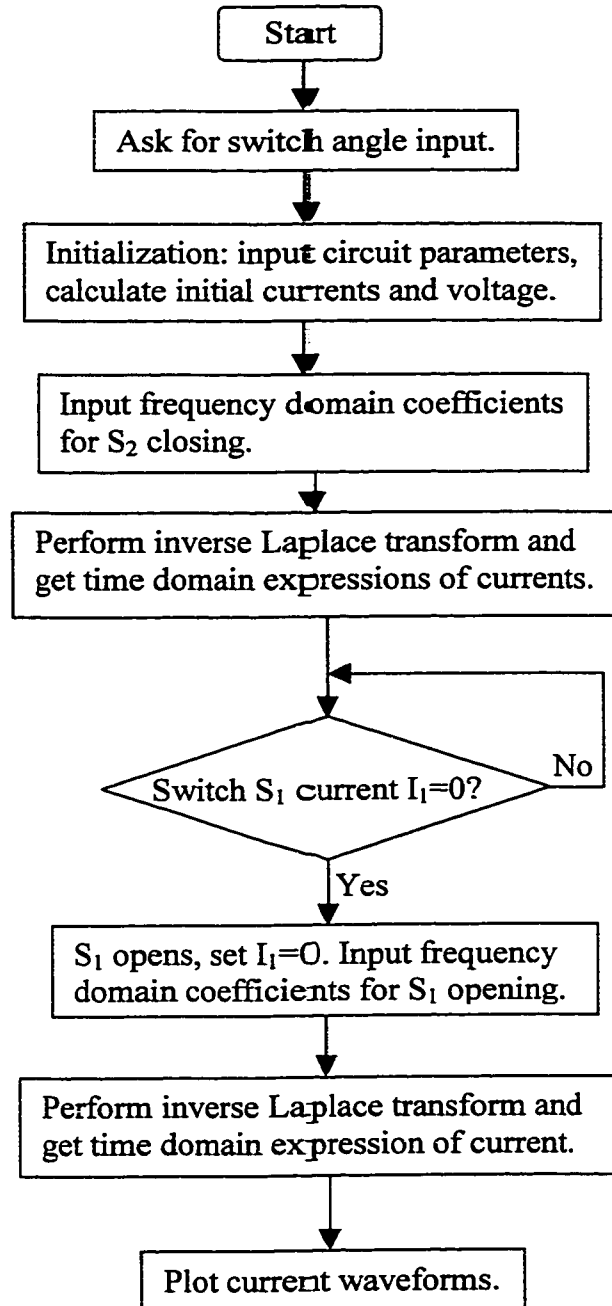


Fig. 4.4: Flow chart of the Matlab program.

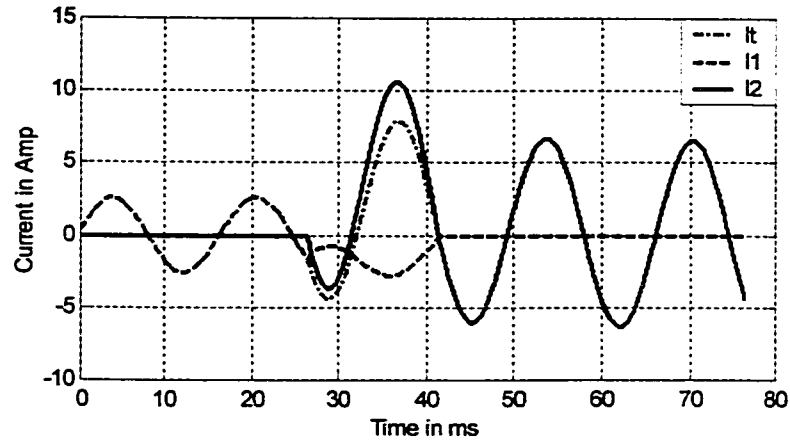


Fig. 4.5: Switch transient at $Angle=210^\circ$.

From the waveforms, it can be observed that:

- There is a period during which the two switches S_1 and S_2 are both on. This is caused by the characteristic of thyristor. S_2 closes at the switching time t , but at this point the current flowing through S_1 (i_1) is not zero. Thus, S_1 keeps conducting till i_1 crosses zero.
- There is a relatively large transient current before S_1 opens. There are basically two factors that contribute to this large transient current. The first one is *the initial current*. The second one is *the induced voltage across the bypassed inductor*. When S_1 and S_2 are all on, this voltage is short-circuited, which introduces a large short circuit current.

From Equations 4.12 and 4.13, it can be seen that the currents consist of two parts: natural part and forced part. The forced part is determined by the voltage source and the natural part is proportional to the initial current. *Therefore, it is possible to reduce the transient current by operating the switch at a lower initial current, or in other words, by switch timing.*

4.2.2 Simulation and Experimental Study

An EMTP script is written to simulate the inductor bypassing transient. The complete script is attached in Appendix A. The following circuit parameters are applied: $R=3.3922\Omega$, $L_1=0.0455H$, $L_2=0.0463H$, $M=0.0414H$, $V_m=80\sqrt{2} V$; simulating time period $0 \sim 0.1s$, step $0.00033s$; switch operation time: $0.0264s$, corresponding to source voltage angle 210° . For comparison, the simulation results and theoretical results are plotted in the same figure in Fig. 4.6.

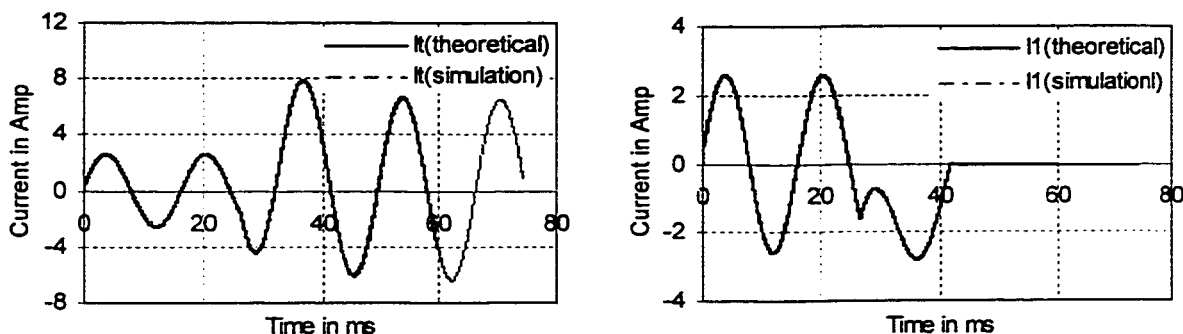


Figure 4.6: Comparison of simulation and theoretical results of inductor bypassing.

The simulation result and the theoretical result are identical, which verifies the correctness of the theoretical analysis. Matlab program based on theoretical analysis is used in further investigation.

An experimental circuit shown in Fig. 4.1 is set up and tested. Inductor bypassing operations are performed, and the transient current waveforms are recorded by the Nicolet system. Fig. 4.7 shows a typical case of inductor bypassing transient. The simulation results obtained by EMTP are plotted side by side with the measuring result.

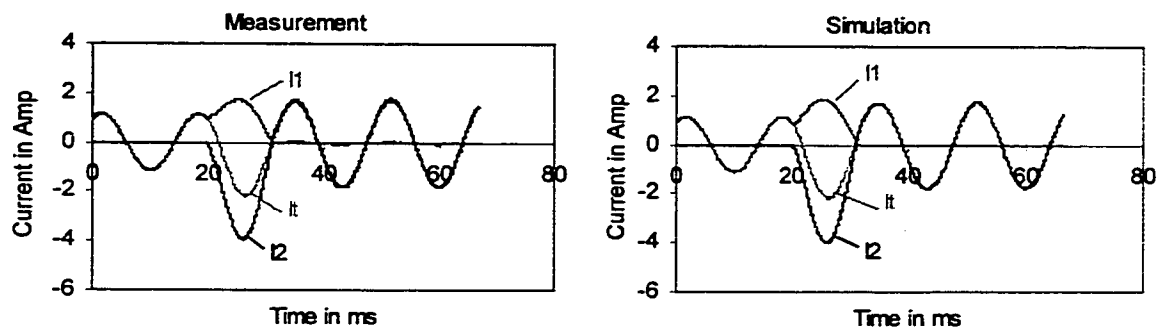


Fig. 4.7: Measurement and simulation current waveforms of inductor bypassing.

From Fig. 4.7, it can be concluded that the results obtained from both methods are identical to one another. They imply not only that the Matlab-based analysis is working properly and can be used in further analysis but also that the proposed variable inductor works as expected. The next few sections will use the Matlab-based theoretical analysis to conduct sensitivity studies and other investigations.

4.2.3 Sensitivity Study on the Switch Timing

As mentioned earlier, the instant of switch operation affects the transient response. It is therefore important to examine the relationship between the switch time and the transient response, thereby finding a way to minimize the switching transients. Two important indices that describe transients are *peak* and *duration*. The effect of switch timing on peak transient current and the duration of the transient is evaluated. Matlab-based theoretical analysis is used to perform the sensitivity study.

Definition of Transient Duration: it refers to the time period during which two switches conduct at the same time and the inductor is short-circuited. This definition is reasonable since the transient starts when S_2 closes, and S_1 opens only at zero current, which causes little transient for switch opening, and the transient, caused by S_2 closing, decays to an insignificant level at the time when S_1 opens. As a matter of fact, this definition is a reasonable approximation of the real case.

Fig. 4.8 is used to explain the definition of the transient duration. The switch S_2 closes at time t_1 and current begins to flow through S_2 after the switch closing. Current i_l is not zero at the time t_1 , so switch S_1 keeps conducting till the current becomes zero. At time t_2 when $i_l=0$, the switch S_2 opens. The time period between t_1 and t_2 is the duration of transient.

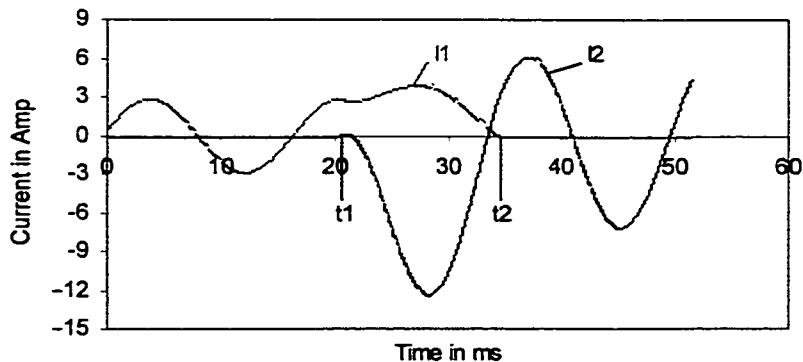


Fig. 4.8: Definition of transient duration.

Fig. 4.9 shows the transient current waveforms of I_l at different switch times. It is noted that the severity and duration of switching transient is highly dependent on the instant of switch operation.

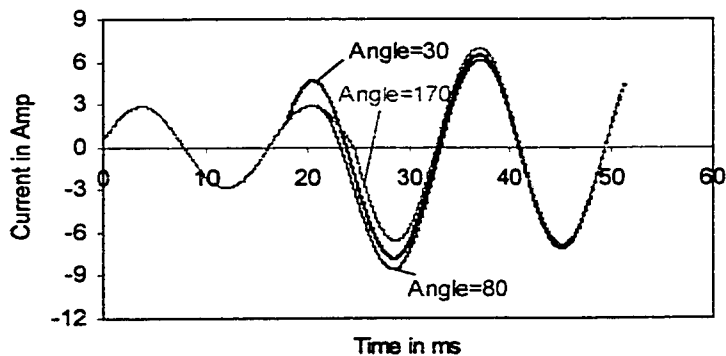


Fig. 4.9: Sensitivity study on switch timing for inductor bypassing.

To get further understanding, the peak transient current and duration corresponding to different switch time are computed. Here the switch time is represented by switch angle. Referring to Fig. 4.5, it is obvious that I_2 has the highest peak current during transient. Thus, here the peak transient current is the peak current of I_2 , which is in per unit, based on the steady-state current after switching. The duration is in milliseconds. The plots of peak current and duration versus switch angle are given in Fig. 4.10. The measured parameters are used in the analysis, i.e., $R=3.3922\Omega$, $L_1=0.0455H$, $L_2=0.0463H$, $M=0.0114H$.

Fig. 4.10 indicates that the maximum peak current occurs at $Angle=90^\circ$ and $Angle=270^\circ$, corresponding to the peak source voltage, and the zero duration occurs at $Angle=-8^\circ$ and $Angle=172^\circ$. It is interesting to notice that there are two ranges within which both the peak current and the duration are very low, $-8^\circ \sim 16^\circ$ and $172^\circ \sim 196^\circ$. In our case, the impedance angle before switching is 82° , so at $Angle=172^\circ$, the initial current is

$$I_1(0) = \frac{V_m}{z} \cos(\theta - \varphi) = \frac{V_m}{z} \cos(172^\circ - 82^\circ) = 0$$

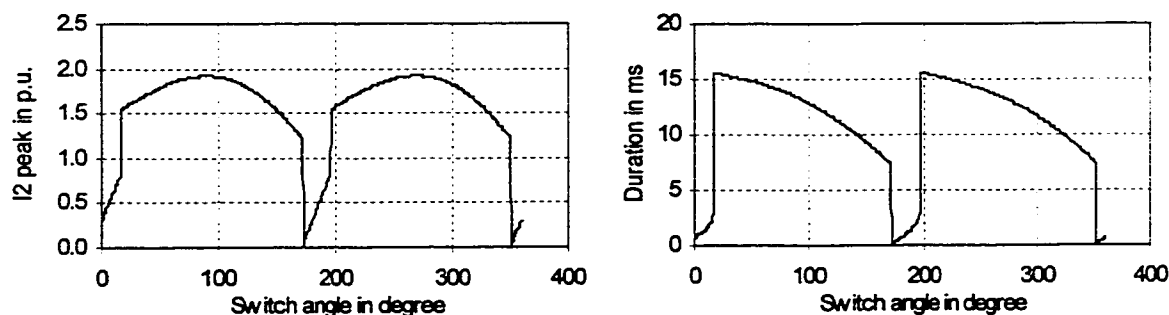


Fig. 4.10: Curves of peak transient current and duration vs. switch angle.

Similarly, the initial current for -8° is also zero. Therefore, we can say that *no transient will occur when the switches are operated at zero initial current*. In this case,

theoretically the switches S_1 and S_2 will operate at the same time under this condition. The angles 16° and 196° correspond to the last point when I_2 can be forced to cross zero before it increases. Obviously, the transient response is highly dependant on the instant of switch operation. *Therefore, by operating the switches within a certain range, the transient severity and the duration can be minimized.*

4.2.4 Effect of Some Factors on the Switching Transients

There are several factors that affect the transient response. These factors include resistance of the circuit, inductor self-inductance and the mutual coupling inductance. It is difficult to obtain an analytical relationship between the peak transient current and these factors. Therefore, a numerical technique is employed to perform the investigation.

Resistance is an important factor that affects the transient current and duration; it usually lowers the severity and shorten the duration. In this case, the inductance parameters are $L_1=0.0455H$, $L_2=0.0463H$, $M=0.0414H$, the resistance is variable and the switch is operated at $Angle=100^\circ$, assuming a 10° error for the worst case of 90° . The curves of I_2 peak and transient duration versus ratio R/X are obtained and shown in Fig. 4.11. The per unit current is based on the steady state current after switching. Here X is the self inductive impedance of a inductor segment. It is observed that

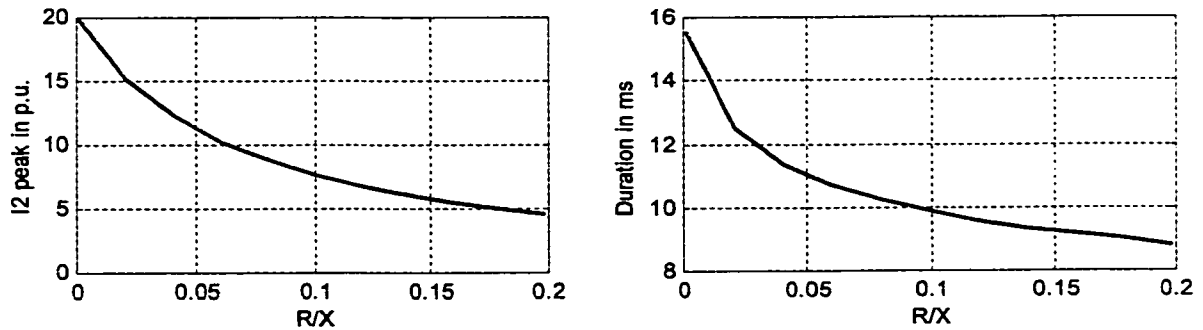


Fig. 4.11: Curves of transient current and duration vs. R for inductor bypassing.

- The peak transient current decreases with the increase of resistance. It is worth mentioning that the switch transient could be very severe if the resistance is very small.
- The duration of the transient also decreases with the increase of the resistance.

At extreme case when $R=0$, the frequency domain current formulas become

$$I_t = \frac{I_0}{s} - \frac{L_2 V(s)}{(L_1 L_2 - M^2)} = \frac{K_1}{s} - \frac{K_2}{s^2 + \omega^2}$$

$$I_1 = \frac{I_0}{s} - \frac{M V(s)}{(L_1 L_2 - M^2)} = \frac{K_3}{s} - \frac{K_4}{s^2 + \omega^2}$$

$$I_2 = \frac{(M - L_2) V(s)}{s(L_1 L_2 - M^2)} = \frac{K_5}{s} + \frac{K_6}{s^2 + \omega^2}$$

It is clear that in the time domain, there will be a DC component without decay in all three currents. This DC offset will delay the opening of switch S_1 , if it ever opens. It is important to know that if the mutual coupling is not strong enough to introduce an AC component to force the current to cross zero, the switch will never open, as indicated in Fig. 4.12.

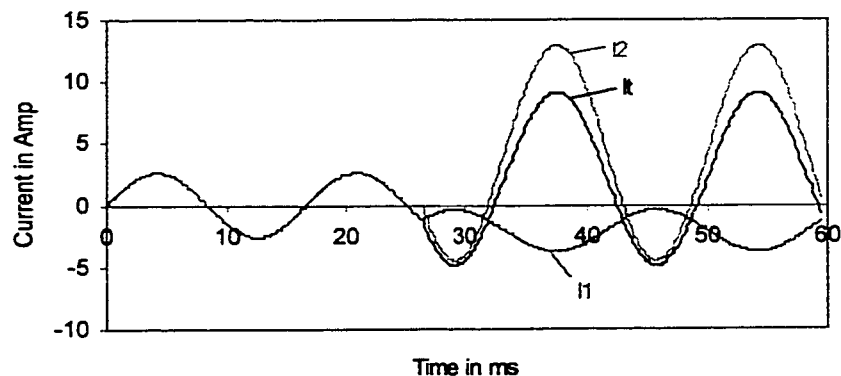


Fig. 4.12: Simulation of inductor bypassing transient for $R=0$.

The effect of L and M on switch transient is also investigated numerically. The curves of peak transient current and duration versus M for different L at worst case are obtained and shown in Fig. 4.13. In this case, R is constant: $R=3.3923\Omega$, the self-inductance and mutual inductance are variable.

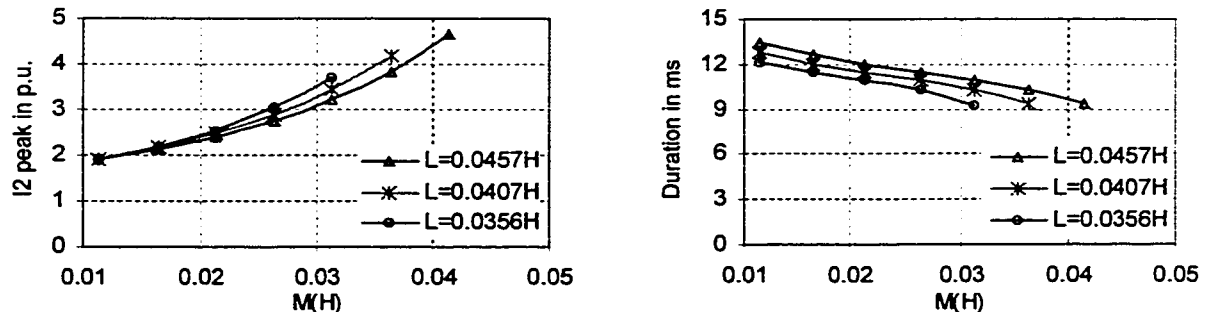


Fig. 4.13: Curves of I_2 peak and transient duration vs. M for different L .

- From the curves of I_2 peak vs. M in Figure 4.13, the peak transient current increases with the increase of mutual coupling inductance. With the same mutual coupling, I_2 peak is larger for smaller self-inductance. Therefore, we can conclude that *the peak transient current increases with the increase of the ratio M/L .*
- From the curves of duration vs. M in Figure 4.13, it is observed that the transient duration is shorter for closer mutual coupling. With the same mutual coupling, the duration is longer for larger self-inductance. In terms of ratio M/L , *the duration decreases with the increase of the ratio M/L .*

4.3 Transient Caused by Inductor Insertion

The initial state of the switches for inductor insertion is opposite to that of inductor bypassing, i.e., initially S_1 is open and S_2 is closed. The total inductance is increased after this operation.

4.3.1 Theoretical Analysis

Similar to inductor bypassing, the switching transient of inductor insertion consists of two phases. The first phase is the period when S_1 closes and S_2 is still conducting. The second phase is the period after S_2 opens.

The analysis of the first phase is the same as that of inductor bypassing except for different initial current conditions. The circuit when S_1 closes and S_2 is still conducting is the same as that of inductor bypassing shown in Fig. 4.2, and the frequency domain equivalent circuit is shown in Fig. 4.14.

Suppose the voltage source has the same form as before, $V_m \cos \omega t$. The steady-state current can be obtained as below:

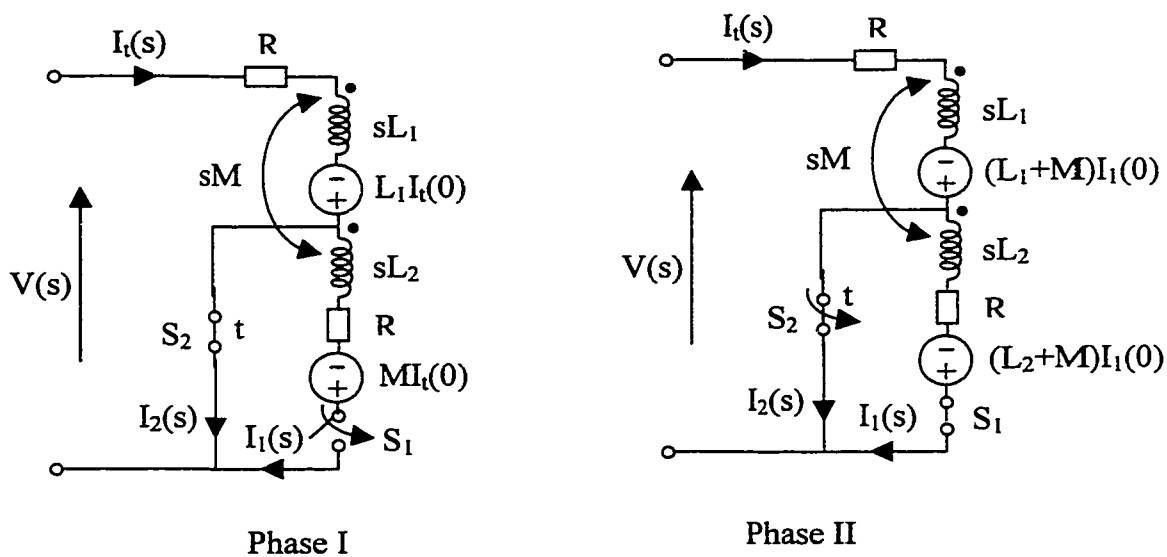


Fig. 4.14: Frequency domain equivalent circuit of inductor insertion.

$$Z = R + j\omega L_1 = z \angle \phi \ \Omega \quad (4.18)$$

$$i_t(t) = \frac{V_m}{Z} \cos(\omega t - \varphi) \text{ A} \quad (4.19)$$

The switch is operated at time t when $\omega t = \theta$, and the initial current $I_t(0)$ is

$$I_t(0) = \frac{V_m}{Z} \cos(\theta - \varphi) \text{ A} \quad (4.20)$$

Similarly with inductor bypassing, the voltage source is represented as

$$u(t) = V_m \cos(\omega t + \theta) \text{ V} \quad (4.21)$$

The Laplace transform of it is

$$V(s) = \frac{V_m (s \cos \theta - \omega \sin \theta)}{s^2 + \omega^2} \quad (4.22)$$

The voltage equations of Fig. 4.14, Phase I are

$$\begin{cases} I_t(R + sL_1) + sMI_1 = L_1 I_t(0) + V(s) \\ I_t sM + I_1(R + sL_2) = MI_t(0) \end{cases} \quad (4.23)$$

Solving the equations for I_t and I_1 , we have

$$\begin{aligned} I_t &= \frac{RI_t(0)L_1 + sI_t(0)(L_1L_2 - M^2) + (R + sL_2)V(s)}{s^2(L_1L_2 - M^2) + sR(L_1 + L_2) + R^2} \quad (4.24) \\ &= \frac{[RI_t(0)L_1 + sI_t(0)(L_1L_2 - M^2)](s^2 + \omega^2) + V_m(R + sL_2)(s \cos \theta_1 - \omega \sin \theta_1)}{[s^2(L_1L_2 - M^2) + sR(L_1 + L_2) + R^2](s^2 + \omega^2)} \end{aligned}$$

$$I_1 = \frac{RI_{i(0)}M - sMV(s)}{s^2(L_1L_2 - M^2) + sR(L_1 + L_2) + R^2} \quad (4.25)$$

$$= \frac{RMI_t(0)(s^2 + \omega^2) - V_m sM(s \cos \theta_1 - \omega \sin \theta_1)}{[s^2(L_1L_2 - M^2) + sR(L_1 + L_2) + R^2](s^2 + \omega^2)}$$

$$I_2 = I_t - I_1 \quad (4.26)$$

The poles of Equations 4.24 and 4.25 are the same as for Equations 4.10 and 4.11. However, since the initial conditions are different, the residues are different. The time domain currents have the same form as that of inductor bypassing currents.

When the current i_2 crosses zero, the switch S_2 opens and the second phase of transient begins. Suppose the second phase begins at t_1 , the initial current of L_1 and L_2 are the same $I_1(0)$, which is the instantaneous value of i_t at the instant t_1 . Suppose the voltage source has the form $V_m \cos(\omega t + \theta_1)$. The Laplace transform of the voltage source is of the same pattern as Equation 4.8. The voltage equation for the second phase is

$$(2R + s(L_1 + L_2 + 2M))I_t = V(s) + (L_1 + L_2 + 2M)I_1(0) \quad (4.27)$$

Solving the equation for I_t , we have

$$I_t = \frac{s^2(L_1 + M)I_1(0) + sV_m \cos \theta_1 - V_m \omega \sin \theta_1 + \omega^2(L_1 + M)I_1(0)}{S^3(L_1 + L_2 + 2M) + S^2 2R + s(L_1 + L_2 + 2M)\omega^2 + 2R\omega^2} \quad (4.28)$$

The time domain current can be obtained by inverse Laplace transform, which has the same pattern as in Equation 4.17. The above derivation is programmed in Matlab. The flow chart of the program is the same as Fig. 4.4. Fig. 4.15 shows the transient current when switches operate at $Angle = 30^\circ$, plotted by the Matlab program.

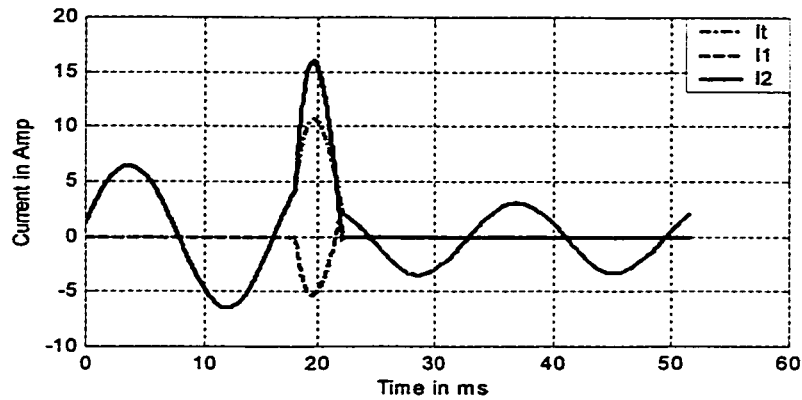


Fig. 4.15: Inductor insertion transient current waveforms.

4.3.2 Simulation and Experimental Study

An EMTP script is written to simulate the inductor insertion transient. The following circuit parameters are applied: $R=3.3922\Omega$, $L_1=0.0455H$, $L_2=0.0463H$, $M=0.0414H$, $V_m=80\sqrt{2}V$. Simulating time period $0 \sim 0.1s$, step $0.00033s$. Switch operation time: $0.018s$, corresponding to source voltage angle 30° . For comparison, the simulation and theoretical results are plotted in the same figure in Fig. 4.16.

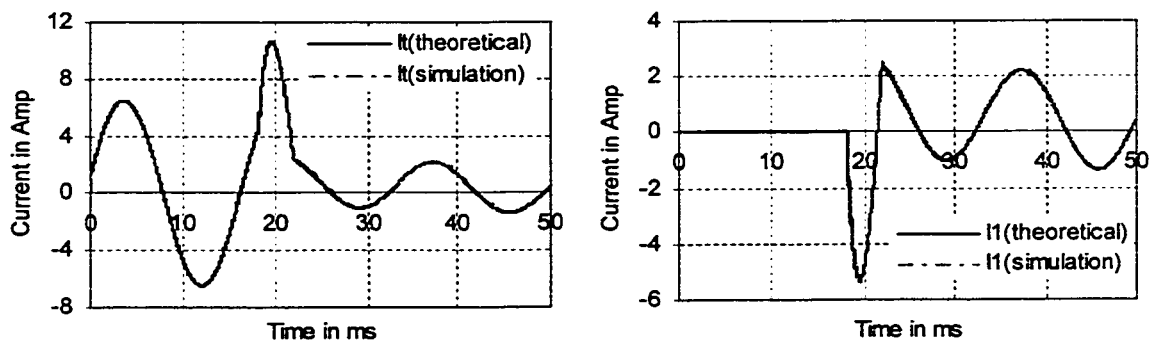


Fig. 4.16: Comparison between simulation and theoretical results.

It is obvious that the theoretical results are identical to the simulation results. The slight different is caused by the low numerical accuracy of EMTP. Therefore, it is reliable to use the theoretical analytical results to perform further investigation.

An experimental circuit is set up as shown in Fig. 4.1 and several measurements are taken on inductor insertion transient. The Nicolet system is used to record the transient waveforms. Several cases with different switching times are recorded. Fig. 4.17 shows a typical transient waveform we have recorded. The transient currents obtained by EMPT are plotted side by side with the measurement results. The waveforms are almost identical. Fig 4.17 indicates that the experimental circuit works as expected, and the conclusions of theoretical analysis can be considered applicable to the practical circuit.

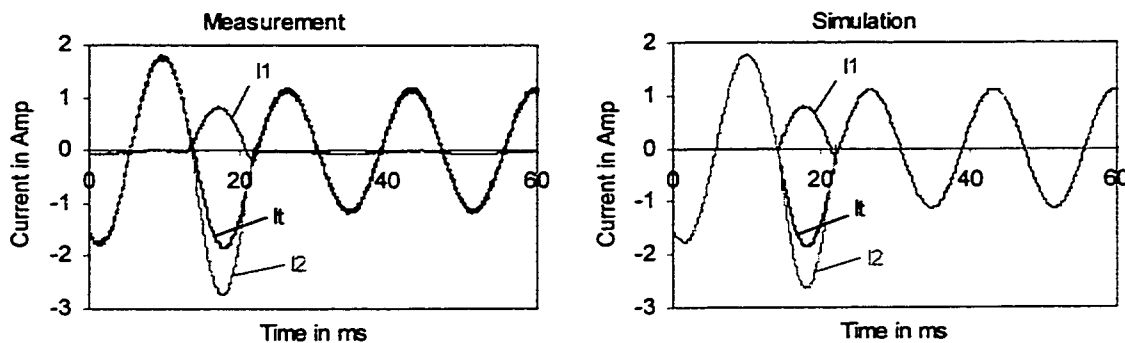


Fig. 4.17: Measurement and simulation current waveforms of inductor insertion.

4.3.3 Sensitivity Study on the Switch Timing

As concluded earlier, the severity of switch transient of inductor insertion is also determined by the instant of switch operation. To observe the effect of switch time on the transient current, current waveforms at different switch times are obtained from the Matlab program and demonstrated in Fig. 4.18.

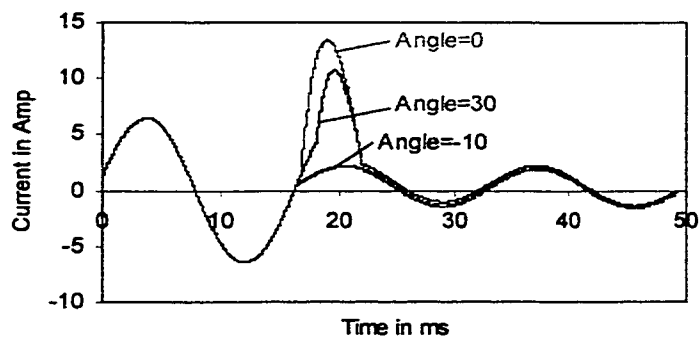


Fig. 4.18: Sensitivity study on switch timing.

Fig. 4.18 illustrates that the transient currents change significantly in response to the switch angle. Following the same procedure as 4.2.3, the relationship between the switch angle and I_2 peak current and transient duration is investigated. Fig. 4.19 shows the curves of I_2 peak and duration versus switch angle. The measured parameters are used in this analysis, i.e. $R=3.3922\Omega$, $L_1=0.0453H$, $L_2=0.0463H$, $M=0.0114H$. Different from the inductor bypassing, *the transient current is larger when the operating point is closer to zero-cross point of i_t .*

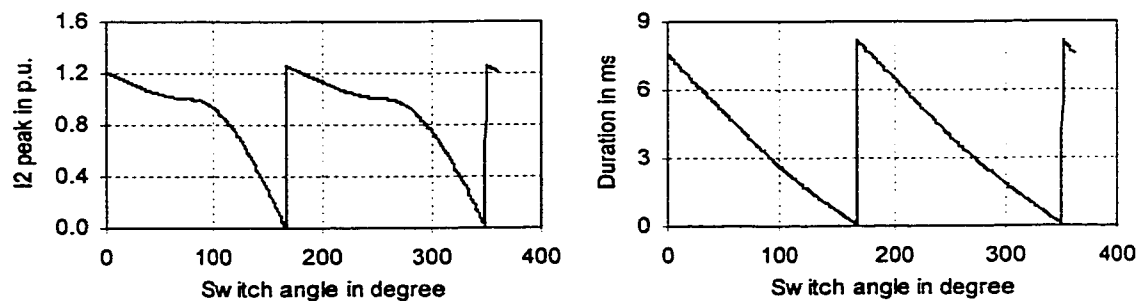


Fig. 4.19: Curves of I_2 peak and duration vs. switch angle.

In this case, when the initial current of inductor L_2 is zero, the transient current is determined solely by the induced voltage across the inserted inductor. This voltage can be represented as

$$V_{L_2} = j\omega M I_{total} = j\omega M \times \frac{V}{Z_1}$$

$$u_{L_2}(t) = \frac{\omega M V_m}{z_1} \cos(\omega t + 90 - \varphi_1)$$

A larger instantaneous value of this voltage at switch point will introduce a larger transient current. For *±maximum* voltage, corresponding to the minimum I_t

$$\omega t + 90^\circ - \varphi = \begin{cases} 180^\circ \\ 360^\circ \end{cases} \Rightarrow \omega t = \begin{cases} 90^\circ + \varphi \\ 270^\circ + \varphi \end{cases}$$

Taking the parameters given at 4.3.2, $\varphi = 78.82^\circ$. So the angles for maximum inducing voltage are

$$Angle_1 = \omega t = 168.82^\circ \text{ \& \ } Angle_2 = \omega t = 348.82^\circ$$

Fig. 4.19 shows that the maximum transient current occurs at $Angle = 169^\circ$ and $Angle = 349^\circ$, respectively, which confirms our analysis.

The transient current can be minimized by operating the switches at zero initial current. It is noticed that there is a period in Fig. 4.19 during which the transient current and duration are relatively low. Fig. 4.18 also shows a case that has almost no transient when the switch operates at zero initial current.

4.3.4 Effect of Some Factors on the Switching Transients

The effect of resistance, self-inductance and mutual inductance on the transient indices is investigated numerically. The same procedures are followed as in 4.2.4. To examine the effect of R , the resistance is variable and the inductance keeps constant. *The*

switch operates at zero current for the worst case. The curves of I_2 peak and transient duration versus R are obtained and shown in Fig. 4.20. The per unit current is based on the steady-state current before switch operation. It is observed that

- The peak transient current decreases with the increase of resistance. It worths mentioning that the switch transient could be very large if the resistance is very small.
- The duration of the transient also decreases with the increase of the resistance.

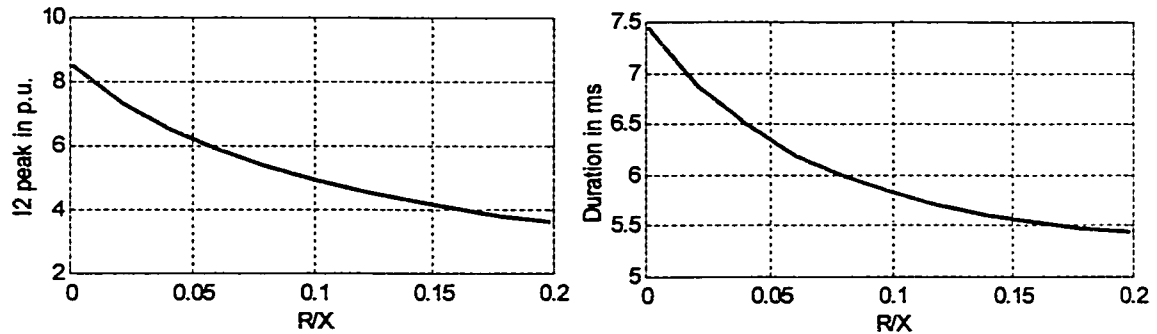


Fig. 4.20: Curves of transient current and duration vs. R .

At extreme case when $R=0$, the frequency domain currents are

$$I_t = \frac{I_0}{s} + \frac{L_2 V(s)}{s(L_1 L_2 - M^2)}, \quad I_1 = \frac{M V(s)}{s(M^2 - L_1 L_2)},$$

$$I_2 = I_t - I_1 = \frac{I_0}{s} + \frac{(L_2 + M)V(s)}{s(L_1 L_2 - M^2)}$$

It is clear that there is a DC component in I_2 and it remains in I_t without decay, as illustrated in Fig. 4.21. This DC offset delays the opening of switch S_2 . However, the delay could not be long since the forced part of I_2 will force the current to cross zero and allow the switch to turn off.

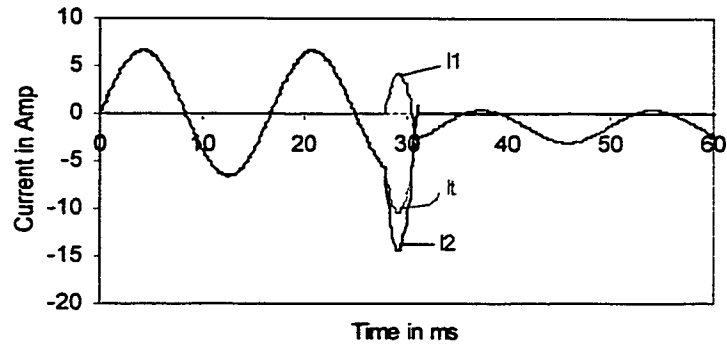


Fig. 4.21: Simulation of inductor insertion transient for $R=0$.

For the investigation of the effect of L and M on switching transient, the switches are still operated at the worst case. The curves of peak transient current and duration versus L and M are obtained and shown in Fig. 4.22.

- From Fig. 4.22, it is noted that the peak transient current increases with the increase of mutual coupling inductance. With the same mutual coupling, I_2 is larger for smaller self-inductance. Therefore, we can conclude that *the peak transient current increases with the increase of the ratio M/L* .
- Also from Fig. 4.22, it is observed that the transient duration is shorter for closer mutual coupling. With the same mutual coupling, the duration is longer for larger self-inductance. In terms of ratio M/L , *the duration decreases with the increase of the ratio M/L* .

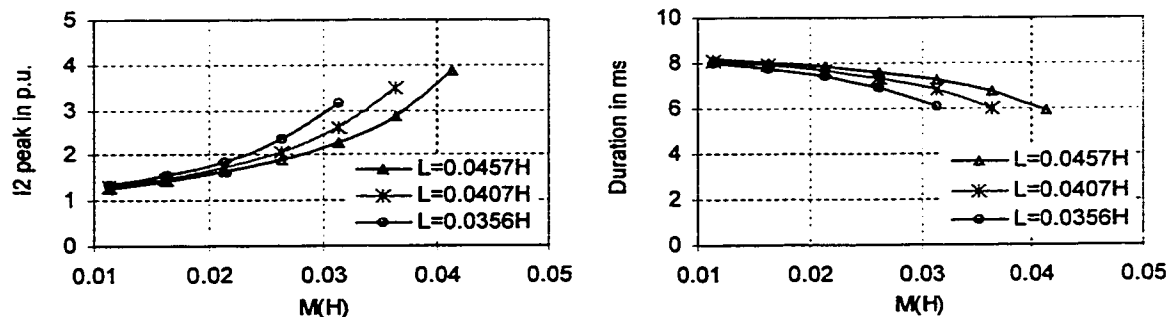


Fig. 4.22: Curves of I_2 peak and duration vs. M at different L .

4.4 Conclusions

Transient performance of the thyristor linked reactor is investigated to reveal the characteristics of the switching transient response. Although only a prototype is tested, the results shed light on the transient behavior of a practical device. There are two kinds of switch operations analyzed, inductor bypassing and inductor insertion. After its results are verified by EMTP simulation, the analytical method is used to conduct the switch sensitivity study. It is found that

- There are periods within which the peak transient current and duration are all low for inductor bypassing and insertion, respectively. These results provide a possible strategy to control the switch operation.
- The increase of the resistance can significantly reduce the switching transient. Whereas obviously the power loss will increase with the resistance, it is therefore a trade-off between switch performance and power loss at practical design.
- The increase of M/L causes higher peak transient current and shorter transient duration. This is useful information for the device design.
- The experimental results are precisely consistent with the analytical and simulation results.

The analysis presented in this chapter provides a basic understanding of the nature of the transient characteristic of the device, which facilitates further investigation of the performance of the device in other applications.

Chapter 5

Transient Performance of the Thyristor Linked Reactor in RLC Circuit

In this chapter, the transient performance of the thyristor linked reactor in a *RLC* circuit is analyzed. Laplace transform is applied to conduct the theoretical analysis. The sensitivity study of switch timing is performed and the impact of resistance, self inductance and mutual inductance on the switching transients is also investigated. Damping coefficient is used to evaluate the duration of the transient. EMTP simulation and experimental test are taken to confirm the analytical results.

5.0 Introduction

The primary potential application of the thyristor linked reactor is a tunable filter, which can be simply viewed as a *RLC* circuit. The analysis in chapter 4 indicates that the transient performance of the device in a *RL* circuit is determined by the parameters of the device and the switch operation. In *RLC* circuit, we still expect certain impacts of those factors on the transient performance of the device. The transient performance of the device in *RLC* circuit is analyzed in this chapter for providing the necessary information for the design of a good performing variable inductor.

The analysis of switching transient of a variable inductor in a *RLC* circuit will use similar procedures as used in chapter 4 except for the study of transient duration. Sensitivity study of switch timing is still an important aspect to be investigated and the impact of resistance, self impedance and mutual coupling impedance on the transient response will also be examined. Noting that the components of transient currents of the

RLC circuit are different from that of the *RL* circuit, the definition of transient duration in chapter 4 is not applicable here. The duration of the switch transient is thereby evaluated by the damping coefficient, which reflects the damping process of the natural component of the transient current.

5.1 Transient Caused by Inductor Bypassing

Fig. 3.12 of chapter 3 can be referred to for the circuit of a tunable filter, and the frequency domain equivalent circuit of inductor bypassing is shown in Fig. 5.1. For inductor bypassing, S_1 is initially closed and S_2 is open. S_2 closes at a certain time and S_1 opens when the current flowing through it hits zero.

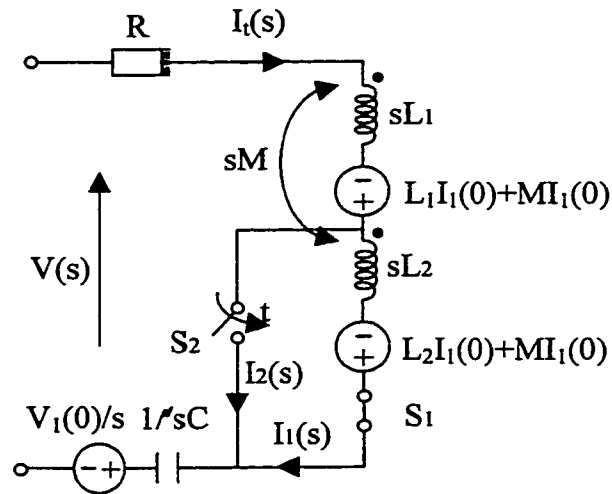


Fig. 5.1: Frequency domain equivalent *RLC* circuit.

5.1.1 Theoretical Analysis

The transient response of the *RLC* circuit is also divided into two phases. The first phase is the time period from switch S_2 closes till S_1 opens, and the second phase begins when S_1 opens. Fig. 5.1 is a simple second order circuit with sinusoidal voltage source. The steady state voltage and current can be calculated by phasors and complex impedance. Laplace transform is used to conduct transient analysis. Suppose the voltage

source has the form of $V_m \cos \omega t$. Similar to the analysis of RL circuit, the steady-state condition before switching can be obtained as follows:

$$Z = R + j\omega(L_1 + L_2 + 2M) - j\frac{1}{\omega C} = z \angle \varphi \quad \Omega \quad (5.1)$$

$$i_t(t) = \frac{V_m}{z} \cos(\omega t - \varphi) \text{ A} \quad (5.2)$$

The switch is operated at time t when $\omega t = \theta$, and the initial current $I_1(0)$ and capacitor voltage $V_1(0)$ are

$$I_1(0) = \frac{V_m}{z} \cos(\theta - \varphi) \text{ A} \quad (5.3)$$

$$V_1(0) = \frac{V_m}{z\omega C} \cos(\theta - \varphi - 90^\circ) \text{ V} \quad (5.4)$$

The voltage equations are

$$\begin{cases} I_t(R + sL_1 + \frac{1}{sC}) + sMI_1 = (L_1 + M)I_1(0) - \frac{V_1(0)}{s} + V(s) \\ I_t sM + I_1(R + sL_2) = (L_2 + M)I_1(0) \end{cases} \quad (5.5)$$

Solve the equations to get the current I_t and I_1 ,

$$I_t = \frac{[V(s) + I_1(0)(L_1 + M) - \frac{V_1(0)}{s}](sL_2 + R) - sM(L_2 + M)I_1(0)}{(R + sL_1 + \frac{1}{sC})(sL_2 + R) - s^2 M^2} \quad (5.6)$$

$$I_1 = \frac{(R + sL_1 + \frac{1}{sC})(L_2 + M)I_1(0) - sM[I_1(0)(L_1 + M) - \frac{V_1(0)}{s}] - sMV(s)}{(R + sL_1 + \frac{1}{sC})(sL_2 + R) - s^2M^2} \quad (5.7)$$

Given the initial voltage of the capacitor and the current i_t , the capacitor voltage can be expressed as

$$V_c = \frac{V_1(0)}{s} + \frac{I_t}{sC} \quad (5.8)$$

Use the measurement parameters of resistance and inductance, as well as the capacitance $C=40.1\mu F$. Suppose the switch is operated at Angle $\theta=190^\circ$, substitute the parameters in Equations 5.6 and 5.7 and inverse transform the current to time domain expressions,

$$i_t = 0.001e^{-73.31t} + 4.9165e^{-42.11t} \cos(763.8t - 98.54^\circ) + 2.2488\cos(377t - 84.09^\circ) \quad (5.9)$$

$$i_1 = -0.4046e^{-73.31t} + 1.2105e^{-42.11t} \cos(763.8t + 86.94^\circ) + 0.5435\cos(377t + 106.9^\circ) \quad (5.10)$$

$$i_2 = i_t - i_1 \quad (5.11)$$

$$v_c = -0.37e^{-73.31t} + 165.4e^{-42.11t} \cos(762.9t - 168^\circ) + 149.2\cos(377t - 174^\circ) \quad (5.12)$$

Observe the expressions, it is noticed that there are two decaying components in the switching transient response; one is a DC component and the other is a sinusoidal component with natural frequency of $f_N = 736.8/2\pi = 117.27\text{ Hz}$. The natural frequency can also be calculated from the following formula:

$$f_N = \frac{1}{2\pi\sqrt{LC}} \quad (5.13)$$

where L is the total inductance after switching,

C is the capacitance of the circuit.

This is the first phase of the transient. The second phase begins when S_1 opens. Suppose the switch opens at t_l when $i_l=0$. The initial inductor current $I_l(0)$ for S_1 opening is the instantaneous current of i_l at the time t_l and the capacitor voltage at this point is the initial voltage $V_2(0)$. The voltage equation for the second phase is

$$(R + sL_1 + \frac{1}{sC})I_t = V(s) + L_1I_l(0) - \frac{V_2(0)}{s} \quad (5.14)$$

Solving the equation for I_t , we have

$$I_t = \frac{V(s) + L_1I_l(0) - \frac{V_2(0)}{s}}{R + sL_1 + \frac{1}{sC}} \quad (5.15)$$

Following the calculation of the first phase, the time domain current of the second phase can be computed and expressed as

$$i_t = 3.79e^{-37.28t} \cos(739.4t - 131.7^\circ) + 2.3 \cos(377t - 31.2^\circ) \quad (5.16)$$

It is interesting to note that there is no DC component in the second phase response. The reason is that the switch S_1 only opens at zero current, i.e., the initial inductor current is zero.

The derivation above is programmed in Matlab to demonstrate the analytical results. The flow chart is almost the same as in Fig. 4.4, with addition of the calculation

of capacitor voltage. The current waveforms for switch $Angle=190^\circ$ are shown in Fig. 5.2.

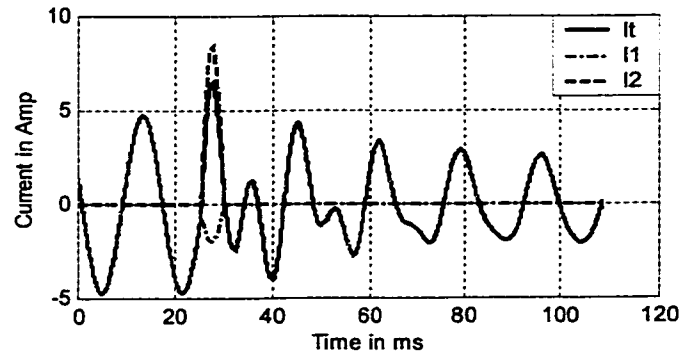


Fig. 5.2: Switch transient current of RLC circuit.

5.1.2 Simulation and Experimental Study

An EMTP script is written to simulate the inductor bypassing transient in the RLC circuit. The results are taken as reference to verify the analytical results. The following circuit parameters are applied: $R=3.3922\Omega$, $L_1=0.0455H$, $L_2=0.0463H$, $M=0.0414H$, $C=40.1\mu F$, $V_m=80\sqrt{2}V$; simulating time period $0 \sim 0.1s$, step $0.00033s$; switch operation time: $0.0138s$, corresponding to source voltage angle 300° .

The theoretical results are plotted in the same figure as the simulation result and are shown in Fig. 5.3. It can be seen that the simulation result and the theoretical result are identical, which indicates that the theoretical analysis is correct and can be applied to further study.

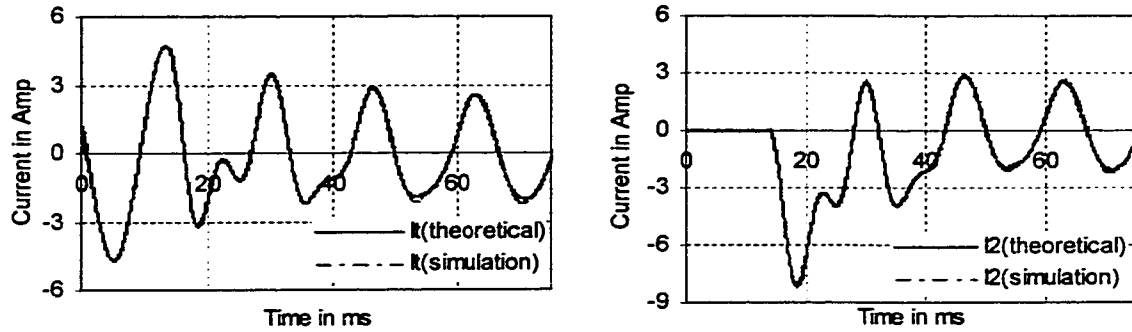


Fig. 5.3: Comparison between simulation and theoretical result.

An experimental circuit as in Fig. 3.13 is set up to conduct a practical test. The switching transient waveforms are captured by the Nicolet system. Fig. 5.4 shows a typical recorded case, and simulation waveforms are plotted side by side with it. It is observed that the measurement and simulation waveforms are almost identical to each other. The slight difference between them could be due to the error of the parameters used in the simulation script. Observing the waveforms, we can see that

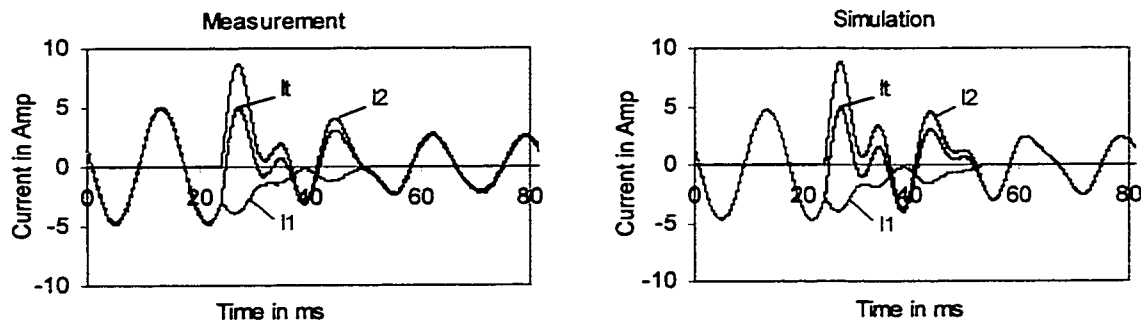


Fig. 5.4: Measuring current waveforms for RLC switch transient.

- Similar to the RL circuit, the variation of inductance in the RLC circuit causes a relatively large transient current.
- Different from the RL circuit, the transient does not die out immediately after the series switch opens due to the natural frequency component in i_t . Thus the duration of the switch transient in the RLC circuit is longer than in that of the RL circuit.

- The results once again confirm the correctness of the theoretical analysis and also indicate that the experimental circuit works as expected. The next few sections will conduct other analysis using the Matlab program based on the theoretical analysis.

5.1.3 Sensitivity Study on Switch Timing

Based on the Matlab program developed in the last section, a sensitivity study of switch timing is conducted theoretically. Consider a more realistic case, $R/X=0.1$, $M/L=0.5$, i.e., $R=1.71\Omega$, $L_1=0.0455H$, $L_2=0.0463H$ and $M=0.0229H$. Now examine the effect of switch angle on I_2 peak current. The switch angle is changed from $0 \sim 360^\circ$ and the corresponding peak transient currents are obtained. The per-unit current is based on the steady-state current before switching, which is larger than the post-switching steady-state current. According to formula 5.13, the natural frequency of the post-switching circuit is $117.8Hz$. The curve of I_2 peak versus switching angle is shown in Fig. 5.5. Fig. 5.6 shows the best case when the switch Angle = 14° . The impedance angle before switching is

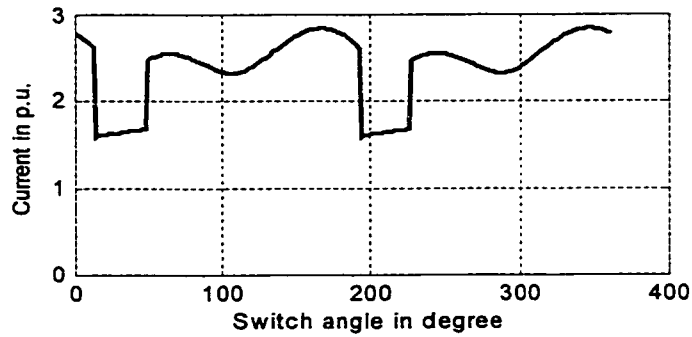


Fig. 5.5: I_2 peak in p. u. vs. switch angle.

$$\begin{aligned}
 Z &= 2R + j\omega(L_1 + L_2 + 2M) - j\frac{1}{\omega C} \\
 &= 2 \times 1.71 + j2 \times \pi \times 60(0.0455 + 0.0463 + 2 \times 0.0229) - j\frac{1}{2\pi \times 60 \times 40.1 \times 10^{-6}} \\
 &= 3.42 - j14.275 = 14.769 \angle -76^\circ \Omega
 \end{aligned}$$

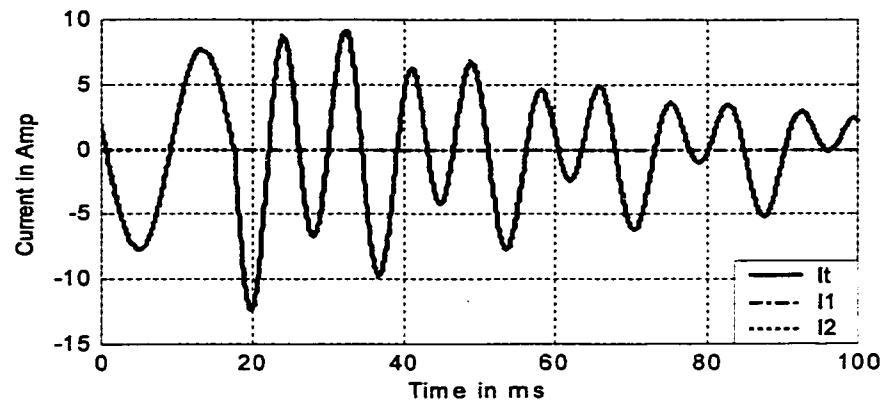


Fig. 5.6: Current waveforms when switch angle is 14° .

Observing the curve, it can be seen that

- The smallest transient occurs at 14° . The impedance angle is -76° . So when the voltage phase angle is 14° , the current phase angle is 90° , which is the current zero cross point. Therefore, the best case happens at zero initial current for the *RLC* circuit. The peak current in this case is $1.6 p. u.$
- It is important to note that the severest transient does not occur at peak initial current. This is different from the inductor bypassing transient in the *RL* circuit, due to the fact that the transient response in the *RLC* circuit is not only determined by the initial current but also by the initial voltage, i.e., the capacitor voltage at the switch instant. When the effect of these two initial conditions is added, the severest transient occurs. In this case, it happens at source voltage phase angles of 167° and 347° . Observation of some other cases indicates that the worst case occurs about $20^\circ \sim 30^\circ$ before the current zero cross point.
- In Fig. 5.5, there are periods within which the peak transient currents are relatively low, They are $14^\circ \sim 47^\circ$ and $194^\circ \sim 227^\circ$, the peak current is around $1.65 p. u.$
- It is obvious that the peak transient current does not change much with the switch angle. The problem here is the transient duration. It takes a long time for the natural frequency component to die out, even in the best case.

5.1.4 Effect of Some Factors on the Switching Transients

Resistance is a factor that damps the transient currents. It plays an important role in a *RLC* switch transient. To examine the impact of resistance on the transient response, the self and mutual inductance are kept constant, while the R/X ratio is variable, where X is the self inductive impedance of one inductor segment. Fig. 5.7 is a curve of I_2 peak current in per unit versus R/X ratio. Parameters applied in this study are as follows: $M=0.0229H$, $L_1=0.0455H$, $L_2=0.0463H$. The switch is operated at time t when $\omega t = 270^\circ + \varphi - 30^\circ = 240^\circ + \varphi$, corresponding to the worst case, as discussed earlier. It is noted that the peak transient current decreases almost linearly with the increase of R/X , which means that the resistance can effectively mitigate the transient current.

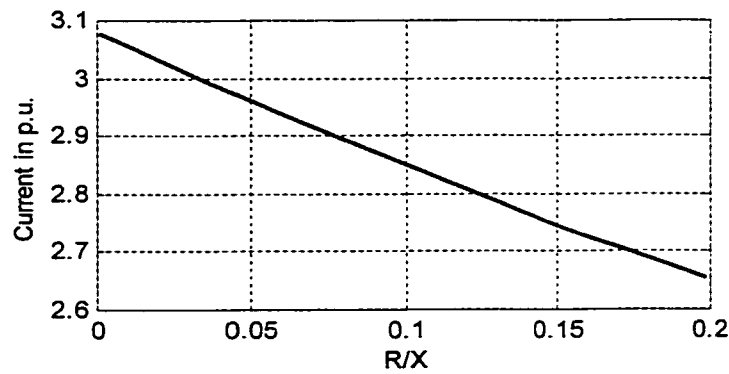


Fig. 5.7: Curve of I_2 peak in p. u. vs. R/X .

The duration of the transient is hard to define for the *RLC* circuit due to the presence of the natural frequency component. In this case, the transient process can be explored through a damping coefficient. This coefficient is defined as $\delta = \frac{R}{2L}$ and the attenuation factor of the natural frequency component is $e^{-\delta t}$. Therefore, the smaller the damping coefficient the faster the natural frequency component decays; in other words, it takes a shorter time for the transient to settle down when the system has bigger

resistance. The effect of resistance on the transient duration will be further investigated later.

The effect of L and M on the switching transient in the RLC circuit is also examined. In this case, the resistance is a constant of 1.71Ω while the self and mutual inductance are variable. Fig. 5.8 shows the curves of the peak transient current versus M . The switch is operated at t when $\omega t = 270^\circ + \varphi - 30^\circ = 240^\circ + \varphi$ for the worst case. The per-unit peak current is based on the steady-state current before switching.

From Fig. 5.8, it is noted that the peak transient current increases with the increase of M and that for the same M , the peak current is larger for smaller L . I.e., the peak current increases with the increase of M/L . Moreover, when the mutual coupling is very strong, the peak transient current could be very high. For example, in Fig. 5.8 when $M/L=0.91$, the peak transient current is 7 p. u..

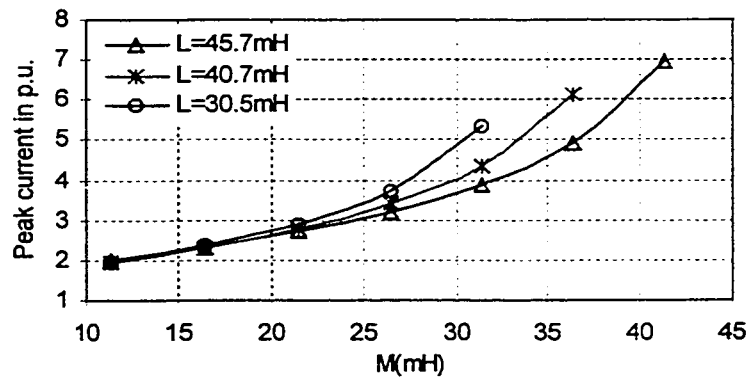


Fig. 5.8: The effect of L and M on transient peak current in RLC circuit.

5.2 Transient Caused by Inductor Insertion

Inductor insertion is a reverse operation to inductor bypassing. The circuit is the same as with inductor bypassing, but the status of the switches are different. In this case,

S_1 is initially open and S_2 is closed. Thus, the initial current of L_1 is zero. Following the same procedures as inductor bypassing, the initial conditions of inductor($I_t(0)$) and capacitor($V_c(0)$) can be obtained.

5.2.1 Theoretical Analysis

The switching transient of the inductor insertion consists of two phases; Phase I is the period when S_1 closes while S_2 is still conducting. Phase II is the period after S_2 opens. Assuming switch S_1 closes at time t when $\alpha t = \theta$, the corresponding frequency domain voltage equations are shown below:

$$\begin{cases} I_t(R + sL_1 + \frac{1}{sC}) + sMI_1 = L_1 I_t(0) - \frac{V_1(0)}{s} + V(s) \\ I_t sM + I_1(R + sL_2) = MI_t(0) \end{cases} \quad (5.17)$$

Solving the equations to get the current I_t and I_1 ,

$$I_t = \frac{[V(s) + I_t(0)L_1 - \frac{V_1(0)}{s}](sL_2 + R) - sM^2 I_t(0)}{(R + sL_1 + \frac{1}{sC})(sL_2 + R) - s^2 M^2} \quad (5.18)$$

$$I_1 = \frac{(R + sL_1 + \frac{1}{sC})MI_t(0) - sM[I_t(0)L_1 - \frac{V_1(0)}{s} + V(s)]}{(R + sL_1 + \frac{1}{sC})(sL_2 + R) - s^2 M^2} \quad (5.19)$$

$$I_2 = I_t - I_1 \quad (5.20)$$

$$V_c = \frac{V_1(0)}{s} + \frac{I_t}{sC} \quad (5.21)$$

The time domain current expressions can be obtained by a reverse transform of Equations 5.18 and 5.19. The same as with the inductor bypassing, the currents consist of three components: decaying DC component, decaying sinusoidal component with natural frequency, and forced component with a frequency of 60Hz. The natural frequency is not the same as that of inductor bypassing. Time domain capacitor voltage can also be obtained by the inverse transform of Equation 5.21.

Switch S_2 opens when its current is zero, supposedly at time t_l , which means inductor L_1 and L_2 have the same initial current. The initial capacitor voltage is determined by the instantaneous value of the capacitor voltage expression at t_l . Supposing the initial current and voltage are $I_l(0)$ and $V_2(0)$, respectively, the frequency domain voltage equation is

$$(2R + sL_1 + sL_2 + s2M + \frac{1}{sC})I_t = V(s) + (L_1 + L_2 + 2M)I_1(0) - \frac{V_2(0)}{s} \quad (5.22)$$

$$I_t = \frac{V(s) + (L_1 + L_2 + 2M)I_1(0) - \frac{V_2(0)}{s}}{s(L_1 + L_2 + 2M) + 2R + \frac{1}{sC}} \quad (5.23)$$

A time domain expression is attained by partial fraction expansions. Following the same procedures as in the inductor bypassing, a Matlab program is developed to demonstrate the theoretical results. The measured parameters are applied. The waveforms at switch angle $\theta = 300^\circ$ are illustrated in Fig. 5.9.

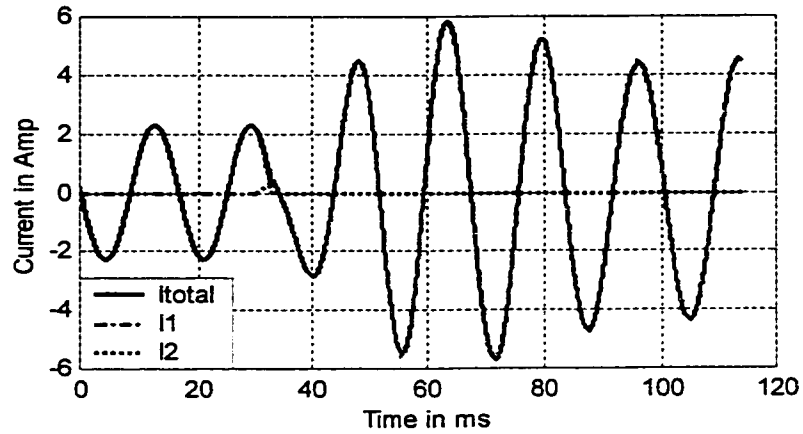


Fig. 5.9: Transient current for inductor insertion.

5.2.2 Simulation and Experimental Study

An EMTP script is written to simulate the inductor insertion transient in the RLC circuit. The following circuit parameters are applied: $R=3.3922\Omega$, $L_1=0.0455H$, $L_2=0.0463H$, $M=0.0114H$, $C=40.1\mu F$, $V_m=80\sqrt{2} V$; simulating time period $0 \sim 0.1s$, step $0.00067s$; switch operation time: $0.0138s$, corresponding to source voltage angle 300° . The theoretical results at the same situation as simulation are also obtained and plotted together with the simulation results for comparison, as shown in Fig. 5.10.

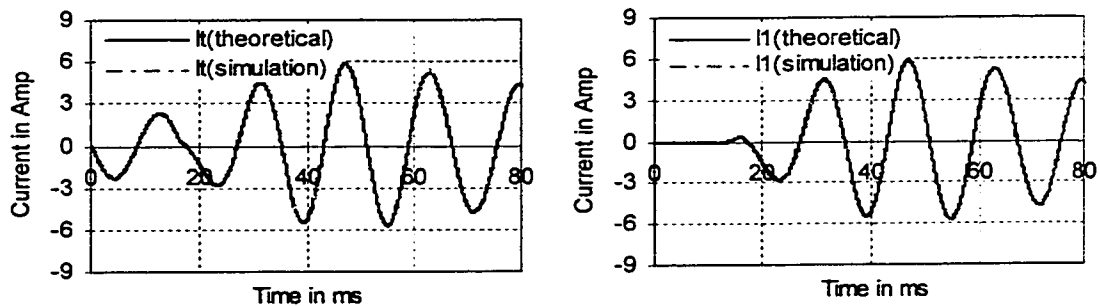


Fig. 5.10: Comparison between analysis and simulation results of inductor insertion.

It is obvious that the theoretical and simulation results are perfectly identical; therefore, the correctness of the theoretical analysis is verified. The Matlab program based on theoretical analysis will be used for further investigation.

An experimental circuit is set up to observe the operation of a practical variable inductor. The transient current waveforms are recorded by the Nicolet system when inserting an inductor segment into the circuit. The simulation results under the same condition as measurement are shown side by side with the recorded waveforms in Fig. 5.11.

Not surprisingly, the measurement results and the simulation results are almost identical to one another. This, once again, assures that the theoretical analysis is correct and the proposed variable inductor can work as expected.

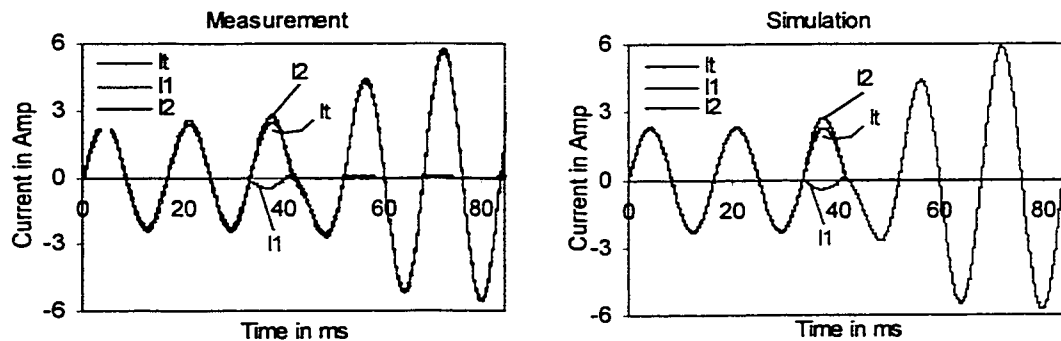


Fig. 5.11: Measurement and simulation current waveforms of inductor insertion.

5.2.3 Sensitivity Study on the Switch Timing

Based on the Matlab program developed in the last section, the impact of the switch operation time on the transient current is examined analytically. The switch angle is changed from 0° ~ 360° and the corresponding peak transient currents are obtained. Hence, a curve of per unit peak current versus the switch angle is plotted and shown in Fig. 5.12. The per-unit current is based on post-switching steady-state current. The

following parameters are used for a more realistic case: $R=1.71\Omega$, $L_1=0.0455H$, $L_2=0.0463H$, $M=0.0214H$. The natural frequency of the post-switching circuit is $f_N=67.6Hz$. The impedance angle before switching is

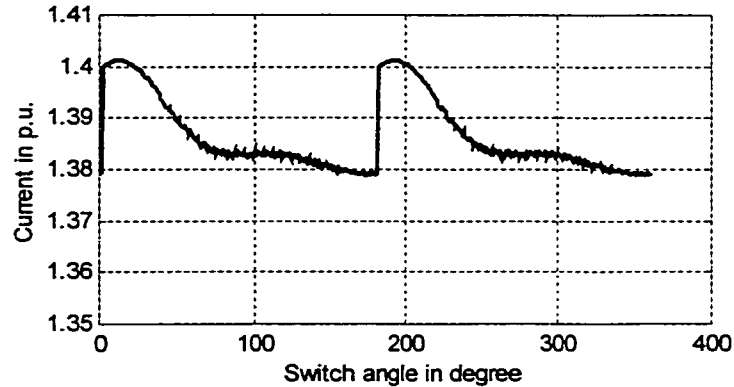


Fig. 5.12: I_1 peak current in p. u. vs. switch angle.

$$\begin{aligned}
 Z &= R + j\omega L_1 - j\frac{1}{\omega C} \\
 &= 1.71 + j2\pi \times 60 \times 0.0455 - j\frac{1}{2\pi \times 60 \times 40.1 \times 10^{-6}} \\
 &= 1.71 - j49 = 49.07 \angle -88^\circ \Omega
 \end{aligned}$$

Fig. 5.12 indicates that

- The peak transient currents are not very large, ranging from $1.38 \sim 1.4$ p. u. It is important to note that the peak current does not change much with the variation of switch angle. *Therefore, we can conclude that the current stress is not high for inductor insertion.*
- The slightest transient occurs when the switch angle is 2° , corresponding to the zero initial current, similar to inductor bypassing, while the severest transient occurs at about $10^\circ \sim 20^\circ$ after the current zero cross point.

5.2.4 Effect of Some Factors on the Switching Transients

First, we want to examine the effect of resistance on the switching transients of inductor insertion. As pointed out earlier, the severest transient occurs when the switch operates right after the zero cross point of the inductor current. Take 10° after the current zero cross point as the switch operation point for the worst case. Keeping the self and mutual inductance constant and varying the resistance, the corresponding peak transient currents are obtained. The following parameters are applied: $L_1=0.0455H$, $L_2=0.0463H$, $M=0.0229H$. The curve of I_1 peak versus R/X ratio is plotted and shown in Fig. 5.13. We can see from Fig. 5.13 that the peak transient still decreases with the increase of resistance, which clearly shows the damping effect of the resistance.

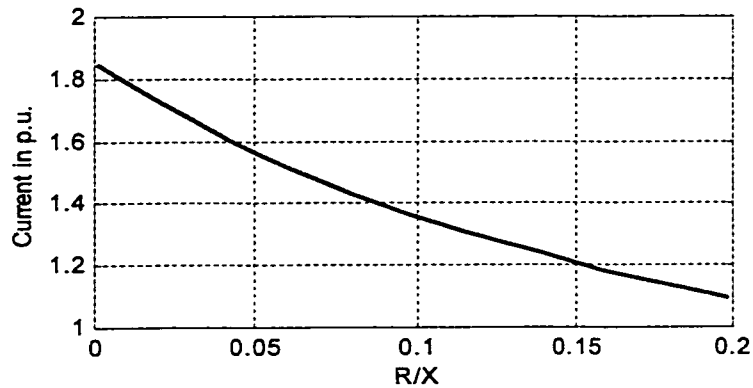


Figure 5.13: Curve of I_1 peak vs. R/X ratio.

The effect of L and M on the transient current is also investigated. In this case, the resistance is kept constant while the self and mutual inductance are variable. The switch is operated at 10° after the current zero cross point. The corresponding peak transient currents are obtained and the curves of peak current versus M are shown in Fig. 5.14. The per-unit current is based on the steady-state current before switching. The figure shows that

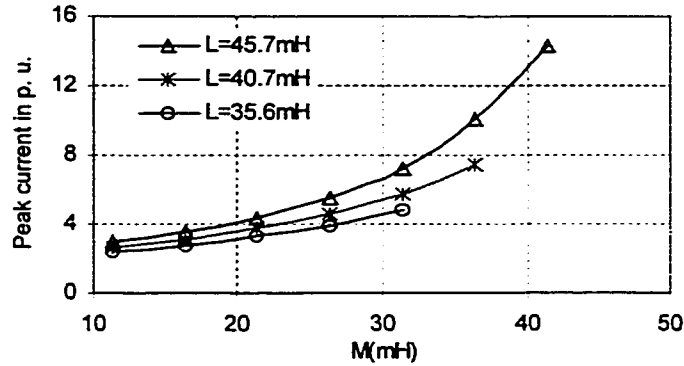


Fig. 5.14: Peak current I_l in per unit vs. M.

- The peak current vs. M increases with the increase of M. As well, for the same M, the peak current is larger for smaller L; i.e., the peak current increases with the increase of M/L .
- In this case, the pre-switching steady-state current is taken as the base, which results in high per unit current. For example, the last point of curve for $L=45.7mH$ is more than $14 p. u.$. These per unit values actually do not reflect the real current situation, since this base current is much smaller than the post-switching steady-state current and the circuit should be designed according to the largest steady-state current. Taking the pre-switching current as base yields the advantage that each curve has only one base current. Based on the post-switching steady-state current, the peak current is less than $1.5 p. u.$
- The severest transient happens after S_2 opens, which is different from that in inductor bypassing.

5.3 Analysis of Voltage Stress on the Switches

The voltage stress on the switches of a TLR in RLC circuit is investigated. Both switching transients of inductor bypassing and insertion are analyzed.

5.3.1 Inductor Bypassing

Refer to Fig. 5.1 for the frequency domain equivalent circuit. As analyzed earlier, the switching transient consists of two phases. The first phase is the time period when two switches are all conducting. During this period, the voltages on the two switches are all zero. The second phase is the time after S_1 opens. In this phase, S_2 is conducting and the voltage drop on the switch is zero. S_1 is open and the voltage across it is the voltage induced on L_2 by mutual coupling. Therefore, the only transient voltage needs to be derived is the voltage on S_1 at second phase.

5.3.1.1 Theoretical Analysis

As analyzed before, the frequency domain current at second phase is

$$I_t = \frac{V(s) + L_1 I_t(0) - \frac{V_2(0)}{s}}{R + sL_1 + \frac{1}{sC}} \quad (5.24)$$

The voltage on switch S_1 is

$$V_{s1} = MI_t(0) - sMI_t \quad (5.25)$$

The time domain voltage can be obtained by partial fraction expansions. Use the measurement parameters in the calculation, i. e., $R=3.3922\Omega$, $L_1=0.0455H$, $L_2=0.0463H$, $M=0.0114H$, $C=40.1\mu F$. The initial conditions of the circuit are determined by the time of switch operation. Now take the time corresponding to the switch angle= 190° as switching time. The time domain voltage is expressed as

$$u_{s1} = 32.01e^{-37.28t} \cos(739.4t + 43.93^\circ) + 9.912 \cos(377t - 58.77^\circ)V \quad (5.26)$$

The derivation above is programmed in Matlab and the voltage waveforms of switch S_1 and S_2 are shown in Fig. 5.15. The steady state voltage on S_2 before switching can be calculated as

$$V_{s_2,pre} = \left| \frac{V_m(R + j\omega L_2 + j\omega M)}{2R + j\omega(L_1 + L_2 + M) - j1/(\omega C)} \right| = 102.8V \quad (5.27)$$

From the waveforms, it is observed that the post switching voltage of S_1 is much lower than the pre-switching voltage, due to the fact that this voltage is resulted only from mutual coupling. The forced voltage component is only 9.9V, with a decaying natural component imposed on it. Therefore, comparing with the steady state switch voltage before switching, which is 102.8V, the transient voltage is not high at all.

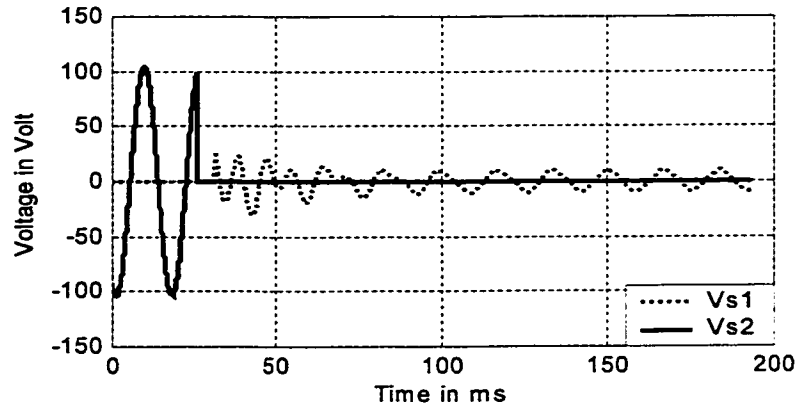


Fig. 5.15: Switch voltage waveforms for inductor bypassing.

5.3.1.2 Sensitivity Study of Switch Timing

Similar to the impact of switch timing on transient current, the transient voltage is also affected by the instant of switch operation. The peak transient voltages are calculated corresponding to different switch angle. The following parameters are used in the computation: $R/X=0.1$, $M/L=0.5$, i.e., $R=1.17\Omega$, $L_1=0.0455H$, $L_2=0.0463H$, $M=0.0229H$.

The peak voltage is in per-unit based on the steady state voltage on the switch before switch operation. Fig. 5.16 shows the curve of peak voltage versus switch angle.

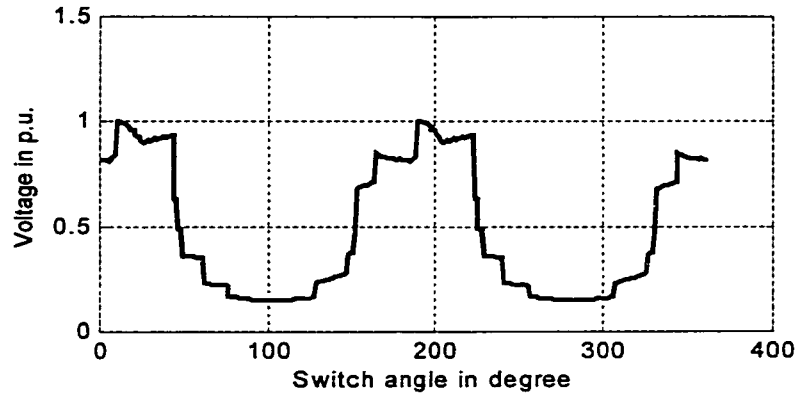


Fig. 5.16: Curve of peak transient voltage v. s. switch angle ($M/L=0.5$).

Fig. 5.16 indicates that the peak voltage varies with the switch angle. However, the maximum peak voltage never goes higher than the steady state voltage (per unit voltage is always less than 1). Therefore, the voltage stress at this case is not a big concern. For a higher M/L ratio, we can expect severer voltage transient since the energy stored in the inductor is larger. The curve of peak transient voltage versus switch angle when $M/L=0.95$ is obtained and shown in Fig. 5.17. It can be seen that the peak transient voltage can be as high as 1.9 p. u..

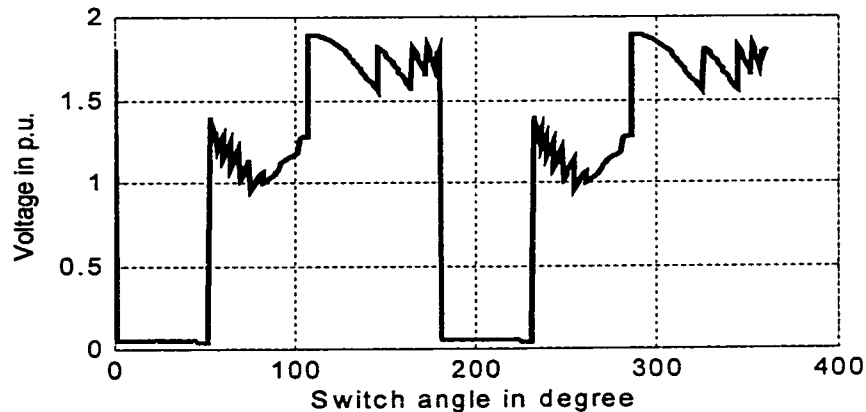


Fig. 5.17: Curve of peak transient voltage versus switch angle ($M/L=0.95$).

5.3.2. Inductor Insertion

Inductor insertion is the opposite operation to inductor bypassing. Referring to Fig. 5.14, S_1 is initially open and S_2 is closed. Therefore, before switch operation the voltage across S_1 is the steady state voltage induced on L_2 and the voltage on S_2 is zero. When S_1 closes and S_2 is still conducting, the voltage on both S_1 and S_2 are zero. After S_2 opens, the voltage on S_1 is zero and the voltage on S_2 is the voltage drop on L_2 .

5.3.2.1 Theoretical Analysis

Same as inductor bypassing, the only transient voltage needs to be analyzed is the voltage on S_2 at second phase. Knowing the second phase current from the current analysis, the frequency domain current is expressed as below:

$$I_t = \frac{V(s) + (L_1 + L_2 + 2M)I_1(0) - \frac{V_2(0)}{s}}{s(L_1 + L_2 + 2M) + 2R + \frac{1}{sC}} \quad (5.28)$$

The voltage on S_2 is

$$V_{s2} = -(L_2 + M)I_1(0) + I_t(sL_2 + sM) \quad (5.29)$$

The time domain voltage can be obtained by partial fraction expansions. Use the measurement parameters in the calculation, i. e., $R=3.3922\Omega$, $L_1=0.0455H$, $L_2=0.0463H$, $M=0.0114H$, $C=40.1\mu F$. The initial conditions of the circuit are determined by the time of switch operation. Now take the time corresponding to the switch angle=300° as switching time. The time domain voltage is expressed as

$$u_{s1} = 82.6e^{-29.5t} \cos(465.5t - 21.85^\circ) + 102.8 \cos(377t - 158.2^\circ)V \quad (5.30)$$

The steady state voltage on S_1 before switching can be calculated as follows:

$$V_{s_1,pre} = \left| \frac{V_m \times j\omega M}{R + j\omega L_1 - j1/(\omega C)} \right| = 9.9V \quad (5.31)$$

The voltage waveforms are shown in Fig. 5.18. From the time domain voltage expression, it is observed that the magnitude of the forced voltage component of S_2 is 102.8V. With a decaying natural component superposed on the force component, the transient voltage can be expected much higher than that of inductor bypassing.

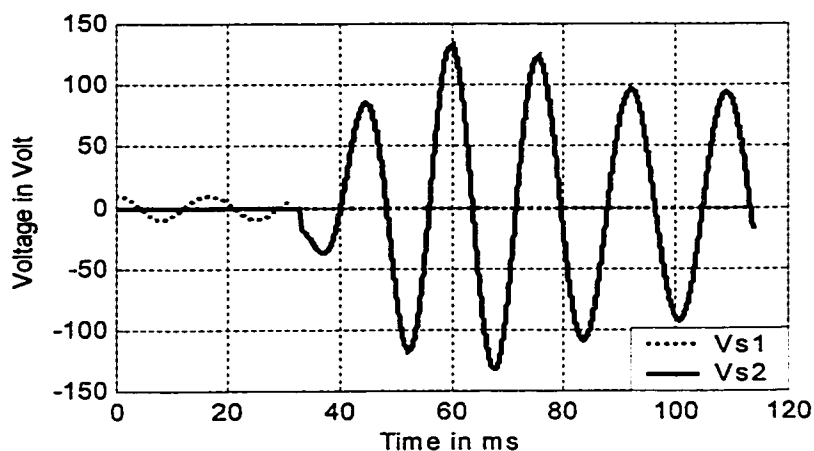


Fig. 5.18: Switch voltage waveforms for inductor insertion.

5.3.2.2. Sensitivity Study of Switch Timing

The peak transient voltage corresponding to different switch angle is calculated. The following parameters are used in the computation: $R/X=0.1$, $M/L=0.5$, i. e., $R=1.17\Omega$, $L_1=0.0455H$, $L_2=0.0463H$, $M=0.0229H$. The peak voltage is in per-unit based on the steady state voltage on the switch after switch operation. Fig. 5.19 shows the curve of peak voltage versus switch angle.

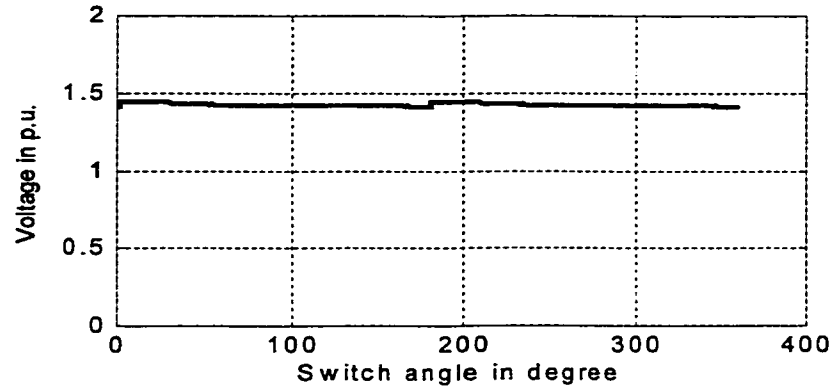


Fig. 5.19: Curve of peak transient voltage v. s. switch angle.

It is interesting to note that the peak transient voltage does not change much with the switch angle in this particular case. The peak voltage is around 1.44 p. u., which is apparently higher than that of inductor bypassing in Fig. 5. 16. Generally speaking, however, this voltage is not considered high. Moreover, this curve is the instantaneous peak voltage, which does not last due to the damping effect. For a closely coupled inductor, for example, $M/L=0.95$, the voltage transient lasts for a long time. Therefore, the main problem in this case is the transient duration. Fig. 5.20 shows the switch voltage for M/L .

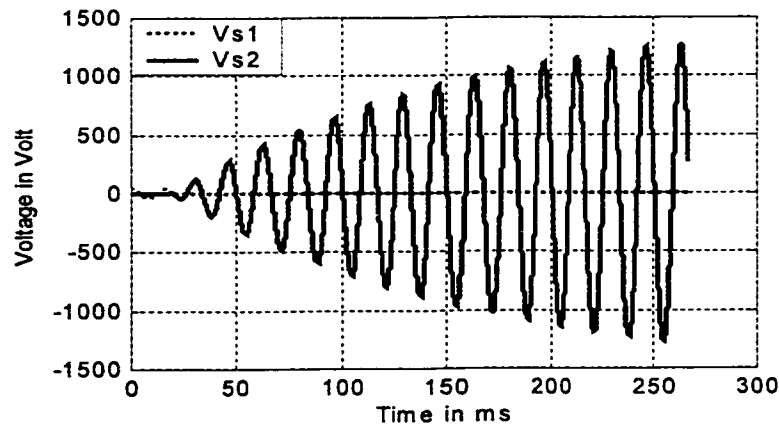


Fig. 20: Switch voltage waveforms for inductor insertion ($M/L=0.95$).

Following the same procedures as the analysis of transient current, the duration of the voltage transient and the impact of resistance and the mutual coupling can be investigated. Similar conclusions can be expected as that of transient current since the natural component of the transient voltage has both the same damping coefficient and frequency as the transient current.

From the analysis above, we can conclude that the switching transient caused by inductor insertion is severer than that of inductor bypassing. However, basically the voltage stress for both inductor bypassing and insertion are not high. In high M/L ratio, the transient duration of the inductor insertion has to be dealt with.

5.4 The Duration of Switching Transients of RLC Circuit

Unfortunately, the definition of the transient duration for the RL circuit is not applicable to the RLC circuit, due to the presence of the natural frequency component in the transient current. As an important index, the duration of the transient needs to be evaluated and a way should be found to do it. We will try to relate the circuit loss to the damping coefficient to evaluate the transient duration.

Recalling the analysis conducted earlier in this chapter, the second phase of the transient response includes only two parts. One is the forced response component associated with the circuit source; the other is natural response component associated with initial conditions and circuit parameters. The forced response is a steady-state component without decay whereas the natural response decays with time. The natural component has the form of $i = I(0)e^{-\delta t} \cos(2\pi f_N t + \phi)$, where f_N is the natural frequency, δ is the damping coefficient and $\delta = \frac{R}{2L}$, $I(0)$ is the initial current. It is obvious that the duration of the transient is determined by δ . The reciprocal of δ is the time taken for the

natural component to decay to 36.8% of its initial current, which is taken as the duration of the transient.

The experimental case is taken as an example to demonstrate the procedures to do the calculation. The source voltage is $V_s=80V$, $L_1=0.0455H$, $L_2=0.0463H$, $M=0.0114H$, $C=40.1\mu F$. The resistance can be calculated from the power loss of the circuit. Taking the no-loss apparent power VA as the base,

$$X = \left| \omega(L_1 + L_2 + 2M) - \frac{1}{\omega C} \right| = 22.94\Omega \quad (5.32)$$

where X is the reactive impedance of the circuit, and the current is

$$I = \frac{V_s}{X} = \frac{80}{22.94} = 3.4868A \quad (5.33)$$

then the branch apparent power is

$$S = VI = 80 \times 3.4868 = 278.947Var \quad (5.34)$$

When the loss is 1% and the power $P=2.789W$, for the inductor bypassing, the resistance R is calculated as

$$P = I^2 R \quad (5.35)$$

$$I = \frac{V_s}{\sqrt{R^2 + (\omega L_1 - 1/\omega C)^2}} \quad (5.36)$$

and we get $R=1.0467 \Omega$

The damping coefficient is $\delta = 11.5s^{-1}$, and the time needed for the natural component to decay to 36.8% of its initial value is $0.087s$.

For the inductor insertion, $P = I^2 R$, $P=2.789W$,

$$I = \frac{V_s}{\sqrt{R^2 + (\omega L_1 + \omega L_2 + 2\omega M - 1/\omega C)^2}} \quad (5.37)$$

and we get $R=0.2295\Omega$. The damping coefficient is $1.001s^{-1}$, and the time needed for the natural component to decay to 36.8% of its initial value is $1s$.

Following the procedures above to examine a practical filter branch, suppose the capacitor size is $800Kvar$, the voltage level that the filter is connected to is $480V$ and the filter is tuned to 5th harmonic. The corresponding parameters are $X_C=0.288\Omega$, $X_L=0.005998\Omega$. The inductor is divided into two parts evenly to perform inductor bypassing and insertion. The resistance and the damping coefficient are calculated for different power loss. The results are given in Table 5.1. The *Cycles* is the transient duration in cycles. The curves of duration cycles versus percent of loss are obtained for inductor bypassing and insertion. (See Fig. 5.21.)

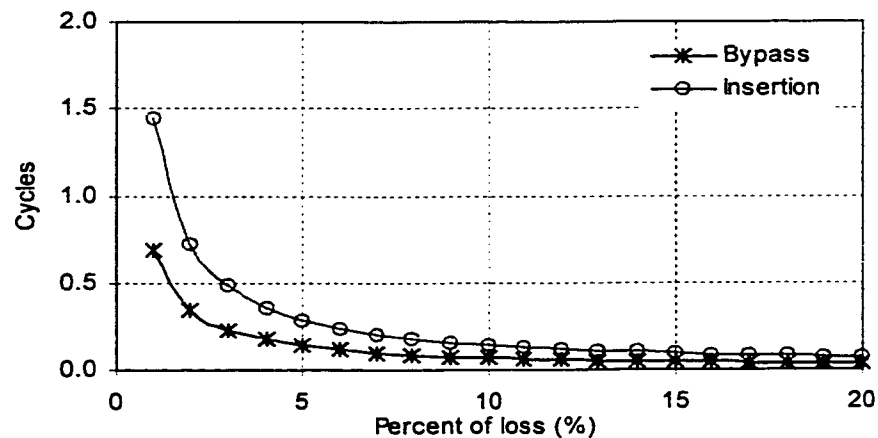


Fig. 5.21: Duration cycles vs. percent of loss for a filter.

Table 5.1 Calculation results of R & δ for different power loss

Loss(%)	Loss(W)	Bypass			Insertion		
		R	δ	Cycles	R	δ	Cycles
1	8	0.0028	86.80	0.69	0.00	41.57	1.44
2	16	0.0055	173.64	0.35	0.01	83.17	0.72
3	24	0.0083	260.59	0.23	0.01	124.81	0.48
4	32	0.0111	347.68	0.17	0.01	166.51	0.36
5	40	0.0138	434.98	0.14	0.01	208.32	0.29
6	48	0.0166	522.53	0.11	0.02	250.23	0.24
7	56	0.0194	610.39	0.10	0.02	292.29	0.21
8	64	0.0222	698.61	0.09	0.02	334.52	0.18
9	72	0.0250	787.24	0.08	0.02	376.93	0.16
10	80	0.0279	876.35	0.07	0.03	419.56	0.14
11	88	0.0307	966.00	0.06	0.03	462.44	0.13
12	96	0.0336	1056.23	0.06	0.03	505.59	0.12
13	104	0.0365	1147.13	0.05	0.03	549.03	0.11
14	112	0.0394	1238.75	0.05	0.04	592.81	0.10
15	120	0.0424	1331.17	0.05	0.04	636.96	0.09
16	128	0.0453	1424.46	0.04	0.04	681.50	0.09
17	136	0.0483	1518.70	0.04	0.05	726.47	0.08
18	144	0.0514	1613.96	0.04	0.05	771.91	0.08
19	152	0.0544	1710.36	0.04	0.05	817.86	0.07
20	160	0.0575	1807.96	0.03	0.06	864.36	0.07

It can be seen that the transient duration decreases with the increase of power loss. Therefore, in practical design, a balance should be found between the transient performance and the power loss. It can also be observed that the inductor bypassing transient has a shorter duration compared with the inductor insertion. The long duration of the inductor insertion transient is due to the fact that the current after insertion is much higher than before the operation. For a higher current and certain power loss, the resistance is smaller, and hence, of longer duration. Generally speaking, the transient duration for this specific case is acceptable for almost all loss levels.

5.5 Conclusions

The transient performance of the proposed variable inductor in the *RLC* circuit is investigated in this chapter. The results reveal several aspects of the transient characteristic of the variable inductor, which provides the necessary insight to guide the design of the device.

The switching transients of inductor bypassing and insertion are theoretically analyzed. The results are verified by simulation and experiments, which not only imply that the theoretical analysis is correct but also assure us that the proposed device works in practice. The theoretical method is further used to conduct a sensitivity study of switch timing and investigate the impact of resistance, self inductance and mutual inductance on the transient process. The results of analysis indicate that

- There are periods within which the peak transient current are low for inductor bypassing and insertion. However, generally speaking, the peak transient current does not change much with the variation of the switch angle for both inductor bypassing and insertion; and the current stress is within an acceptable level. For example, the inductor bypassing and insertion transient currents are around 2.0 and 1.5 p. u., respectively. This is a good relief to the switch control.
- The stronger mutual coupling causes a higher peak transient current. This is a factor should be considered in the device design.
- The transient duration decreases with the increase of power loss. The damping coefficient is used to evaluate the duration of the transient, which is closely related to the power loss. A typical case is studied to demonstrate the method of evaluation. In this case, the transient duration is 0.14 cycle when the power loss is 10%, which is quite acceptable.
- The voltage stress on the switches for inductor insertion is higher than that of inductor bypassing. However, generally speaking, the voltage stress is not high for both switch operation. It is important to point out that the transient duration is very long for inductor insertion if the coupling coefficient is high.

From the analysis, we know that the transient performance of the device is highly dependant on its parameters. By arranging the parameters according to its nature as revealed in this study, a better performance device can be designed.

Chapter 6

Design Issues of the Thyristor Linked Reactor

This chapter deals with the design issues of the thyristor linked reactor. The procedures of the design of the inductor are discussed. Key thyristor indices are introduced to facilitate the selection of suitable thyristors for certain applications.

The device basically consists of two kinds of components. One is the inductor segment and the other is the thyristor. The design of the device is, therefore, the design of inductors and the selection of suitable thyristors. The procedures of the design of inductors will be discussed, and several thyristor indices will be identified.

6.0 Inductor Design Issues

The design of the inductor starts from the determination of the inductor parameters. Suppose we design inductor segments for a tunable filter as the one in chapter 3. The total inductance is first determined from the capacitor size and the desired harmonic frequency the filter tuned to. Then the inductance is divided into several segments according to a certain order, for example a binary order. If the inductor segments are separate from each other without mutual coupling, the inductance can be simply split by binary order, and adding or removing inductor segments will be in binary. However, if the segments are coupled together and we still want the inductance to vary in binary order, the parameter arrangement will not be as simple.

Take the case in chapter 3 as example. The parameters without coupling are

$$X_L = \begin{bmatrix} 16.41 & 0 & 0 & 0 \\ 0 & 8.205 & 0 & 0 \\ 0 & 0 & 4.102 & 0 \\ 0 & 0 & 0 & 2.05 \end{bmatrix} \Omega \quad (6.1)$$

When switches operate, the total inductance changes linearly in binary order. The parameters with the mutual coupling coefficient of 0.9 are

$$X = \begin{bmatrix} 16.41 & 10.44 & 7.384 & 5.221 \\ 10.44 & 8.205 & 5.221 & 3.692 \\ 7.384 & 5.221 & 4.102 & 2.611 \\ 5.221 & 3.692 & 2.611 & 2.051 \end{bmatrix} \Omega \quad (6.2)$$

Obviously, the inductance of Equation 6.2 is not changing in binary order when a segment is switched in or out. The problem here is how to arrange the segment parameters to achieve the effect as in Equation 6.1 when mutual coupling exists. Suppose the mutual coupling coefficient is 0.9. The corrected impedance matrix is expressed as

$$X_{corrected} = \begin{bmatrix} \omega L_{11} & 0.9\omega\sqrt{L_{11}L_{22}} & 0.9\omega\sqrt{L_{11}L_{33}} & 0.9\omega\sqrt{L_{11}L_{33}} \\ & \omega L_{22} & 0.9\omega\sqrt{L_{22}L_{33}} & 0.9\omega\sqrt{L_{22}L_{44}} \\ & & \omega L_{33} & 0.9\omega\sqrt{L_{33}L_{44}} \\ & & & \omega L_{44} \end{bmatrix} \Omega \quad (6.3)$$

where L_{ii} are self-inductance and i is the row and column number.

With the existence of mutual coupling, the self-impedances in the corrected matrix will not be in binary order. But what we really care about here is the total impedance for each switch state. The total impedance of the variable reactor can be obtained by summation of certain self-impedances and mutual coupling impedances

according to the switch state. The calculation of total impedance can be demonstrated by an example. When inductor segments L_{11} and L_{22} are switched in, the total impedance is

$$X_T = \omega L_{11} + \omega L_{22} + 2 \times 0.9 \omega \sqrt{L_{11} L_{22}} \Omega \quad (6.4)$$

Eight total impedances can be obtained corresponding to 8 switch states. Similarly, the total impedances X_T' can also be derived from Equation 6.1. The difference between X_T and X_T' is

$$error = X_T - X_T' \quad (6.5)$$

Now, let the first self-impedance ωL_{11} in the Equation 6.3 equal to the corresponding impedance in the Equation 6.1; change the other self-impedances in the Equation 6.3 of the corrected matrix and, hence, the total impedance X_T , till the minimum errors are reached. The resultant impedance matrix is

$$X = \begin{bmatrix} 16.41 & 3.431 & 1.913 & 0.989 \\ 3.431 & 0.885 & 0.444 & 0.230 \\ 1.913 & 0.444 & 0.275 & 0.128 \\ 0.989 & 0.230 & 0.128 & 0.074 \end{bmatrix} \Omega \quad (6.6)$$

The impedances at different switch states are shown in Table 6.1 and comparison plots are shown in Fig. 6.1. Here *Coupled* is the total impedance at each switch state derived from Equation 6.2; **Error** is the difference between X_T and X_T' .

Table 6.1 Parameter comparison

Switch	Coupled	X_r'	X_r	Error	Error%
1000	16.41	16.41	16.41	0.00	0.00
1001	28.90	18.46	18.46	0.00	0.00
1010	35.28	20.51	20.51	0.00	0.00
1011	53.00	22.56	22.56	0.00	0.00
1100	45.50	24.62	24.16	0.46	1.86
1101	65.38	26.67	26.67	0.00	0.00
1110	74.82	28.72	29.15	-0.43	-1.50
1111	99.92	30.77	31.91	-1.15	-3.72

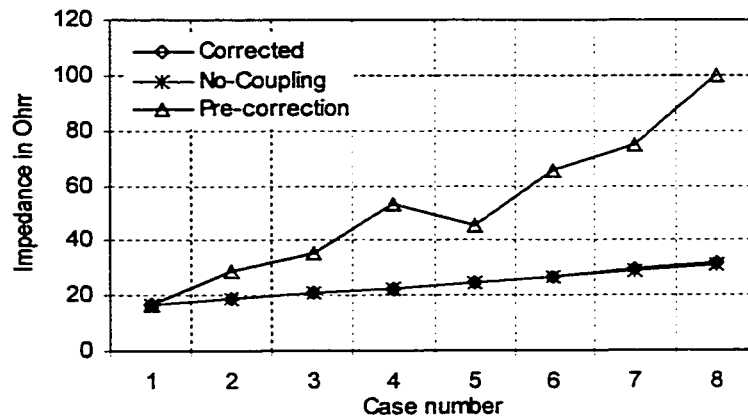


Fig. 6.1: Parameter comparison.

From the figure and the table, it can be seen that the calculated results are almost identical to the non-coupling case. Moreover, the calculated parameters in Equation 6.3 are much smaller than that of the non-coupling case in Equation 6.1, which means less turns of coil are needed for the coupled case and, therefore, the cost is lower.

After the parameters are determined, the voltage and current rating can be obtained following the same procedures as in chapter 3. Considering the transient performance of the reactor at different resistance level analyzed in chapters 4 and 5, certain wire sizes can be selected. The mechanical design of the inductor has standard procedures to follow, which is out of the scope of this thesis.

6.1 Selection of Thyristors

A thyristor is one of the most important types of power semiconductor devices. Thyristors are used extensively in power electronic circuits. They are operated as bi-stable switches, operating from non-conducting state to conducting state. Thyristors can be assumed to be ideal switches for many applications. It is a critical, relatively expensive component of the thyristor linked reactor.

All semiconductor devices have operating limits to their capability, and exceeding these limits, even for short times, will result in failure, loss of control or irreversible damage. All thyristors, therefore, must be used within their capability at all times and those must include extreme conditions such as may exist during circuit transients and faults. A data sheet is usually provided by the manufacturer to give the specifications of the thyristor. Among the data provided, the following indices are of great importance in selecting a thyristor:

- Current rating,
- Voltage rating,
- di/dt rating, and
- dv/dt rating.

6.1.1 Thyristor Current Rating

The thyristor being composed of semiconductor material having a small thermal capacity is extremely sensitive to current flowing through it that is larger than the rated value [21]. The size of the thyristor may be chosen from the level of the continuous current required through it and from the level of the fault current that can occur in the circuit. The fault current is also known as a non-repetitive surge current, which is usually about 10 times that of the continuous current with a duration of half of a cycle. For example, from an ABB thyristor data sheet, the continuous current is $550A$ and the non-

repetitive surge current is $4850A$ with a duration of $8.3ms$. The principle most often used in choosing the correct thyristor is to study both of these conditions carefully.

The continuous RMS current can be estimated by conducting an analysis following the same procedures as in chapter 3. The analysis of the transient performance provides the peak transient current. Therefore, the current rating can be determined by taking the maximum steady state current as continuous current rating and peak transient current as maximum peak surge current. Of all the cases studied in chapters 4 and 5, all the peak transient currents are less than 7 times of the continuous RMS currents except for one extreme case. The duration of the whole transient process is less than 20ms and the duration of the peak transient current is actually very short.

6.1.2 Voltage Rating

The device voltage rating is a measure of the maximum voltage that can be applied across the device without causing a breakdown or failure. It is essential that the voltage capability of a thyristor is not exceeded during operation even for a very short period of time. The different ratings related to the voltage are *peak repetitive forward blocking voltage* (V_{DRM}), *peak repetitive reverse voltage* (V_{RRM}) and *non-repetitive peak reverse voltage* (V_{RSM}) [21]. V_{DRM} and V_{RRM} are the peak voltages that the thyristor can block without breakdown at the maximum allowable junction temperature in forward and reverse direction, respectively. These two indices are usually set to the same value. V_{RSM} is the maximum transient reverse voltage that can be safely blocked by the thyristor with a short duration of about $10ms$ [22]. V_{RSM} is not much higher than V_{RRM} and V_{DRM} . For example, in an ABB thyristor data sheet, the V_{DRM} and V_{RRM} are $5600V$ and the V_{RSM} is $6500V$ with a duration of $10ms$. In selecting voltage ratings, steady state analysis as in chapter 3 has to be conducted to decide the peak repetitive voltage, and transient analysis should also be performed to estimate the peak transient voltage.

6.1.3 di/dt Rating

It is important that the rate of rise of the anode current be kept less than the maximum value given on the thyristor specification sheet. If di/dt exceeds this maximum rate, the device may be damaged. Such damage may occur because large rates of current growth mean that the rise time will be short and, consequently, a localized 'hot-spot' heating will occur due to the high current density and the device may fail, as a result of excessive temperature. Therefore, the limit of the di/dt at turn-on is specified for all thyristors usually in Amps/ μ sec. The typical values lie in the range of 50 to 800A/ μ sec [21]. The practical devices must be protected against high di/dt . In practice, the di/dt is limited by adding a series inductor L_s [23]. The thyristor linked reactor does not need a series inductor to limit the di/dt because the thyristors are always in series with working inductors.

6.1.4 Forward dv/dt Rating

If the rate of rise of forward voltage is higher than the specified maximum value, it may cause switching from the off-state to the on-state. Since gate pulse triggering is commonly used for the turn on of a thyristor, the high dv/dt causes unscheduled turn on of a thyristor. This kind of switching is to be avoided as this may lead to the destruction of the thyristor through high local current density [21]. The dv/dt can be limited by connecting a capacitor with a resistor in parallel with the thyristor. This circuit is known as a RC snubber. With the presence of a snubber circuit, the voltage of the thyristor will rise exponentially [23]. Detailed design of a snubber circuit is out of the scope of this thesis. Referring to Fig. 3.6 in chapter 3, it can be seen that there are voltage sparks across thyristor switches due to the thyristor commutation. There is, therefore, potential possibility of a false trigger of the thyristor. A snubber circuit should be considered to limit the dv/dt level.

6.2 Conclusions

This chapter discussed the design issues of the thyristor linked reactor. The design is divided into two parts; one is the design of the inductor and the other is the selection of thyristors. The procedures of the design of the inductor are discussed and a method is introduced to calculate the inductor parameters, which results in a cheaper inductor. In selection of the thyristors, some key indices are highlighted. To use thyristors successfully it is most important that all conditions of operation are fully understood. Therefore, the determination of these indices must be based on the analysis in chapters 3, 4 and 5.

Chapter 7

Conclusions and Recommendations

This work has investigated the operating characteristics of a novel thyristor linked reactor. The objective is to determine the main design parameters of the device and the key factors affecting the design. This objective is achieved through a series of steps consisting of literature review, analytical study, computation simulation and prototype experiments.

The operating principle of the device and its potential applications are first discussed. They are presented in Chapters 1 and 2 along with a review of other similar devices. The literature review results showed that the TLR is new and has some advantages over existing devices. The potential applications of the device include tunable harmonic filter and a new type of static shunt compensator.

The steady state performance of the TLR is presented in Chapter 3. A prototype device was constructed to demonstrate its practicability and to guide subsequent investigations. Experimental results have confirmed that the prototype works in a desired manner and there are no unexpected operating problems. The steady state voltage stress on the TLR switches is then analyzed and compared to that of the tapped reactor. It was found that the TLR switches experience lower voltage stress than that of the tapped reactor. The TLR provides more flexible and accurate inductance variation comparing with the tapped reactor. The economical feasibility of the device was demonstrated.

The third step, presented in Chapter 4, is the analysis of the transient performance of the device in a RL circuit. Two indices, current peak and duration, are used in this thesis to characterize the behavior of transients. The study results show that the two

indices are highly dependent on the instant of switching operation. There are ranges of switch angles within which the peak and the duration of the transients are low. They can be utilized to design a thyristor control strategy that minimizes stress on the TLR components and thereby reduces the cost of the device. Other factors affecting the behavior of switching transients were also examined. They include the resistance, self-inductance and mutual inductance of the device. It was found that the resistance could significantly reduce the transient peak and duration. The higher M/L ratio can cause higher peak current and shorter duration.

The transient performance of the TLR in a RLC circuit is presented in Chapter 5. The device behavior is more complicated in this case but is more important since the RLC circuit is the intended application. Sensitivity studies on switch timing yielded an interesting finding - the transient peak current does not change significantly with the switching instant. The resistance was found effective in damping the transient, and stronger mutual coupling would cause severer transients. The transient duration was investigated in terms of power loss of the device. A method was developed to estimate the transient duration at different power loss levels. The conclusions are (1) the peak transient current is not very sensitive to the switching instant for the RLC circuit and (2) the duration of the transient can be confined to an acceptable range with an acceptable level of losses.

Experimental tests have been conducted to support both steady state and transient performance studies. The prototype parameters and responses were measured and were used to verify the validity of analytical studies. EMTP simulations were further conducted as a cross verification of the analytical and experimental results. A good agreement was found among the experimental, simulation and analytical results. The analytical study was then selected as the main approach for sensitivity studies.

The design issues of the thyristor linked reactor are discussed in Chapter 6. A method to calculate the sizes of inductor segments is introduced. For the subject of

thyristor selections, several indices were discussed with respect to the results presented in the previous chapters.

The work presented in this thesis is just the first step towards the development of a practical and economical design for the thyristor linked reactor. It has demonstrated that such a device can be constructed economically and there are no major technical problems associated with the device. There is a need, however, to further investigate the design issues quantitatively with respect to specific applications. One of the future researches in this subject could be the design of a real device with a specific application objective. For example, research could be conducted to design and construct a 208V tunable harmonic filter that can be installed and tested in a commercial power system.

The thyristor linked reactor has several promising applications. Further research work could also be conducted to explore such applications. Example research subjects are the control strategies of the device and the impact of the application on the power system performance. New applications of the device could be found in the process.

References

- [1] Roger C. Dugan; Mark F. McGranaghan; H. Wayne Beaty, *Electrical Power Systems Quality*. McGraw-Hill, New York, 1996.
- [2] Nelson David Epp, *A Self-Tuning Filter for the Mitigation of Power System Harmonics*, Thesis of Master of Science, University of Alberta, Canada, 1999.
- [3] Emad Ezat Ahmed Hassan, *Electric Arc Furnace Harmonics*. Thesis of Master of Science, Cairo University, Egypt, 1998.
- [4] Task Force on Harmonics Modeling and Simulation, "Modeling and Simulation of the Propagation of Harmonics in Electric Power Networks, Part I: Concepts, Models, and Simulation Techniques, *IEEE Trans. on Power Delivery*, 11(1), January 1996, 452-465.
- [5] R. E Owen, M. F. McGranaghan, J. R. Vivirito, "Distribution System Harmonics: Controls for Large Power Converters", *IEEE Trans. on Power Apparatus and Systems*, Vol. PAS -101, No. 3 March 1982
- [6] Gerald Robrge, Andre Deyon, *Variable Inductor*, U. S. Patent 4393147, December 5, 1978.
- [7] Johnson, Leopold J., *Current Controlled Variable Inductor*, U. S. Patent 5426409, June 20, 1995.
- [8] Bruno Bambozzi, *Variable Three Phase Inductor*, U. S. Patent 4347489, October 16, 1984.

- [9] Hua Jin; Geza Goos; Luiz Lopes, "An Efficient Switched-Reactor-Based Var Compensator", *IEEE Trans. on Industry Applications*, Vol. 30, No. 4 July/August 1994.
- [10] A. E. Lashine, "A Variable Inductor for Power Applications Using Coupled Circuits", *Electric Machines and Power Systems*, Vol. 20, No. 5, Sept./Oct 1992.
- [11] W. M. Gray, M. J. Samotyj, A. H. Noyola, "Survey of Active Power Lined Conditioning Methodologies", *IEEE Trans. on Power Delivery*, Vol. 5, No. 3, July 1990.
- [12] C. Kawann, A. E. Emanuel, "Passive Shunt Harmonic Filters for Low and Medium Voltage: A Cost Comparison Study", *IEEE Trans. on Power Systems*, Vol. 11, No. 4, November 1996.
- [13] P. C. Sen, Paul P. Biringer, R. Sidney Segeworth, "Thyristor-Controlled Single Phase Variable Inductor", *IEEE Trans. on Magnetics*, Vol. Mag-3, No.3 Sep. 1967.
- [14] D. A. Woodford, M. Z. Tarnawecy, "Compensation of Long Distance AC Transmission Lines By Shunt Connected Reactance Controllers", *IEEE Trans. on Power Apparatus and Systems*, Vol. PAS-94, No.2 March/April 1975.
- [15] L. Gyugyi, R. A. Otto, T. H. Putman, "Principles and Applications of Static Thyristor-controlled Shunt Compensators", *IEEE Trans. on Power Apparatus and Systems*, Vol. PAS-97, No. 5, Sep./ Oct. 1978.
- [16] A. E. Hammad, R. M. Mathur, "A New Generalized Concept for The Design of Thyristor Phase-Controlled Var Compensators Part I: Steady state Performance",

IEEE Trans. on Power Apparatus and Systems, Vol. PAS-98, No. 1 Jan./Feb. 1979.

- [17] Laszlo Gyugyi, Edgar R. Taylor, Jr., "Characteristics of Static, Thyristor-Controlled Compensators for Power Transmission System Applications", *IEEE Trans. on Power Apparatus and Systems*, Vol. PAS-99, No.5 Sept/Oct 1980.
- [18] R. M. Mathur, R. S. Basati, "A Thyristor Controlled Static Phase-Shifter for AC Power Transmission", *IEEE Trans. on Power Apparatus and Systems*, Vol. PAS-100, No. 5, May 1981.
- [19] Shashi B. Dewan, Janos Rajda, "Application of 46Kv, 100MVA Smart Predictive Line Controller (SPLC) to AC Electric Arc Furnace", *IEEE PES Proceedings of 1999 Winter Meeting, Part 2*, New York, 1999.
- [20] William H. Hayt, Jr., Jack E. Kemmerly, *Engineering Circuit Analysis*, McGraw-Hill, U. S., 1993.
- [21] G. K. Dubey, S. R. Doradla, A. Joshi and R. M. K. Sinha, *Thyristored Power Controllers*, Halted Press, New York, 1986.
- [22] David Finney, *The Power Thyristor and its Applications*, McGraw-Hill, England, 1980.
- [23] Muhammad H. Rashid, *Power Electronics*, Second Edition, Prentice Hall, New Jersey, 1993.
- [24] H. M Pflanz, G. N. Lester, "Control of Overvoltages on Energizing Capacitor Banks", *IEEE PES* Vol. 92, No. 1, 1973.

- [25] G. Oliver, I. Mougharbel, G. Dobson-Mack, "Minimal Transient Switching of Capacitors", *IEEE Trans. on Power Delivery*, Vol. 8, No. 4, October 1993.
- [26] C. D. Clarrcke, M. J. Johanson-Brown, "The Application of Self-Tuned Harmonic Filters to HVDC Converters", *IEE Conference Publication* No. 22, Conference on High Voltage D. C. Transmission, September 19-23, part I, PP275-276, Paper No. 55.
- [27] Technical Presentation by ABB.
- [28] R. M. Mathur, *Static Compensators for Reactive Power Control*, Canadian Electrical Association, Canada, 1984.
- [29] Michael L. Honig, David G. Messerschmitt, *Adaptive Filters: Structures, Algorithms, and Applications*, Kluwer Academic Publishers, 1984.
- [30] William D. Stevenson, Jr., *Elements of Power System Analysis*, McGraw-Hill, 1975.

Appendices

Appendix A: EMTP Script

Following program is used in chapter 4 for transient simulation of RL circuit.

```
BEGIN NEW DATA CASE                                60 60
.000125      1 1
1  A1  A2      3.647617.161
2  A3  A4          4.2544  3.392217.451
3  A5  A6          1.0746      4.1778  3.059917.353
4  A7  A8          0.4386      1.0889      4.2291
          3.080217.469
$ BLANK card ending branch cards
  A2  A3      -1      10                                1
  A4  A5  0.1664      10
  A3  A5      -1  0.1664          0.0001
  A6  A7      -1  0.2664          0.0001
  A5  A7  0.2664      10          0.0001
  A8          -1  0.4200          0.0001                                1
  A7          0.4200      10          0.0001                                1
$ BLANK card ending switch cards
14  A1  .1697E+3 .6000E+02          -1.
$ BLANK card ending source cards
*  A1  A2
$BLANK card terminating output specifications (node voltages only, here)
```

Appendix B: Matlab Scripts

Following Matlab scripts are used to conduct calculation and generate curves in chapters 3, 4 and 5.

1. Matlab Script 1

This Matlab script is used to calculate steady state voltage stress in chapter 3.

```
% Calculate the voltage stress on each inductor segment when
% thyristor linked reactor is in a filter.

%Initiation.

clear
Voltage=25000; % Voltage rating.
KVA=800; % Capacitor size.
Harmonic=6.9; % Filter tuned harmonic order.
XC=Voltage^2/(KVA*1000);
HalfZ=XC/Harmonic^2;
A=zeros(4,4);
Zseg=zeros(1,4);
Ztotal=0;
ZLCmatrix=zeros(1,8);
CVoltage=zeros(1,8);
Imatrix=zeros(1,8);
ZsegMatrix=zeros(4,8);
fmatrix=zeros(1,8);
Zmiddle=0;
VsegMatrix=zeros(8,4);

%Input impedance and switch state matrix. K=0.9.
%Impedance matrix.
Zmatrix=[HalfZ 0.9*sqrt(HalfZ^2/2) 0.9*HalfZ/2 0.9*HalfZ/sqrt(8);...
          0.9*sqrt(HalfZ^2/2) HalfZ/2 0.9*HalfZ/sqrt(8) 0.9*HalfZ/4;...
          0.9*HalfZ/2 0.9*HalfZ/sqrt(8) HalfZ/4 0.9*HalfZ/sqrt(32);...
```

```

0.9*HalfZ/sqrt(8) 0.9*HalfZ/4 0.9*HalfZ/sqrt(32) HalfZ/8];

%switch state matrix.
Switch=[1 1 1 1 1 1 1 1;0 0 0 0 1 1 1 1;0 0 1 1 0 0 1 1;0 1 0 1 0 1 0
1];

for Nswitch=1:8,
    for L=1:4,
        A(L,L)=Switch(L,Nswitch);
    end
    for L=1:4,
        for M=1:4,
            if L~=M,
                A(L,M)=A(L,L)*A(M,M);
            end
        end
    end
    Zcase=Zmatrix.*A;%Self-inductance and mutual-inductance in effect
                    %according to the switch state.

    for L=1:4,
        for M=1:4,
            Zseg(1,L)=Zcase(M,L)+Zseg(1,L);%impedance of each segment of
                                            %inductor.

        end
    end
    for L=1:4,
        Ztotal=Ztotal+Zseg(L);%Total impedance of all segments.
    end
    ZLC=XC-Ztotal;%Total impedance of the branch.

%Get current and voltage of each segment.

ZLCmatrix(Nswitch)=ZLCmatrix(Nswitch)+ZLC;
frequency=sqrt(XC/Ztotal);%filter tuned harmonic.
fmatrix(Nswitch)=fmatrix(Nswitch)+frequency;
Current=Voltage/ZLC;
Vseg=Current*(Switch(:,Nswitch))'*Zmatrix;

```

```

    Imatrix(Nswitch)=Imatrix(Nswitch)+Current;
    CVoltage(Nswitch)=CVoltage(Nswitch)+XC*Current;%Voltage of the
capacitor.

    for L=1:4,
        VsegMatrix(Nswitch,L)=VsegMatrix(Nswitch,L)+Vseg(1,L);
    end
Zseg=zeros(1,4);
    Ztotal=0;
end

%Output.

Output=[Imatrix' ZLCmatrix' fmatrix' CVoltage' VsegMatrix];
save D:\TLR_LC_Couple.txt Output -ASCII

```

2. Matlab Script 2

This script is used in chapter 5 for switching transient calculation of RLC circuit.

```

% Initialization.

clear
i=sqrt(-1);
j=sqrt(-1);
w=2*pi*60;
L1=0.0457;
L2=0.0463;
Cap=40.1*10^(-6);
M=0.0219;
R=1.71;
Vm=113.1;
Z=2*R+j*w*(L1+L2+2*M)-j/(w*Cap); %Impedance before switching.
Nsample=250; %sample points per cycle.

% Ask for switch angle. Get pre-disturbance current and voltage.

```

```

Angle=input('Please input an angle in degree\n')
sita=Angle*pi/180;
Tswitch=1/60+Angle/(60*360);
Tpre=(0:1/(Nsample*60):Tswitch)';
Itpre=Vm*cos(w*Tpre-angle(Z))/abs(Z);
I1pre=Itpre;
m=max(size(Itpre));
I2pre=zeros(m,1);
Vcpre=Vm*cos(w*Tpre-angle(Z)-pi/2)/(w*Cap*abs(Z));

%Get initial inductor current and capacitor voltage for S2 closing.

I0=Vm*cos(sita-angle(Z))/abs(Z);
V0=Vm*cos(sita-angle(Z)-pi/2)/(abs(Z)*w*Cap);

%Input Laplace coefficients. Get poles and residues.

%Denominator of Itotal and I1.
Midd=L1*L2-M^2;
aa1=1;
aa2=R*(L1+L2)/Midd;
aa3=w^2+(R^2+L2/Cap)/Midd;
aa4=(w^2*R*(L1+L2)+R/Cap)/Midd;
aa5=w^2*(R^2+L2/Cap)/Midd;
aa6=w^2*R/(Cap*Midd);
AA=[aa1 aa2 aa3 aa4 aa5 aa6];

%Denominator of capacitor voltage.
Va1=aa1;
Va2=aa2;
Va3=aa3;
Va4=aa4;
Va5=aa5;
Va6=aa6;
Va7=0;
VA=[Va1 Va2 Va3 Va4 Va5 Va6 Va7];

```

```

%Numerator of Itotal.
b1=I0;
b2=(I0*R*(L1+M)-V0*L2+Vm*L2*cos(sita))/Midd;
b3=w^2*I0-(V0*R-Vm*R*cos(sita)+Vm*w*L2*sin(sita))/Midd;
b4=(w^2*I0*R*(L1+M)-w^2*V0*L2-Vm*w*R*sin(sita))/Midd;
b5=-V0*R*w^2/Midd;
BB1=[b1 b2 b3 b4 b5];

%Numerator of I1.
bb1=I0;
bb2=(R*I0*(L1+M)+M*V0-Vm*M*cos(sita))/Midd;
bb3=w^2*I0+(I0*(L2+M)/Cap+Vm*M*w*sin(sita))/Midd;
bb4=(w^2*R*(L1+M)*I0+w^2*M*V0)/Midd;
bb5=(L2+M)*I0*w^2/(Cap*Midd);
BB2=[bb1 bb2 bb3 bb4 bb5];

%Numerator of Vc.
Vb1=b1/Cap;
Vb2=b2/Cap;
Vb3=b3/Cap;
Vb4=b4/Cap;
Vb5=b5/Cap;
VB=[Vb1 Vb2 Vb3 Vb4 Vb5];

%Get poles and residues.
[RR1,PP1,KK1]=residue(BB1,AA);
[RR2,PP2,KK2]=residue(BB2,AA);
[VR,VP,VK]=residue(VB,VA);

%Obtain time domain currents and voltage.

% kcycles after switch operation.
kcycles=10;
Ttransient=(0:1/(60*Nsample):kcycles/60)';
ItTran=RR1(1)*exp(PP1(1)*Ttransient)+RR1(2)*exp(PP1(2)*Ttransient)+...
        RR1(3)*exp(PP1(3)*Ttransient)+RR1(4)*exp(PP1(4)*Ttransient)+...
        RR1(5)*exp(PP1(5)*Ttransient);

```

```

I1Tran=RR2(1)*exp(PP2(1)*Ttransient)+RR2(2)*exp(PP2(2)*Ttransient)+...
RR2(3)*exp(PP2(3)*Ttransient)+RR2(4)*exp(PP2(4)*Ttransient)+...
RR2(5)*exp(PP2(5)*Ttransient);

```

```

Vcap=V0+VR(1)*exp(VP(1)*Ttransient)+VR(2)*exp(VP(2)*Ttransient)+...
VR(3)*exp(VP(3)*Ttransient)+VR(4)*exp(VP(4)*Ttransient)+...
VR(5)*exp(VP(5)*Ttransient)+VR(6)*exp(VP(6)*Ttransient);

```

```

ItTrans=real(ItTran);

```

```

I1Trans=real(I1Tran);

```

```

VcTrans=real(Vcap);

```

```

%Find the first zero-cross point of I2 after switch operation.

```

```

for l=1:2000,
    if sign(I1Trans(l))~=sign(I1Trans(l+1)),
        stop=l;break;
    end
end

```

```

ItTransient=ItTrans(1:stop);
I1Transient=I1Trans(1:stop);
I2Transient=ItTransient-I1Transient;
VcTransient=VcTrans(1:stop);
duration=stop/(60*Nsample);

```

```

% Get transient current and voltage after S1 opens.

```

```

% Initial conditions for S1 opening.
Tstop=(stop+1)/(60*Nsample);
Tpost=(0:1/(60*Nsample):(kcycles*Nsample-stop-1)/(60*Nsample))';
sital=sita+w*Tstop;
I01=ItTrans(stop);
V01=VcTrans(stop);

```

```

%Input Laplace coefficients.

```

```

%Denominator of current;

```

```

apost1=1;

```

```

apost2=R/L1;
apost3=w^2+1/(L1*Cap);
apost4=R*w^2/L1;
apost5=w^2/(L1*Cap);
Apost=[apost1 apost2 apost3 apost4 apost5];

%Denominator of voltage.
Vapost1=apost1;
Vapost2=apost2;
Vapost3=apost3;
Vapost4=apost4;
Vapost5=apost5;
Vapost6=0;
VApost=[Vapost1 Vapost2 Vapost3 Vapost4 Vapost5 Vapost6];

%Numerator of current.
bpost1=I01;
bpost2=(Vm*cos(sita1)-V01)/L1;
bpost3=w^2*I01-Vm*w*sin(sita1)/L1;
bpost4=-V01*w^2/L1;
Bpost=[bpost1 bpost2 bpost3 bpost4];

%Numerator of voltage.
VBpost=Bpost/Cap;

%Get poles and residues.
[Rpost, Ppost, Kpost]=residue(Bpost, Apost);
[VRpost, VPpost, VKpost]=residue(VBpost, VApost);

%Time domain current after switch S1 opens.
Itafter=Rpost(1)*exp(Ppost(1)*Tpost)+Rpost(2)*exp(Ppost(2)*Tpost)+...
    Rpost(3)*exp(Ppost(3)*Tpost)+Rpost(4)*exp(Ppost(4)*Tpost);

Vcafter=V01+VRpost(1)*exp(VPpost(1)*Tpost)+VRpost(2)*exp(VPpost(2)*
    Tpost)+VRpost(3)*exp(VPpost(3)*Tpost)+VRpost(4)*exp(VPpost(4)*Tpost)+
    VRpost(5)*exp(VPpost(5)*Tpost);

%I1=0 after zero-cross point.

```



```

Itpost=real(Itafter);
Vcpost=real(Vcafter);
I2post=Itpost;
I1post=zeros(kcycles*Nsample-stop,1);

%Total currents.
Ttotal=[Tpre;Ttransient(1:stop)+Tswitch;Tpost+Tswitch+Tstop];
ItTotal=[Itpre;ItTransient;Itpost];
I1Total=[I1pre;I1Transient;I1post];
I2Total=[I2pre;I2Transient;I2post];
VcTotal=[Vcpre;VcTransient;Vcpost];
I=[ItTotal I1Total I2Total VcTotal];
Zpost=R+j*w*L1-j/(w*Cap); %Impedance after switching.

%Plot of the current and voltage waveforms.

figure
plot(Ttotal*1000,ItTotal,'k',Ttotal*1000,I1Total,'r.',Ttotal*1000,
I2Total,'b:')
xlabel('Time in ms');
ylabel('Current in Amp');
legend('It','I1','I2');
grid
figure
plot(Ttotal*1000,VcTotal)
xlabel('Time in ms')
ylabel('Voltage in Volt')
grid

```